2012-12-20

COOPERATIVE COMMUNICATIONS FOR LTE-ADVANCED SYSTEMS: DOWNLINK RELAY AND PERFORMANCE OPTIMIZATION

MAHASNEH, HASSAN ALI SHAKER

UNIVERSITY OF CALGARY

COOPERATIVE COMMUNICATIONS FOR LTE-ADVANCED SYSTEMS: DOWNLINK RELAY AND PERFORMANCE OPTIMIZATION

By

Hassan Ali Shaker Mahasneh

A DISSERTATION

SUBMITTED TO THE FACULTY OF GRADUATE STUDIES

IN PARTIAL FULFILMENT OF THE REQUIREMENTS FOR THE

DEGREE OF DOCTOR OF PHILOSOPHY

DEPARTMENT OF ELECTRICAL AND COMPUTER ENGINEEERING

CALGARY, ALBERTA

December 2012

UNIVERSITY OF CALGARY

FACULTY OF GRADUATE STUDIES

The undersigned certify that they have read, and recommend to the Faculty of Graduate Studies for acceptance, a dissertation entitled " COOPERATIVE COMMUNICATIONS FOR LTE-ADVANCED SYSTEMS: DOWNLINK RELAY AND PERFORMANCE OPTIMIZATION" submitted by Hassan Ali Shaker Mahasneh in partial fulfillment of the requirements of the degree of Doctor of Philosophy.

Supervisor, *DR. Abu Sesay*
Department of Electrical and Computer Engineering

Supervisor Committee Member, *DR. Abraham Fapojuwo*
Department of Electrical and Computer Engineering

Supervisor Committee Member, *DR. Geoffrey Messier*
Department of Electrical and Computer Engineering

Internal/External Examiner, *DR. Gérard Lachapelle*
Department of Geomatics

External Examiner, *DR. Xiaodai Dong*
University of Victoria

Date

Abstract

The Third Generation Partnership Project's Long Term Evolution-Advanced (LTE-A) is considering an option for relay networks to provide cost-effective throughput enhancement and coverage extension. While analog repeaters have been used to enhance coverage in commercial cellular networks, the use of more sophisticated fixed relays is relatively new. The main challenges faced by relay deployments in cellular systems are designing an improved and efficient relaying protocol, improving the desired signal and overcoming the extra interference added by the presence of relays specifically at cell-edge regions. Most prior works on relaying do not consider relay integration in cellular LTE-A systems. In this dissertation, we propose and investigate the performance of a modified relaying protocol, the *Enhanced-Decode-and-Forward* (E-DF), which improves diversity and data rate and reduces the symbol error rate. The dissertation also proposes and analyzes the performance of several half-duplex downlink relay schemes in interference-limited cellular systems. These schemes are – *The Omni-Relay* (OR) *scheme*, *The Directional-Relay* (DR) *scheme* and *The In-band Relay* (IR) *scheme*. The average signal-to-interference plus noise ratio and average capacity performances of each scheme are analyzed for each relay type, antenna pattern as well as power and frequency resources allocation.

Acknowledgements

I would like to thank to my PhD advisor, Professor Abu Sesay, for supporting me during these past four years. Abu has been supportive and has given me the freedom to pursue various projects. He has also provided insightful discussions about the research. I am very grateful to Abu for his scientific advice and knowledge and many insightful discussions and suggestions. He is my primary resource for getting my science questions answered and was instrumental in helping me build this thesis. I hope that I could be as lively, enthusiastic, and energetic as Abu and to someday be able to command an audience as well as he can. I also have to thank the members of my PhD committee, *DR. Abraham Fapojuwo*, *DR. Geoffrey Messier* , *DR. Gérard Lachapelle*, and *DR. Xiaodai Dong* for their helpful comments and suggestions.

I also thank the wonderful staff in the Electrical and Computer Engineering Department for always being so helpful and friendly. People here are genuinely nice and want to help you out and I'm glad to have interacted with many.

I especially thank my mom, dad, brothers, and sisters. My hard-working parents have sacrificed their lives for my brothers, my sisters, and myself and provided unconditional love and care. I love them so much, and I would not have made it this far without them. My brothers and sisters have been my best friends all my life and I love them dearly and thank them for all their advice and support. I know I always have my family to count on when times are rough.

I am most grateful to my in-laws, *Capt. Yousef*, *Dorzyah*, *Feras*, *Fahad*, and *Majd* for providing me with love, caring, and kindness. They are always very supportive

in every step I took academically and personally. I wish I could pay you back one day.

The best outcome from these past four years is finding my best friend, soul-mate, and wife. I married the best person out there for me. Maysa has been a true and great supporter and has unconditionally loved me during my good and bad times. She has been non-judgmental of me and instrumental in instilling confidence. She has faith in me and my intellect even when I felt like digging hole and crawling into one because I didn't have faith in myself. These past several years have not been an easy ride, both academically and personally. I truly thank Maysa for sticking by my side, even when I was irritable and depressed. I feel that what we both learned a lot about life and strengthened our commitment and determination to each other and to live life to the fullest.

I dedicate this thesis to

my family, my wife Maysa, my beloved son Ali, and daughter Tala,

for their constant support and unconditional love.

I love you all dearly.

Table of Contents

List of Tables

List of Figures

List of Abbreviations

Abbreviation	Meaning
1G	The first generation analog cellular systems
2G	The second generation digital cellular systems
3G	The third generation digital cellular systems
3GPP	3G partnership projects
AF	Amplify-and-Forward
AWGN	Additive White Gaussian Noise
BER	Bit Error Rate
BS	Base Station
CAGR	Compound Annual Growth Rate
CDF	Cumulative Density Function
CDMA	Code Division Multiple-Access
CSI	Channel State Information
D-AMPS	Digital-Advanced Mobile Phone Systems
dB	Decibel
DF	Decode-and-Forward
DMF	Demodulate-and-Forward
DR	Directional-Relay
DwPTS	Downlink Pilot Timeslot
E-cell	Evolved-cell
E-DF	Enhanced-Decode-and-Forward
E-DR	Enhanced- Directional-Relay
eNB	Evolved-Node Base station
EVDO	Evolution Data Only system
EVDV	Evolution Data Voice
evolved-UTRA	evolved Universal Terrestrial Radio Access
FDD	Frequency-Division Duplexing

FDMA	Frequency-Division Multiple-Access
FM	Frequency modulation
FRF	Frequency Reuse Factor
Gbps	Giga bit per second
GP	Guard Period
GSM	Global Systems for Mobile communications
HSPA	High Speed Packet Access
HRPA	High Rate Packet Data
Hz	Hertz
ICI	Inter-Cell Interference
IR	In-band Relay
IRC	Interference Rejection Combining
IMT	International Mobile Telecommunication
IMT-2000	International Mobile Telecommunications-2000
ITU-R	International Telecommunications Union-Radiocommunication
LTE	Long-Term Evolution
LTE-A	Long-Term Evolution - Advanced
m/s	meter/second
Mbps	Mega bit per second
MGF	Moment-Generating Function
MIMO	Multiple-Input Multiple-Output
ML	Maximum Likelihood
MLSE	Maximum Likelihood Sequence Estimator
MPSK	*M*-ary Phase Shift Keying
MSs	Mobile Stations
OFDMA	Orthogonal Frequency Division Multiple-Access
OR	Omni-Relay
OSTBC	Orthogonal Space-Time Block Code
PDF	Probability Density Function
PLC	Power Line Communication
RC	Repetition Coding

RN	Relay Node
SC-FDMA	Single Carrier Frequency-Division Multiple-Access
SER	Symbol Error Rate
SINR	Signal-Interference plus Noise Ratio
SNR	Signal-to-Noise Ratio
ST	Space-Time
STC	Space-Time Coding
STTC	Space-Time Trellis Code
STBC	Space-Time Block Code
TDD	Time-Division Duplexing
TDMA	Time-Division Multiple-Access
TD-LTE	Time-Division Long-Term Evolution
UC	Unconstrained Coding
UFRF	Universal Frequency Reuse Factor
UMB	Ultra Mobile Broad Band
UpPTS	Uplink Pilot Timeslot
VoIP	Voice over Internet Protocol
WCDMA	Wideband CDMA
WiMAX	Worldwide Interoperability for Microwave Access
WRC2007	World Radiocommunication Conference 2007
WMAN	Wireless Metropolitan Area Network

List of Symbols

Symbol	Meaning
$..^*$	Conjugate operation
$..^H$	Conjugate transpose operation
$..^{-1}$	Inverse operation
$\|\|..\|\|^2$	Norm-squared operation
$\mathbb{C}$	Complex-valued number
γ_i	Signal-to-noise ratio for i^{th} received signal
γ_i^a	Approximate signal-to-noise ratio upper-bound for i^{th} received signal
γ_i^u	Signal-to-noise ratio upper-bound for i^{th} received signal
η	Power ratio between base station and relay node
$\mathbf{\Theta}$	Combined interference and noise covariance matrix
$\hat{\mathbf{\Theta}}$	Estimate combined interference and noise covariance matrix
$\mathbf{\Lambda}$	Decoder gain matrix
λ	Signal wavelength in m
λ_i	i^{th} diagonal elements of decoder gain matrix
Ξ	Total number of terminals in LTE-A network
σ^2_{eNB}	Variance of channel between base station and mobile station
$\sigma^2_{eNB_i}$	Variance of channel between base station i and mobile station
σ_χ	Shadow standard deviation measured in dB
σ^2_χ	Shadow variance measured in dB
$\sigma^2_{w_i}$	Additive-white Gaussian noise variance at terminal i
$\sigma^2_{RN_i}$	Variance of channel between relay node i and mobile station
σ^2_{RN}	Variance of channel between relay node and mobile station
$\tau_{\max}$	Maximum delay spread
υ	Path loss exponent
$\boldsymbol{\varphi}$	Channel diagonalize matrix
$\boldsymbol{\varphi}_D$	Desired channel diagonalize matrix

φ_{Di}	i^{th} element of desired channel diagonalize matrix
φ_i	i^{th} element of channel diagonalize matrix
Φ	Radio resource allocation factor
χ	Shadow loss
$\mathfrak{R}$	Data rate
a_{inner}	Inner region signal to interference plus noise variable
a_{outer}	Outer region signal to interference plus noise variable
B	System bandwidth allocated to downlink
B_{inner}	Bandwidth resources allocated to inner mobile stations
B_{outer}	Bandwidth resources allocated to outer mobile stations
c	Path loss constant
C	Channel capacity
C_i	Instantaneous channel capacity for system i
$\overline{C}_i$	Average channel capacity for system i
d	Distance
D	Per-user noise power spectral density level in watt.user/Hz
$Det\|..\|$	Determinant operation
$diag(..)$	Diagonal matrix
d_i	Distance from i^{th} terminal to mobile station
d_o	Distance to power measurement reference point
E[..]	Expected value operation
$erfc(..)$	Complementary error function
exp(..)	Exponential function
f_c	Coherence bandwidth
$f_{d,\max}$	Maximum *Doppler* spread
f_i	i^{th} frequency set
$f_I[i]$	Probability density function of random variable i
$f_{I,J}[i,j]$	Joint probability density function of random variables i and j
h_{eNB}	Channel coefficient for base station - mobile station link
h_{eNB_i}	Channel coefficient for i^{th} base station - mobile station link
h_i	Channel coefficient for i^{th} interfering terminal - mobile station link

$\mathbf{H}_D$	Channel matrix for desired signals
$\mathbf{H}_{ICI_1}$	Channel matrix for inter-cell interferers within E-cell
$\mathbf{H}_{ICI_2}$	Channel matrix for inter-cell interferers from other E-cell$s$
h_{RN}	Channel coefficient for relay node - mobile station link
h_{RN_i}	Channel coefficient for i^{th} relay node - mobile station link
$I+N$	The summation of the interference plus noise power
ICI_1	Inter-cell interference from relays within E-cell
ICI_2	Inter-cell interference from terminals in other E-cell$s$
$\mathbf{I}_i$	$i \times i$ identity matrix
I_i	Mutual information of relaying protocol i
$J(..)$	Jacobian matrix
$log(..)$	Logarithm of a number
M	Number of constellation points for phase shift keying modulation
P'_{eNB}	Adjusted transmitted power at base station
P_{eNB}	Transmission power at base station
$PL\ (..)$	Path loss function
$P_{r_{eNB}}$	Instantaneous received power from base station at inner region boundary
$\Pr[..]$	Probability of an event
P_r	Instantaneous received power
P_{RN}	Transmission power at relay node
$P_{r_{RN}}$	Instantaneous received power from relay node at outer region boundary
Q_i	Instantaneous spectral efficiency for system i
$\overline{Q}_i$	Average spectral efficiency for the system i
r	Relay cell radius
R	Cell radius
$R_{\hat{\mathbf{\Theta}}\hat{\mathbf{\Theta}}}$	Covariance matrix of $\hat{\mathbf{\Theta}}$
R_o	Inner region radius
$\mathbf{s}_D$	Desired transmitted signal vector
$\hat{\mathbf{s}}_D$	Desired decoded signal vector
s_i	i^{th} transmitted symbol
$\mathbf{s}_{ICI_1}$	Transmitted signal vector from inter-cell interferers within E-cell

$\mathbf{s}_{ICI_2}$	Transmitted signal vector from inter-cell interferers from other E-cell$s$
$SINR_i$	Instantaneous signal-to-interference plus noise ratio for system i
$\overline{SINR}_i$	Average signal-to-interference plus noise ratio for system i
$\tan(..)$	Tangent function
T_c	Coherence time
T_f	Frame length
T_s	Sample period
U	Average number of MSs users in a cell
U_{inner}	Average number of inner users
U_{outer}	Average number of outer users
v	Relative speed in m/s
$\mathbf{w}$	Additive white Gaussian noise vector
w_i	Additive white Gaussian noise at terminal i
$\mathbf{y}$	Received signal vector
$\hat{\mathbf{y}}$	Decision statistic vector
y_i	Received signal at mobile station from terminal i
$\mathbf{z}$	Combined interference signals plus noise
$\hat{\mathbf{z}}$	Combined interference signals plus noise multiplied by diagonalize matrix

Chapter One: Introduction

One of the main motivations for this work is the various challenges foreseen in the future trends of wireless communications. Recently, there has been a growing interest in high-speed transmission capabilities over wireless channels. Future systems are required to provide a voice and multimedia services. These new demands in cellular mobile radio have brought many issues for researchers in this field. The problems vary from the choice of suitable transmission technology to advanced signal processing techniques required at the receivers.

Among future wireless communication systems are the Long-Term Evolution (LTE) system and its advanced version, LTE-A. LTE-A was standardized to accommodate the growing demand of data traffic. The high requirements of LTE-A systems motivate researchers to invent new technologies or enhance existing technologies to meet such high requirements. A promising example is a cooperative communication system. A cooperative communication is a new paradigm that exploits the broadcast nature of the wireless channel to allow communicating nodes to assist each one another.

In this chapter, some historical footprints and future trends of LTE-A and cooperative communication systems are provided in Section 1.1. The significance and the subject area of this work are introduced in Section 1.2. Section 1.3 discusses the objectives and scope of this dissertation. The outline of the dissertation is detailed in Section 1.4. Finally, the contributions of this dissertation are summarized in Section 1.5.

1.1 Historical View Point

It has been over a century since the landmark invention of the wireless telegraph by Guglielmo Marconi in 1895. Wireless cellular communications has now become a popular means of public and personal communication with wide spread deployment

and ever growing expectations. In this context, it is worthwhile to look back briefly at some of the important footprints of wireless cellular communications.

The cellular wireless communications industry witnessed tremendous growth in the past decade with over four billion wireless subscribers worldwide. The first generation (1G) analog cellular systems were deployed around 1980, which supported voice communication with limited roaming. The 1G systems employed analog frequency modulation (FM) wireless access using narrowband frequency division multiple-access (FDMA) [1]. The second generation (2G) digital systems provided higher capacity and better voice quality than did their analog counterparts. Moreover, roaming became more prevalent because of fewer standards and common spectrum allocations across countries, particularly in Europe. The two widely deployed 2G cellular systems are global systems for mobile communications (GSM) and code division multiple-access (CDMA) [2]. Like the 1G analog systems, 2G systems were designed primarily to support voice communication. In later releases of these standards, capabilities were introduced to support data transmission. However, the data rates were generally lower than that supported by dial-up connections. The international telecommunication Union-Radiocommunication sector (ITU-R) initiative on international mobile telecommunications-2000 (IMT-2000) paved the way for the evolution to 3G. A set of requirements such as a peak data rate of 2Mbps and support for vehicular mobility were published under the IMT-2000 initiative. Both the GSM and CDMA camps formed their own separate 3G partnership projects (3GPP and 3GPP2, respectively) to develop IMT-2000 compliant standards based on the CDMA technology. The 3G standard in 3GPP is referred to as wideband CDMA (WCDMA) [3] because it uses a larger 5MHz bandwidth relative to 1.25MHz bandwidth used in 3GPP2's CDMA2000 [4] system. The 3GPP2 also developed a 5MHz version supporting three 1.25MHz subcarriers referred to as CDMA2000-3×.

The first release of the 3G standards did not fulfill its promise of high-speed data transmissions, as the data rates supported in practice were much lower than that claimed in the standards. A serious effort was then made to enhance the 3G

systems for efficient data support. The 3GPP2 first introduced the high rate packet data (HRPD) [5] system that used various advanced techniques optimized for data. The HRPD system required a separate 1.25MHz carrier and supported no voice service. This was the reason that HRPD was initially referred to as CDMA2000-1×EVDO (evolution data only) system. The 3GPP followed a similar path and introduced high speed packet access (HSPA) [6] enhancement to the WCDMA system. The HSPA standard reused many of the same data-optimized techniques as the HRPD system. A difference relative to HRPD, however, is that both voice and data can be carried on the same 5MHz carrier in HSPA. The voice and data traffic are code-multiplexed in the downlink. In parallel to HRPD, 3GPP2 also developed a joint voice data standard that was referred to as CDMA2000-1×EVDV (evolution data voice) [7]. Like HSPA, the CDMA2000-1×EVDV system supported both voice and data on the same carrier but it was never commercialized. In the later release of HRPD, Voice over Internet Protocol (VoIP) capability was introduced to provide both voice and data service on the same carrier. The two 3G standards, namely HSPA and HRPD, were finally able to fulfill the 3G promise and have been widely deployed in major cellular markets to provide wireless data access.

While HSPA and HRPD systems were being developed and deployed, IEEE802 standard committee introduced the IEEE802.16e standard [6,7] for mobile broadband wireless access. This standard was introduced as an enhancement to an earlier IEEE802.16 standard for fixed broadband wireless access. The IEEE802.16e standard employed a different access technology named orthogonal frequency division multiple-access (OFDMA) and claimed better data rates and spectral efficiency than that provided by HSPA and HRPD. Although the IEEE802.16 family of standards is officially called wireless metropolitan area network (WMAN) in IEEE, it has been called worldwide interoperability for microwave access (WiMAX) by an industry group named the WiMAX Forum. The mission of the WiMAX Forum is to promote and certify the compatibility and interoperability of broadband wireless access products. The WiMAX system supporting mobility as in the IEEE802.16e standard is referred to as Mobile WiMAX. In addition to the

radio technology advantage, Mobile WiMAX also employed a simpler network architecture based on IP protocols. The introduction of Mobile WiMAX led both 3GPP and 3GPP2 to develop their own version beyond 3G systems based on the OFDMA technology and network architecture similar to that in Mobile WiMAX. The beyond 3G system in 3GPP is called evolved universal terrestrial radio access (evolved-UTRA) [8] and is also widely referred to as Long-Term Evolution (LTE) while 3GPP2's version is called ultra mobile broadband (UMB) [9]. All three beyond 3G systems, namely Mobile WiMAX, LTE, and UMB, meet IMT-2000 requirements and hence they are also part of IMT-2000 family of standards.

The goal of LTE is to provide a high-data-rate, low-latency, and packet-optimized radio-access technology supporting flexible bandwidth deployments [10]. In parallel, new network architecture is designed with the goal to support packet-switched traffic with seamless mobility, quality of service and minimal latency [11]. The system supports flexible bandwidths because of the OFDMA access scheme in downlink and single carrier FDMA (SC-FDMA) access scheme in uplink. The radio-interface attributes for Mobile WiMAX and UMB are very similar to those of LTE. All three systems support flexible bandwidths and OFDMA in the downlink. There are a few differences such as – uplink in LTE is based on SC-FDMA compared to OFDMA in Mobile WiMAX and UMB. The performance of the three systems is therefore expected to be similar with small differences.

Similar to the IMT-2000 initiative, ITU-R Working Party 5D has stated requirements for IMT-advanced systems. Among others, these requirements include average downlink data rates of 100Mbps in the wide area network, and up to 1Gbps for local access or low mobility scenarios. Also, at the World Radiocommunication Conference 2007 (WRC2007), a maximum of a 428MHz new spectrum is identified for IMT systems that also include a 136MHz spectrum allocated on a global basis. Both 3GPP and IEEE802 are actively developing their own standards for submission to IMT-advanced standards. The goal for both LTE-A [12] and IEEE802.16m [13] standards is to further enhance system spectral efficiency and data rates while supporting backward compatibility with their

respective earlier releases. As part of the LTE-A and IEEE802.16m standards developments, several enhancements are being discussed to meet the IMT-advanced requirements.

One of the main challenges faced by the developing LTE-A standard is providing high throughput at the cell edge. Technologies like multiple-input multiple-output (MIMO), OFDMA, and advanced error control codes enhance per-link throughput but do not inherently mitigate the effects of interference. Cell edge performance is becoming more important as cellular systems employ higher bandwidths with the same amount of transmission power and use higher carrier frequencies with infrastructure designed for lower carrier frequencies [14]. One solution to improve coverage is combine LTE-A with cooperative communication systems such that, the use of fixed simple and small terminals, called *relays*, may forward messages between the base station (BS) and mobile stations (MSs) through multi-hop communication[15-23].

The basic idea of cooperative communications can be traced back to the 1970s to van der Meulen [24,25], in which a basic three-terminal communication model was first introduced and studied in the context of mutual information. Since it was first introduced, cooperative communications have been extensively studied mostly in communication–related aspects such as, information theory [26-30], the channel effect [32-34], relay selection mechanisms [35-42], differential modulation in cooperative systems [43-52], and so on, for applications such as wireless sensor, ad-hoc, and cellular networks.

Many different relay transmission techniques have been developed over the past ten years. The simplest strategy (already deployed in commercial systems) is the analog repeater, which uses a combination of directional antennas and a power amplifier to repeat the transmission signal [53]. More advanced strategies use signal processing of the received signal. Amplify-and-Forward (AF) relays apply linear transformation to the received signal [54-56] while Decode-and-Forward (DF) relays decode the signal, then re-encode for transmission [30]. In research, relays are often

assumed to be half-duplex (they can either send or receive but not at the same time) or full-duplex (can send and receive at the same time) [58]. While full-duplex relays are under investigation, practical systems are considering half-duplex relay operations, which incur a rate penalty since they require two (or more timeslots) to relay a message. Relaying has been combined with multiple antennas in the MIMO relay channel [60,61] and the multiuser MIMO relay [62]. Despite extensive work on relaying, prior work has not as extensively investigated the impact of interference as seen in cellular systems.

The first commercial wireless network to incorporate multi-hop communication was IEEE802.16j [62]. Its architecture constrained the relays to be served by a single base station and allowed them to communicate in only one direction at a time (i.e., either uplink or downlink). From a design perspective, unfortunately, IEEE802.16j had several restrictions that drastically limited its capability, for example, the transparent mode that supports relaying-ignorant mobile subscribers. Further, the relays were not designed to specifically mitigate interference. Consequently, LTE-A standards may consider more sophisticated relay strategies and thus may expect larger performance gains from the inclusion of relaying.

1.2 The Subject Area

Most future wireless systems, such as ultra mobile broadband (UMB), Long Term Evolution (LTE), and IEEE802.16e (WiMAX), promise very high data rates per user over high bandwidth channels. Cooperative communication is a new promising technology that affords some level of enhancement to the existing communication systems to achieve the requirements of such systems. The principle of cooperative systems is based on deploying a group of relay nodes within the cell to assist the serving base station. The relay can be thought of as an auxiliary node to the direct channel between the base station and the network subscribers. A key aspect of the cooperative communication is the processing of the signal received from the source node at the relay through *cooperative relaying protocols*. The trend is towards

developing cooperative protocols that provide true assistance to the transmitting base station by increasing the data rate and reducing any delay caused by employing cooperative communications.

Although a vast amount of research has been conducted on cooperative communications in the literature, the integration of cooperative relaying into LTE-A-aided cellular networks has received little or no attention. Such integration requires developing suitable transmitting algorithms, frame structure design, interference elimination or reduction techniques, power and frequency resource allocation, and many other communication-related topics.

1.3 Objectives and Scope of the Work

The overall objective of this research is to propose and investigate improved and efficient transmission techniques for LTE-A systems that can achieve high average signal-to-interference plus noise ratio ($SINR$) and high average capacity under various impairments such as fading, interference, and noise in the wireless channels. The following specific issues are addressed in this dissertation.

- **Cooperative Relaying Protocols**

  The objective is to enhance one of the relaying protocols, *the decode-and-forward*, to achieve a higher data rate with diversity. The scheme is referred to as *the enhanced-decode-and-forward*. Semi-analytical and simulation methods are used to evaluate the symbol error rate (SER) performance and other information-theoretic measures when utilizing this proposed enhanced-decode-and-forward.

- **Relay Integration in Cellular LTE-A Systems**

The objective is to improve the desired signal level and cancel the inter-cell interference in a cellular LTE-A systems using relay terminals at the cell edges. The use of relay terminals helps in solving the following specific issues:

1. **Cell-Edge Improvement**

   The objective is to develop a communication scheme for LTE-A systems that eliminate the inter-cell interference by isolating the co-channel base stations geographically. Moreover, there is a need to improve the desired signal level for cell-edge users by deploying distributed relay terminals. Analytical and simulation methods are conducted to compare the developed scheme and conventional schemes.

2. **Frequent Handover Caused by Relay Terminals**

   The objective is to develop a communication scheme for LTE-A systems that reduces frequent handovers caused by relay deployment in a cell. Also, the goal is to enhance further the *SINR* level for cell-edge users by increasing the diversity at cell-edge users.

3. **Interference Caused From Relay Terminals**

   The purpose is to develop a cooperative transmission scheme that exploits the total available bandwidth resources and cancels the mutual interference between deployed relay terminals.

1.4 Assumptions

Numerous assumptions are made in carrying out these studies. Some of the important assumptions and limitations, which are not addressed due to the scope of this research, are listed below.

- When analyzing the cooperative relaying protocol, the effect of non-ideal conditions such as timing and carrier offset errors are not considered in this study. These issues have received considerable attention by many researchers and will not be addressed in this dissertation.

- The channel is assumed to be estimated perfectly, and the receiver has full knowledge of the channel state information (CSI).

- The channel, during the analysis of all schemes, is modeled as uncorrelated frequency-flat but time-selective Rayleigh fading. The channel gains are assumed time-invariant within three signaling intervals but may vary after three signaling intervals.

- For all relay assisted schemes, the transmission power at the relays is assumed to be identical and equals a fraction of the host base station power.

- Only downlink analysis for average *SINR* and capacity are considered. The uplink performance has received much attention in many researches.

- The path loss model being used in the analysis is adopted from the path loss model in [92].

- The case where the MS is receiving interference from all co-channel cells in the first two tiers is considered as the worse-case.

- For analytical convenience, mobile users are distributed uniformly within a cell. This assumption was considered in [63] when deriving area spectral efficiency of cellular mobile radio systems.

1.5 Dissertation Outline

In the first chapter, a brief historical background on the evolution of cellular radio technology, cooperative communications, and LTE-A systems is provided and the

subject area is introduced. The objectives and contributions of the work are also discussed. The rest of this dissertation is organized as follows.

Chapter 2 provides the reader a review of a number of concepts that will be useful throughout this dissertation include – the characteristics of wireless channels, the diversity and MIMO concepts, relay communications, and the LTE and the LTE-A systems.

Chapter 3 provides a brief description of the system model for cooperative communications with the proposed cooperation relaying protocol. It provides a proposed modified decoding mechanism for the system when the channel is assumed to be a quasi-static flat fading channel. Analysis of symbol error rate (*SER*) performance is conducted, in which the exact, an upper bound, and an approximate upper bound expressions for the *SER* are derived. Furthermore, information-theoretic measures such as the mutual information, the rate, and the outage probability are derived. Finally, analytical and simulation results are obtained for the proposed cooperative scheme and other conventional schemes for validation and comparison.

Chapter 4 discusses a relay-assisted scheme with omni-directional antenna for the LTE-A system. The system model and the transmission algorithm with a proposed download frame structure are presented and discussed. Required performance measures such as average *SINR* and average capacity are also derived. Finally, analytical and simulation results for the average *SINR* and capacity are obtained for the proposed scheme and other conventional schemes for validation and comparison.

Chapter 5 discusses the system model of a relay-assisted scheme with directional antennas that provides less frequent handovers and increase the *SINR* at the cell-edge area.. A joint download transmission algorithm is also proposed and discussed for the relay-assisted scheme. In addition, performance measures such as average *SINR* and average capacity are derived. Finally, analytical and simulation results

for the average *SINR* and capacity are obtained for validation and comparison with other conventional schemes.

Chapter 6 discusses the system model of a relay-assisted scheme with omni-directional antennas and same frequency resources allocated to the base station. A joint download transmission algorithm with inter-cell interference cancellation technique is also proposed and discussed for the relay assisted scheme. Finally, analytical and simulation results for *BER* upper bound, the average *SINR*, and capacity are obtained for validation and comparison with other conventional schemes.

Finally, conclusions on the accomplished research objectives are summarized in Chapter 7 and some research topics for future work are suggested.

1.6 Contributions

The following contributions have been made in this dissertation.

- **Chapter 3**

In this chapter, we propose and investigate the performance of a new cooperative relaying protocol called *the Enhanced-Decode-and-Forward* (*E-DF*) *scheme*. Based on the system and the received signal model of the E-DF scheme, we propose a modified maximum likelihood (ML) decoder to recover the received symbols over a quasi-static fading channel. In addition, the analysis of the average signal-to-noise ratio (*SNR*) is conducted, in which the exact, an upper bound, and an approximate average *SNRs* are derived. Also, we perform the analysis of the symbol error rate (*SER*) via the moment generating function (*MGF*) and the approximate average *SNRs*. Expressions for a worse-case *SER* upper bound and an approximate worse-case *SER* are derived to simplify the calculations when obtaining the exact *SER* expression. We also conduct the analysis of other information-theoretic measures include – mutual information, the achieved rate, and the outage probability. Finally, semi-analytical and simulation results for – *SER*, outage probability, and

achieved rate are obtained and compared with other conventional schemes. The results show significant improvement for the E-DF scheme over the direct transmission and other conventional relaying protocols. Specifically, the results show that low *SER*, high transmission rate, and low outage probability are achieved when employing the E-DF scheme.

- **Chapter 4**

In this chapter, we propose a relay-assisted scheme with omni-directional antennas called *the omni-relay* (*OR*) *scheme*. Also, we propose a relay frame structure that is compatible with the long-term evolution (LTE) standard. In addition, the analysis of the average signal-to-interference plus noise ratio (*SINR*) and the average capacity are carried out for the OR scheme. Finally, semi-analytical and simulation results for the achieved average *SINR* and the achieved average capacity are obtained and compared with other conventional schemes. The results show that the desired signal level is improved for the cell-edge users, and the interference level is reduced when the OR scheme is utilized. Also, the average capacity of the OR scheme is improved significantly when compared to other conventional schemes.

- **Chapter 5**

In this chapter, we propose the use of relay terminals at the cell-edges, where each relay is equipped with directional antennas. This scheme is called *the directional-relay* (*DR*) *scheme*. We also propose a new cooperative download transmission scheme for the DR, called *Enhanced-DR* (*E-DR*) *scheme*, to overcome the issues of interference and low desired signal level at cell-edge users. In addition, the analysis of the average signal-to-interference plus noise ratio (*SINR*) and the average capacity are carried out for the DR and the E-DR schemes. Finally, semi-analytical and simulation results for the achieved average *SINR* and the achieved average capacity are obtained and compared with other conventional schemes. The results show that, when utilizing the download transmission scheme E-DR, the average *SINR* and the average capacity are improved remarkably for the cell-edge users when compared to the DR and the OR schemes.

- **Chapter 6**

In this chapter, we propose the use of relay terminal at the cell edges, each with omni-directional antennas and same frequency resources allocated to the base station. This scheme is called *the in-band relay* (*IR*) *scheme*. We also propose the concept of *the evolved-cell* (*E-cell*) for the IR scheme that can perform joint cooperative transmission of information between the involved terminals within the E-cell. The joint cooperative transmission is accomplished by using the E-DF relaying protocol (introduced in Chapter 3) to increase the diversity and the data rate. Due to high interference, we propose the use of the interference cancelling technique, *Interference Rejection Combining* (*IRC*), in each E-cell. In addition, we investigate the decoding of the received symbol sequences as well as the derivations of the *BER* upper bound, average *BER* upper bound, average *SINR*, and average capacity for this IRC-aided IR with E-DF scheme. Finally, we obtain semi-analytical and simulation results for the achieved average *SINR* and the achieved average capacity when utilizing the IRC-aided IR with E-DF scheme. The results show that, when utilizing the IRC-aided IR scheme, the average *SINR* and the average capacity are improved remarkably for the cell-edge users when compared to the IR that has no joint transmission scheme.

Chapter Two: Background

Wireless communications have seen a remarkably fast technological evolution. Although separated by only a few years, each new generation of wireless devices has brought significant improvements in terms of link communication speed, device size, battery life, applications, etc. In recent years, the technological evolution has reached a point where researchers have begun to develop wireless network architectures that depart from the traditional idea of communicating on an individual point-to-point basis with a central controlling base station. Such is the case with ad-hoc and wireless sensor networks, where the traditional hierarchy of a network has been relaxed to allow any node to help forward information from other nodes, thus establishing communication paths that involve multiple wireless hops. One of the most appealing ideas within these new research paths is the implicit recognition that, contrary to being a point-to-point link, the wireless channel is broadcast by nature. This implies that any wireless transmission from an end-user, rather than being considered as interference, can be received and processed at other nodes for a performance gain. This recognition facilitates the development of new concepts on distributed communications and networking via cooperation.

The technological progress seen with wireless communications follows that of many underlying technologies such as integrated circuits, energy storage, antennas, etc. Digital signal processing is one of these underlying technologies contributing to the progress of wireless communications. One of the most important contributions to the progress in recent years has been the advent of multiple-input multiple-output (MIMO) technologies. In a very general way, MIMO technologies improve the received signal quality and increase the data communication speed by using digital signal processing techniques to shape and combine the transmitted signals from multiple wireless paths created by the use of multiple receive and transmit antennas. Cooperative communications is a new proposal that draws from the ideas of using the broadcast nature of the wireless channel to make communicating nodes help each other, of implementing the communication process in a distribution

fashion and of gaining the same advantages as those found in MIMO systems. The end result is a set of new tools that improve communication capacity, speed, and performance; reduce battery consumption and extend network lifetime; increase the throughput and stability region for multiple access schemes; expand the transmission coverage area; and provide cooperation trade-off beyond source–channel coding for multimedia communications.

In this chapter, we begin with the study of basic communication systems and concepts that are highly related to user cooperation, by reviewing a number of concepts that will be useful throughout this dissertation. The chapter starts with a brief description of the relevant characteristics of wireless channels in Section 2.1. It then follows by discussing diversity concept followed by the MIMO wireless communications in Section 2.2. After this, we describe the concept of relay communications in Section 2.3. The chapter concludes by describing the LTE and the LTE-A system in Section 2.4.

2.1 The Wireless Channel Characteristics

Communication through a wireless channel is a challenging task because the medium introduces much impairment to the signal. Wireless transmitted signals are affected by effects such as noise, attenuation, and interference. It is then useful to briefly summarize the main impairments that affect the signals.

2.1.1 *Additive White Gaussian Noise*

Some impairments are additive in nature, meaning that they affect the transmitted signal by adding noise. Additive white Gaussian noise (AWGN) and interference of different nature and origin are good examples of additive impairments. The additive white Gaussian channel is perhaps the simplest of all channels to model. The relation between the output $y\big(t\big)$ and the input $s\big(t\big)$ signal is given by

$$y(t) = s(t) + w(t)$$

where $w(t)$ is noise. The additive noise $w(t)$ is a random process with each realization modeled as a random variable with a Gaussian distribution. This noise term is generally used to model background noise in the channel as well as noise introduced at the receiver front end.

2.1.2 *Large-Scale Propagation Effects*

2.1.2.1 Path Loss

Path loss is an important effect that contributes to signal impairment by reducing its power. Path loss is the attenuation suffered by a signal as it propagates from the transmitter to the receiver. Path loss is measured as the value in decibels (dB) of the ratio between the transmitted and received signal power. The value of the path loss is highly dependent on many factors related to the entire transmission setup. In general, the path loss is characterized by a function of the form

$$PL(d) = 10\upsilon \log\left(\frac{d}{d_o}\right) + c$$

where PL is path loss function measured in dB, d is the distance between transmitter and receiver, υ is the path exponent, c is a constant, and d_o is the distance to a power measurement reference point (sometimes embedded within the constant c). In many practical scenarios this expression is not an exact characterization of the path loss, but is still used as a sufficiently good and simple approximation. The path loss exponent υ characterizes the rate of decay of the signal power with the distance, taking values in the range of 2 to 6. The constant c includes parameter related to the physical setup of the transmission such as signal wavelength, antennas height, etc.

2.1.2.2 Shadowing

In practice, path losses of two receive antennas situated at the same distance from the transmit antenna are not the same. This is, in part, because the transmitted signal is obstructed by different objects as it travels to the receive antennas. Consequently, this type of impairment has been named *shadow loss* or *shadow fading*. Since the nature and location of the obstructions causing shadow loss cannot be known in advance, path loss introduced by this effect is a random variable. Denoting by χ the value of the shadow loss, this effect can be added to path loss equation by writing

$$PL\left(d\right) = 10\upsilon \log\left(\frac{d}{d_o}\right) + \chi + c$$

It has been found through experimental measurements that χ when measured in dB can be characterized as a zero-mean Gaussian distributed random variable with variance σ_χ^2 (also measured in dB). Because of this, the shadow loss value is a random value that follows a log-normal distribution and its effect is frequently referred as *log-normal fading*.

2.1.3 *Small-Scale Propagation Effects*

From the explanation of path loss and shadow fading it should be clear that the reason why they are classified as large-scale propagation effects is because their effects are noticeable over relatively long distances. There are other effects that are noticeable at distances in the order of the signal wavelength; thus being classified as small-scale propagation effects. We now review the main concepts associated with these propagation effects.

In wireless communications, a transmitted signal encounters random reflectors, scatterers, and attenuators during propagation, resulting in multiple copies of the signal arriving at the receiver after each has traveled through different paths. Such

a channel where a transmitted signal arrives at the receiver with multiple copies is known as a *multipath channel*. Several factors influence the behavior of a multipath channel. One is the already mentioned random presence of reflectors, scatterers, and attenuators. In addition, the speed of the mobile terminal, the speed of surrounding objects, and the transmission bandwidth of the signal are other factors determining the behavior of the channel. Furthermore, due to the presence of motion at the transmitter, receiver, or surrounding objects, the multipath channel changes over time. The multiple copies of the transmitted signal, each having different amplitude, phase, and delay, are added at the receiver creating either constructive or destructive interference with each other. This results in received signal whose shape changes over time.

2.1.3.1 Slow and Fast Fading

The distinction between *slow* and *fast fading* is important for the mathematical modeling of fading channels and for the performance evaluation of communication systems operating over these channels. The *coherence time* T_c of the channel is the key factor to distinct between slow and fast fading. The coherence time measures the period of time over which the fading process is correlated. In other words, coherence time is the period after which the correlation function of two samples of the channel response taken at the same frequency but different time instants drops below a certain predetermined threshold. The coherence time is also related to the channel maximum *Doppler spread* $f_{d,\max}$ by [64]

$$T_c \approx \frac{9}{16\pi f_{d,\max}}$$

where Doppler spread is caused by the relative movements of the transmitter, receiver, and/or the objects in between, which cause the carrier frequency of the received signal gets altered. The maximum Doppler spread (in units of Hz) is given as [65],

$$f_{d,\max} = \frac{v}{\lambda}$$

where v and λ denote the relative speed (m/s) of the receiver with respect to the transmitter and the wavelength (m) of the carrier signal, respectively. The fading is said to be slow if the symbol time duration T_s is smaller than the channel's coherence time T_c; otherwise it is considered to be fast. In slow fading a particular fade level will affect many successive symbols, which leads to burst errors, whereas in fast fading the fading de-correlates from symbol to symbol.

2.1.3.2 Frequency-Flat and Frequency-Selective Fading

Frequency selectivity is also an important characteristic of fading channels. If all the spectral components of the transmitted signal are affected in a similar manner, the fading is said to be *frequency-non selective* or equivalently *frequency-flat*. This is the case for *narrowband* systems, in which the transmitted signal bandwidth is much smaller than the *coherence bandwidth* f_c of the channel. Coherence bandwidth measures the frequency range over which the fading process is correlated and is defined as the frequency bandwidth over which the correlation function of two samples of the channel response taken at the same time but different frequencies falls below a suitable value. In addition the coherence bandwidth is related to the *maximum delay spread* $\tau_{\max}$ by

$$f_c \approx \frac{1}{\tau_{\max}}$$

where the *delay spread*, by definition, quantifies the average length of overlapping received multipath pulses over which most of energy is concentrated [66]. On the other hand, if the spectral components of the transmitted signal are affected by different amplitude gains and phase shifts, the fading is said to be *frequency-selective*. This applies to *wideband* systems in which the transmitted bandwidth is bigger than the channel's coherence bandwidth.

2.2 Diversity in Wireless Channels

As we have explained, wireless fading channels present the challenge of being changing over time. In communication systems designed around a signal path between transmitter and receiver, a crippling fade on this path is a likely event that needs to be addressed with such techniques as increasing the error correcting capability of the channel coding block, reducing the transmission rate, using more elaborate detectors, etc.

Nevertheless, these solutions may still fall short for many practical channel realizations. Viewing the problem of communication through a fading channel with a different perspective, the overall reliability of the link can be significantly improved by providing more than one signal path between transmitter and receiver, each exhibiting a fading process as much independent from the others as possible. In this way, the chance that there is at least one sufficiently strong path is improved. Those techniques that aim at providing multiple, ideally independent, signal paths are collectively known as *diversity techniques*. The concept of *diversity* means receiving redundantly the same information-bearing signal over two or more fading channels, then combining these multiple replicas at the receiver in order to increase the overall received signal-to-noise ratio. The intuition behind this concept is to exploit the low probability of concurrence of deep fades in all the diversity channels to lower the probability of error and of outage. These multiple replicas can be obtained by extracting the signals via different radio paths…

- in time by using multiple time slots separated by at least the coherence time of the channel,
- in frequency by using multiple-frequency channels separated by at least the coherence bandwidth of the channel, and/or
- in space by using multiple-receiver antennas.

In its simplest form, the multiple paths may carry multiple distorted copies of the original message. Nevertheless, better performance may be achieved by applying some kind of coding across the signals sent over the multiple paths and by combining in a constructive way the signals received through the multiple paths. Also important is the processing performed at the receiver, where the signals arriving through the multiple paths are constructively combined. The goal of combining is to process the multiple received signals so as to obtain a resulting signal of better quality or with better probability of successful reception than each of the received ones.

For any diversity technique, the performance improvement is manifested by the communication error probability decreasing at a much larger rate at a high channel signal-to-noise ratio than systems with less or no diversity. When using log–log scales, this rate of decrease in the communication error probability becomes the slope of the line representing the communication error probability at high signal-to-noise ratio and is known as the *diversity gain*. This definition establishes an implicit behavior at high signal-to-noise ratio for the probability of symbol error as being a linear function of the signal-to-noise ratio when seen in a plot with log–log scales. Then it can be seen that, as previously stated, in these conditions the diversity gain is the slope of the linear relation. It is better to have as large a diversity gain as possible, since it means that the probability of symbol error is reduced at a faster rate. Also, it is important to note that, depending on the particular diversity scheme and the system setup, other measures of probability of error can be used. For example, the outage probability is used in some cases, instead of the probability of symbol error.

2.2.1 *Temporal Diversity*

It is quite common to find communication scenarios where the channel coherence time equals or exceeds several symbol transmission periods. This implies that two symbols transmitted with a separation in time longer than the coherence time will

experience channel realizations that are highly uncorrelated and can be used to obtain diversity. The simplest way to achieve this is to form the two symbols by using a repetition coding scheme.

Also, in temporal diversity, transmitted bits may be interleaved into time-separated packets at a transmitter, spreading and thereby reducing the effect of burst noise or multipath fading in particular packets. The interleaved bits are then deinterleaved at the receiver to recreate their original order.

2.2.2 *Frequency Diversity*

Analogous to time diversity, in wideband systems where the available bandwidth exceeds the channel coherence bandwidth, it is possible to realize diversity by using channels that are a partition of the available bandwidth and that are separated by more than the channel coherence bandwidth.

Realizing frequency diversity as a partition of the whole system bandwidth into channels with smaller bandwidth and independent frequency response is perhaps the most intuitively natural approach. This approach is applicable in multicarrier systems, where transmission is implemented by dividing the wideband channel into non-overlapping narrowband sub-channels. The symbol used for transmission in each sub-channel has a transmission period long enough for the sub-channel to appear as a flat fading channel. Different sub-channels are used together to achieve frequency diversity by ensuring that each is separated in the frequency domain from the rest of the sub-channels in the transmission by more than the coherence bandwidth. In this way, the fading processes among the sub-channels show small cross-correlation. Examples of these systems are those using orthogonal frequency-division multiplexing (OFDM).

Frequency diversity can also be achieved through processing based on a time-domain phenomenon. Recall that the frequency response of multipath channels is not of constant amplitude and linear phase because each spectral component of the

signal undergoes destructive or constructive interference of different magnitude depending on the delay of each path and the frequency of the spectral component. These multipath channels provide diversity through each of the copies of the signal arriving through each path and, consequently, the overall channel appears as frequency selective. It is then possible to achieve diversity of an order equal to the number of independent paths.

2.2.3 *Spatial Diversity and MIMO Systems*

By using multiple transmit antennas and multiple receive antennas, we may exploit diversity in the spatial domain which is called *spatial diversity*. Systems utilizes spatial diversity are often referred as *multiple-input multiple-output* (*MIMO*) *systems*. Spatial diversity or MIMO improves the performance of communication systems. Signal will not suffer the same level of attenuation as it propagates along different paths. Spatial diversity can be efficiently exploited when the antenna array configuration at receive and transmit sides is properly performed to the propagation environment characteristic. This could be achieved if multiple branches which are combined are ideally uncorrelated in order to reduce probability for deep fades in fading channels.

One of the major benefits of spatial diversity systems is the reliable communication through the use of multiple receive and transmit antennas. The system reliability is represented by the diversity gain. As mentioned earlier, the signal level at a receiver in a wireless system fluctuates or fades. Spatial diversity gain mitigates fading and is realized by providing the receiver with multiple (ideally independent) copies of the transmitted signal in space. With an increasing number of independent copies (the number of copies is often referred to as the diversity order), the probability that at least one of the copies is not experiencing a deep fade increases, thereby improving the quality and reliability of reception.

Moreover, spatial diversity systems offer a linear increase in data rate through spatial multiplexing [67-70], i.e., transmitting multiple, independent data streams within the bandwidth of operation. Under suitable channel conditions, such as rich scattering in the environment, the receiver can separate the data streams. Furthermore, each data stream experiences at least the same channel quality that would be experienced by a direct transmission system, effectively enhancing the capacity by a multiplicative factor equal to the number of streams. In general, the number of data streams that can be reliably supported by a MIMO channel equals the minimum of the number of transmit antennas and the number of receive antennas [71]. The spatial multiplexing gain leads to an increase in the system spectral efficiency without any need for additional bandwidth or for additional power allocation.

MIMO system can achieve both spatial diversity and temporal diversity by exploiting space-time (ST) coding technique. ST coding is a class of a linear processing of the transmitted signals at each transmitting antenna of MIMO system. ST codes are designed in order to achieve both maximum coding gain and diversity gain. ST codes may be split into two main types which are listed in the following.

- *Space-Time Trellis Code* (STTC) was invented by Vahid Tarokh in 1998. This coding scheme transmits multiple redundant copies of trellis code which are distributed in time and space [72].

- *Space-Time Block Code* (STBC) aims to provide a diversity gain by transmitting block codes distributed over the transmit antennas. Development of STBC is based on complex orthogonal design. The most well-known orthogonal STBC (OSTBC) design is the Alamouti scheme which was invented in 1998 for a MIMO system for two transmit and two receive antennas [73]. At the receiver, the transmitted signal is easily recovered as a result of the orthogonality of ST code. OSTBCs have received

much attention from the coding community as compared to STTCs owing to their simple design and low complexity receivers [74].

2.3 Cooperation Diversity

The continually increasing number of users and the rise of resource-demanding services require a higher link data rate than the one that can be achieved in current wireless networks [30]. Wireless cellular networks, in particular, have to be designed and deployed with unavoidable constraints on the limited radio resources such as bandwidth and transmit power [75]. As the number of new users increases, finding a solution to meet the rising demand for high data rate services with the available resources has became a challenging research problem. The primary objective of such research is to find solutions that can improve the capacity and utilization of the radio resources available to the service providers [76]. While in traditional infrastructure networks the upper limit of the transmitter – receiver link's data capacity is determined by the Shannon capacity [70], advances in radio transceiver techniques such as MIMO architectures and cooperative or relay-assisted communications have led to an enhancement in the capacity of contemporary systems.

In the MIMO technique diversity relies on uncorrelated channels, and is achieved by employing multiple antennas at the receiver side, the transmitter side, or both,

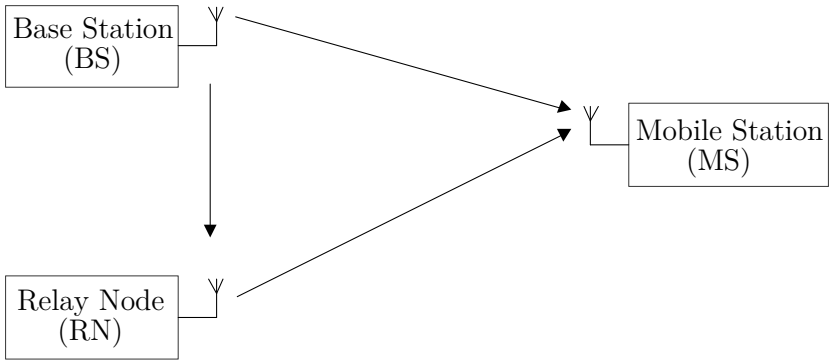

Figure 2.1: Illustration of cooperative diversity.

and by sufficiently separating the multiple antennas [77]. The MIMO technique can be used to increase the robustness of a link as well as the link's throughput. Unfortunately, the implementation of multiple antennas in most modern mobile devices may be challenging due to their small sizes [76].

Cooperative diversity or relay-assisted communication has been proposed as an alternative solution where several distributed terminals cooperate to transmit/receive their intended signals. In this scheme, Figure 2.2, the base station (BS) wishes to transmit a message to the mobile station (MS), but obstacles degrade the BS-MS link quality. The message is also received by the relay terminals, which can retransmit it to the MS, if needed. The mobile station may combine the transmissions received by the base station and relays in order to decode the message.

The limited power and bandwidth resources of the cellular networks and the multipath fading nature of the wireless channels have also made the idea of cooperation particularly attractive for wireless cellular networks [30]. Moreover, the desired ubiquitous coverage demands that the service reaches the users in the most unfavorable channel conditions (e.g., cell-edge users) by efficient distribution of the high data rate across the network [78]. In conventional cellular architectures (without relay assistance) increasing capacity along with coverage extension dictates dense deployment of base stations which turns out to be a cost-wise inefficient solution for service providers [15]. A relay node (RN), which has less cost and functionality than the base station, is able to extend the high data rate coverage to remote areas in the cell under power and spectral constraints [79–82].

By allowing different nodes to cooperate and relay each other's messages to mobile stations, cooperative communication also improves the transmission quality [83]. This architecture exhibits some properties of MIMO systems; in fact a virtual antenna array is formed by distributed wireless nodes each with one antenna. Since channel impairments are assumed to be statistically independent, in contrast to conventional MIMO systems, the relay-assisted transmission is able to combat

these impairments caused by shadowing and path loss in BS-MS and RN–MS links. To this end, an innovative system has been proposed in which the communication between transmitter and receiver is done in multiple hops through a group of relay nodes. This cooperative MIMO relaying scheme creates a virtual antenna array by using the antennas of a group of relay nodes [84]. These relay nodes transmit the signal received from the base station cooperatively on a different channel to the mobile station.

2.3.1 *Cooperative Relaying Protocols*

The performance of relay transmissions is greatly affected by the rules or conventions, called *cooperative relaying protocols*, which control the exchange of information between terminals on the network [30]. Many cooperative relaying protocols have been proposed to establish a two-hop communication between a base station and a mobile station through a relay [85-88].

2.3.1.1 Amplify-and-Forward (AF)

In this relay-assisted protocol, the relay amplifies the received signal from the base station and retransmits it to the mobile station without doing any decoding. For this reason, it is also called non-regenerative relaying. The main drawback of this strategy is that the relay terminal amplifies the received noise at the same time. Applying this strategy to cooperative communication leads to a lower bit error rate (*BER*) than direct transmission [54-56]. The outage probability of the cooperative communication derived in [89], demonstrates that a diversity order of 2 is obtained for two cooperative users.

2.3.1.2 Decode-and-Forward (DF)

In this relaying protocol, relay terminal has to decode the message received from the base station. Therefore, the total performance depends on the success of this message decoding [89]. Depending on the type of symbols retransmitted, the strategy at the relay is repetition coding (RC) or unconstrained coding (UC). In RC, the relay retransmits the same symbols previously estimated, while in UC the symbols transmitted are not the same as the received ones, but are related to the same information sent by the source. Hence, this protocol is also called regenerative relaying. The DF can effectively avoid error propagation through the relay, but the processing delay is quite long.

2.4 Long-Term Evolution (LTE) Systems

The third generation partnership project (3GPP) long-term evolution (LTE) is one of the most promising standards for the next generation wireless communications systems. LTE is a candidate for the International Mobile Telecommunication (IMT) of International Telecommunications Union-R (ITU-R). It is being designed to utilize techniques such as MIMO and relay technologies in the air interface to provide high-speed data transmission and high channel-capacity transmission [90,91].

2.4.1 *From LTE to LTE-A: System Specifications and Requirements*

The 3GPP LTE standard was developed between 2004 and 2009 with the goal of providing a high-data rate, low-latency, and packet-optimized radio-access technology supporting flexible bandwidth deployments. The air-interface-related attributes of the LTE system are summarized as follows. The system supports flexible bandwidths using OFDMA and single-carrier FDMA (SC-FDMA) schemes. In addition to frequency-division duplexing (FDD) and time-division duplexing

(TDD), half-duplex FDD is allowed to support low-cost mobile stations. The system is primarily optimized for low speeds, up to 15km/h. However, the system specifications allow mobility support in excess of 350km/h with some performance degradation. The uplink access is based on SC-FDMA, which provides increased uplink coverage due to low peak-to-average power ratio (PAPR) relative to OFDMA [92]. The system supports a downlink peak data rate of 326Mbps with 4×4 MIMO within 20MHz bandwidth. Since uplink MIMO is not employed in the first release of the LTE standard, the uplink peak data rate is limited to 86Mbps within 20MHz bandwidth. In terms of latency, LTE radio-interface and network are capable of delivering a packet from the base station to the mobile station in less than 10ms. The LTE standard was finalized in 2009 and some initial commercial LTE deployments are already underway in the USA, Japan, and Europe to accommodate the growing data traffic demands.

The mobile data traffic continues to grow and is expected to grow at a compound annual growth rate (CAGR) of 131% [93] over the next years, increasing more than 65 fold in 5 years. In order to meet this spectacular growth in data traffic, continuous improvements in air-interface efficiency as well as allocation of new spectrum has lead the stage for the future evolution of radio technologies towards IMT-Advanced. IMT-Advanced is an ITU-R initiative for developing the fourth generation global mobile broadband wireless standard. A major effort was started by the 3GPP and IEEE802.16 standards to develop the IMT-Advanced compliant fourth generation mobile broadband standards. This effort made IMT-Advanced to standardize LTE-A as a candidate technology for the 4G mobile broadband with the following requirements for peak data rate, average cell spectrum efficiency and cell-edge users' spectrum efficiency.

- **Peak Data Rate:** As for the peak data rate, the system should target a downlink peak data rate of 1Gbps and an uplink peak data rate of 500Mbps.

- **Average Spectral Efficiency:** According to LTE-A, average spectral efficiency for mobile broadband standard is defined as *the aggregate throughput of all users, or the number of correctly received bits over a certain period of time, normalized by the overall cell bandwidth divided by the number of cells*. In the LTE-A standard, the system should target average downlink spectral efficiency of 2.6bps/Hz and average uplink spectral efficiency of 2bps/Hz.

- **Cell-Edge User Throughput:** The cell-edge user throughput is defined as *the* 5% *point of the cumulative density function* (*CDF*) *of the user throughput normalized with the overall cell bandwidth*. LTE-A should allow cell-edge user throughput to be 0.09bps/Hz for downlink and 0.07bps/Hz for uplink.

2.4.2 *Relay Technologies in LTE-A Cellular Systems*

When introducing LTE-A systems, 3GPP considered relay technologies in the standardization process [91]. The relay transmission can be achieved by forwarding information from a local evolved-base station (eNB) to a neighboring mobile station using a relay node. In doing this, an RN can effectively extend the signal and service coverage of an eNB and enhance the overall throughput performance of a wireless communication system [85,91]. Figure 2.3 shows an example of deploying a relay node in a cellular LTE-A system. The figure shows that the relay nodes can be placed at the cell-edge to increase the transmission range of the cell.

2.4.3 *Relays classifications*

A variety of different classifications have been used to categorize relay nodes in the LTE-A standard. In one category, relays may be distinguished based on the functionality [86] as …

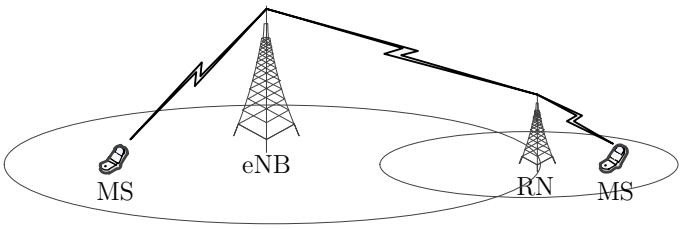

Figure 2.2: Relaying in LTE-A systems.

- **a repeater**: This type of relays is the simplest in terms of implementation and functionality. The relay simply receives the signals from the base station, amplifies it and then forwards it to the mobile station.

- **a decoder/encoder**: This relay is able to decode the received signals and re-code the transmit signals in order to achieve higher RN-MS link quality. The advantage of achieving higher link quality comes at the expense of higher cost and complexity of the relay and also adds delay to the communication link.

- **a base station**: This type of relay has the functionality of a base station like mobility management, session set-up, and handover. Such functionality adds more complexity to the implementation of this relay and the delay budget is further increased.

A different classification is used in 3GPP standardization where two types of relays have been defined in 3GPP LTE-A standard, Type I and Type II in [91], or non-transparency and transparency in [85].

- **Type I (or non-transparent)**: This relay type can help a remote mobile station unit, which is located far away from a base station, to access the base station. So a Type I relay needs to transmit the common reference signal and the control information for the base station, and its main objective is to extend signal and service coverage, as shown in Figure 2.4 (a). Type I relays can mainly make some contributions to the overall system

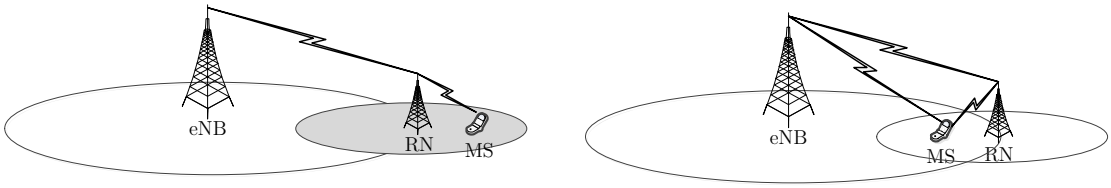

(a) Type I (non-transparent) (b) Type II (transparent)

Figure 2.3: Relay types.

capacity by enabling communication services and data transmissions for remote mobile station units.

- **Type II (or transparent)**: the relays can help a local mobile station unit, which is located within or outside the coverage of a base station and has a direct communication link with the base station, to improve its service quality and link capacity, as shown in Figure 2.4 (b). So a Type II relay does not transmit the common reference signal or the control information, and its main objective is to increase the overall system capacity by achieving diversity and transmission gains for local mobile station units.

2.4.4 *Relay Terminals in Cellular Systems*

Relay technology is considered in cellular networks to assist base stations for coverage extension and throughput enhancement. The information theoretical properties of the relay channel have already been studied in the 1970s by Cover [33]. However the integration of relays into a cellular system has only gained attention around the year 2000 for example in [94] when the concepts of Single-hop Cellular Network (SCN) and Multihop Cellular Network (MCN) were introduced. In SCN, base and mobile stations in the same cell are always mutually reachable in a single hop. When having data to send, mobile stations always send them to the base within the same cell. If the destination and the source are in the same cell, the base directly forwards packets to the destination. On the other hand, the

architecture of MCN resembles that of SCN except that bases and mobile stations are not always mutually reachable in a single hop. Similar to ad-hoc network, a key feature of MCN is that mobile stations can directly communicate with each other if they are mutually reachable. This feature leads to multihop routing.

The research in [94] motivated to study the effect of relay deployment in cellular network. In [95], for example, it was shown that deployments based on in-band relays can increase the high bit rate coverage at the cell border; thereby provide the means to balance the capacity within the cell and increase the coverage area of a single BS. Not surprisingly relays as part of infrastructure based networks have been standardised in the Technical Specification Group j (TSG j) of IEEE802.16j [96] and a study item on relaying has been formed in 3GPP.

Moreover, the authors in [97] showed through simulation-based results, that relays provide range extension and spectral efficiency enhancement when deployed in different location in the cell. Multiple relay deployment in cellular networks is also discussed in [98]. Simulation results showed that deploying multiple relays per cell can significantly improve system capacity and coverage.

The effect of using multiple antennas at relay terminals is also addressed in [99] where the effect of using N antennas at the relay terminal is studied in terms of data rate enhancement. The results showed that employing several antennas at each relay terminal and proper space-time coding improve downlink data rate, however it required to have more complex receiver structure at the mobile station in order to achieve such high rate and decode correctly.

The performance of relay deployment on the uplink was also addressed in several researches like in, for example, [100]-[102]. Most research concerning uplink analysis considered different relay types and relaying protocol.

Although several research dealt with relay terminals deployment in cellular systems, most of the obtained results were based on system-level simulation and not analytical or semi-analytical results. Also, the frequency and power resources

allocation for each relay terminal are not discussed when providing system models. Furthermore, the coordination between terminals (base stations, relays, and mobile stations) is not considered for such system. Finally, most researches do not consider analytical performance for the interference stem from relay deployment.

Chapter Three: An Enhanced Decode-and-Forward (E-DF) scheme over quasi-static flat fading channel

3.1 Introduction

Most future wireless systems promise very high data rates per user over high bandwidth channels such as ultra mobile broadband (UMB), Long Term Evolution (LTE), and IEEE802.16e (WiMAX). Cooperative communication is a new technology that can achieve the requirements of such systems and provide some level of enhancement to future communication systems. The principle of cooperative communications is based on the deployment of a group of relay nodes within a cell-site to assist the base station. The relay can be thought of as an auxiliary node to the direct channel between the base station and the network subscribers. A key aspect of the cooperative communication is the processing of the signal received from the base station at the relay. In the literature, two key types of cooperative protocols exist. These are [30]– *amplify-and-forward* (AF) and *decode-and-forward* (DF) relaying protocols. In the AF protocol, the relay receives the data from the base station, amplifies it, and then retransmits it to the mobile station. In the DF protocol, the relay decodes the received signal, re-encodes, and then retransmits it to the subscriber. In Chapter 3, the main focus is on the enhancement of the conventional DF relaying protocol performance.

3.1.1 *The Conventional DF Relaying Protocol*

In the conventional DF scheme, time-division multiple-access (TDMA) is employed, and symbol transmission from the base station to the mobile station can be accomplished by three different schemes [89], each in two phases.

(a) Phase 1 (b) Phase 2

Figure 3.1: Conventional *DF* Scheme I.

In the first scheme, the base station (or eNB according to LTE-A standard[103]) communicates with the relay node (RN) and mobile station (MS) during the first phase as shown in Figure 3.1 (a). In the second phase, both the relay and eNB terminals communicate with the mobile station terminal as illustrated in Figure 3.1 (b). Scheme I provides a transmission of two symbols over two phases and diversity only for symbol s_1.

In the second scheme, the base station communicates with the relay and the mobile station terminals over the first phase as illustrated in Figure 3.2 (a). In the second phase, only the relay terminal communicates with the mobile station as illustrated in Figure 3.2 (b). Scheme II provides a transmission of one symbol over two phases and diversity only for the symbol s_1.

In the third scheme, the base station communicates with the relay only over the first phase as shown in Figure 3.3 (a). In the second phase, the relay and the base

(a) Phase 1 (b) Phase 2

Figure 3.2: Conventional DF Scheme II.

(a) Phase 1 (b) Phase 2

Figure 3.3: Conventional DF Scheme III.

station terminals communicate with the mobile station as shown in Figure 3.3 (b). Cooperative scheme III provides a transmission of two symbols over two phases and no diversity for any transmitted symbols.

3.1.2 *Space-Time-Coded DF scheme*

In order to increase diversity, space-time coding (STC) is used [73]. To use STC coding in the conventional DF relaying protocols, for example Scheme I, and a 2×1 Alamouti ST coding [73], the base station first broadcasts the first data symbol s_1 to the relay and to the MS in phase 1 as shown in Figure 3.4 (a). In the second phase, the base station transmits the second symbol, s_2, to the MS. The relay decodes s_1 and forwards it to the MS as shown in Figure 3.4 (b). In the third phase, the base station broadcasts the second symbol to the relay and the MS as shown in Figure 3.4 (c). In the fourth phase, the base station changes the constellation of the first symbol, s_1, into $-s_1^*$ and transmits to the MS. At the same time, the relay changes the constellation of the decoded s_2 into s_2^* and relays it to the MS as shown in Figure 3.4 (d). The transmission over the four phases is equivalent to a 2×1 Alamoti ST coding [73] as (the second and the fourth rows)

$$\begin{matrix} \\ \rightarrow \\ \\ \rightarrow \end{matrix}\begin{bmatrix} s_1 & 0 \\ s_2 & s_1 \\ s_2 & 0 \\ -s_1^* & s_2^* \end{bmatrix}\begin{bmatrix} h_{eNB} \\ h_{RN} \end{bmatrix} \equiv \begin{bmatrix} s_2 & s_1 \\ -s_1^* & s_2^* \end{bmatrix}\begin{bmatrix} h_{eNB} \\ h_{RN} \end{bmatrix}$$

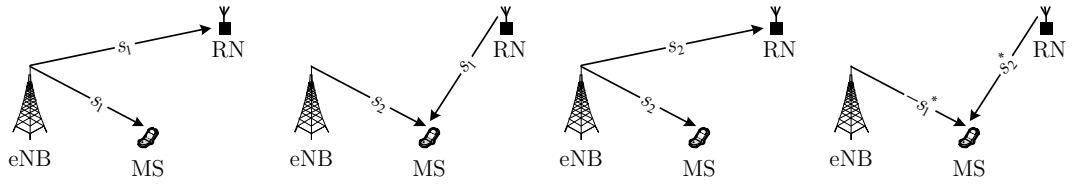

(a) Phase 1 (b) Phase 2 (c) Phase 3 (d) Phase 4

Figure 3.4: The ST-coded conventional DF Scheme I.

where h_{eNB} and h_{RN} are the channel coefficients from eNB to MS and from RN to MS, respectively. Similar steps can be considered for ST-coded Scheme III; however, ST-coding is not applicable to Scheme II since it receives only one symbol every phase from either the base station or the relay.

If direct transmission of one symbol requires one signaling interval, four signaling intervals are required to transmit two symbols from the base station to the mobile station using a ST-coded conventional DF relay scheme. Therefore, the data rate is half of the data rate of the direct or non-cooperative transmission. In communication systems where high data rate is required, this issue is considered a major drawback.

For the conventional DF protocol, many previous proposals attempt to design relay cooperative protocols to obtain full spatial diversity with high data rate [29-40]. However, this comes with new cost of hardware implementation such as employing multiple antennas at the base station, the mobile station, and/or the relay.

In Chapter 3, we propose a modified relaying protocol that enhances the conventional DF protocol to achieve a higher data rate transmission with diversity. *This new scheme is referred to as the enhanced-decode-and-forward* (*E-DF*). Based on the E-DF's received signal model, we proposed a modified ML decoder. Moreover, we conduct the analysis of the symbol error rate (*SER*) and compare it with the performances of the conventional DF protocol and the direct transmission to measure the improvement achieved by E-DF.

Chapter 3 is organized as follows. In Section 3.2, we present a brief description of the system model for the proposed E-DF cooperation protocol as well as modified maximum likelihood (ML) decoder when the channel is assumed to be quasi-static flat fading channel. In Section 3.3, we analyze the symbol error rate performance for the E-DF scheme with an exact, upper bound, and tight approximation for systems with MPSK modulation. In addition, we derive some information-theoretic measures such as – the mutual information, the rate, and the outage probability for the proposed E-DF, direct transmission, and the conventional DF schemes. Finally, performance comparisons are made between the direct transmission, the conventional DF, and the E-DF schemes.

3.2 An Enhanced-Decode-and-Forward (E-DF) Scheme

We propose the enhanced-decode-and-forward (E-DF) scheme to overcome the issues of low data rate found in the conventional DF schemes. The scheme uses two relay nodes for more reliable transmission between the transmitter and the receiver. Multiple-relay communication is part of the LTE-A standard [104] to enhance the coverage and capacity. In the following, we describe the system model for the E-DF scheme together with the proposed ML decoder.

3.2.1 *System Model*

We present a cooperative communication scheme with three transmission phases for wireless networks such as mobile ad hoc, wireless sensor, or cellular networks. In all phases, terminals transmit signals through orthogonal channels by using TDMA. The proposed scheme targets *downlink transmissions* where the data source terminal, eNB, transmits information to the data source terminal, MS, with the assistance of two relay terminals labeled as RN_1 and RN_2, as shown in Figure 3.5.

At the eNB, the information bit sequence is first mapped from a complex signal constellation into a complex symbol sequence. The complex symbol sequence is

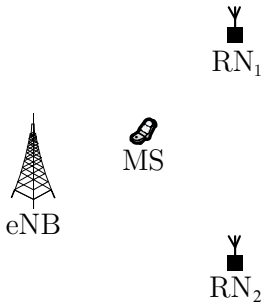

Figure 3.5: System model for the proposed E-DF scheme.

then parsed into code vectors $\mathbf{s} \triangleq \begin{bmatrix} s_1 & s_2 \end{bmatrix}^T$. It is assumed that the channel coherence time is comparable to the symbol duration due to relative motion between transmitter and receiver. The channel between any two terminals is modeled as uncorrelated frequency-flat but time-selective Rayleigh fading. The channel gains are assumed time-invariant within three signaling intervals but may vary between every three signaling intervals. The transmission power at the base station is denoted by P_{eNB}. The transmission power at the relays, RN_1 and RN_2, are assumed to be identical and denoted by P_{RN}. Each relay power is assumed to be a fraction of the base station power according to the following relation

$$P_{RN} = \eta P_{eNB} \tag{3.1}$$

where $0 < \eta < 1$. In the E-DF, the downlink transmission to the MS is accomplished in three phases as illustrated in Figure 3.6.

In phase 1, the eNB broadcasts the first symbol s_1 from the code vector to all terminals, i.e. MS, RN_1 and RN_2 as shown in Figure 3.6 (a). The relay terminals, RN_1 and RN_2, receive and decode s_1. The received signal at the MS is written as

$$y_1 = \sqrt{P_{eNB}}\, h_{eNB} s_1 + w_1 \tag{3.2}$$

where h_{eNB} is the channel coefficient from eNB to MS and w_1 is additive white Gaussian noise (AWGN). In Equation (3.2), h_{eNB} is modeled as zero-mean, complex

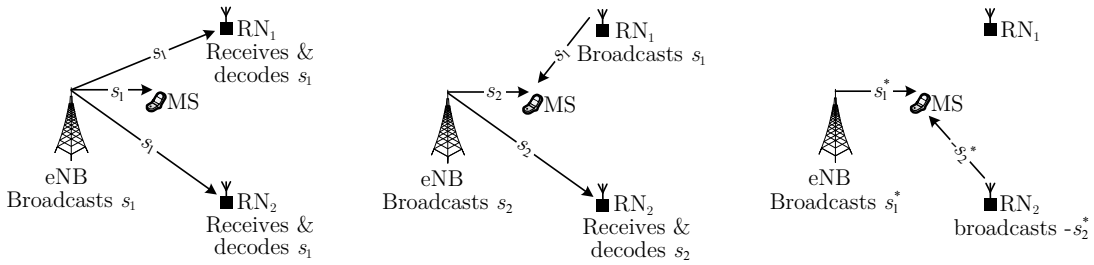

(a) Phase 1 (b) Phase 2 (c) Phase 3

Figure 3.6: The proposed E-DF transmission phases.

Gaussian random variable with variance σ^2_{eNB}. Also, the noise term w_1 is modeled as a zero-mean, complex Gaussian random variable with variance $\sigma^2_{w_1}$.

In phase 2, Figure 3.6 (b), the eNB broadcasts the second symbol s_2 from the code vector to the MS and RN_2. Simultaneously, RN_1 transmits the decoded s_1 to the MS and RN_2. The total received signal at the MS from eNB and RN_1 in phase 2 is written as

$$y_2 = \sqrt{P_{RN}}\, h_{RN_1} s_1 + \sqrt{P_{eNB}}\, h_{eNB} s_2 + w_2 \tag{3.3}$$

where h_{RN_1} is the channel coefficient from RN_1 to MS and w_2 is additive white Gaussian noise (AWGN). In Equation (3.3), h_{RN_1} is modeled as zero-mean, complex Gaussian random variable with variance $\sigma^2_{RN_1}$. Also, w_2 is modeled as a zero-mean, complex Gaussian random variable with variance $\sigma^2_{w_2}$.

In phase 3, Figure 3.6 (c), eNB and RN_2 modify the constellations of the symbols such that, eNB changes s_1 to s_1^* and RN_2 changes s_2 to $-s_2^*$. Both, eNB and RN_2, transmit the modified symbols to the MS simultaneously. Therefore, the signal received at the MS from eNB and RN_2 in phase 3 can be written as

$$y_3 = \sqrt{P_{eNB}}\, h_{eNB} s_1^* - \sqrt{P_{RN}}\, h_{RN_2} s_2^* + w_3 \tag{3.4}$$

where h_{RN_2} is the channel coefficient from RN_2 to the MS and w_3 is AWGN. In Equation (3.4), h_{RN_2} is modeled as zero-mean, complex Gaussian random variable

with variance $\sigma^2_{RN_2}$. Also, w_3 is modeled as a zero-mean, complex Gaussian random variable with variance $\sigma^2_{w_3}$. The three-phase transmission is carried on until the end of the entire symbol sequence. Assuming the channel conditions for all links are quasi-static over three consecutive signaling intervals, and taking the conjugate of y_3 in Equation (3.4), Equations (3.2), (3.3) and (3.4) are combined in matrix form as

$$\begin{bmatrix} y_1 \\ y_2 \\ y_3^* \end{bmatrix} = \begin{bmatrix} \sqrt{P_{eNB}}h_{eNB} & 0 \\ \sqrt{P_{RN}}h_{RN_1} & \sqrt{P_{eNB}}h_{eNB} \\ \sqrt{P_{eNB}}h_{eNB}^* & -\sqrt{P_{RN}}h_{RN_2}^* \end{bmatrix} \begin{bmatrix} s_1 \\ \\ s_2 \end{bmatrix} + \begin{bmatrix} w_1 \\ w_2 \\ w_3^* \end{bmatrix} \tag{3.5}$$

Using the value of P_{RN} in Equation (3.1), Equation (3.5) becomes

$$\underbrace{\begin{bmatrix} y_1 \\ y_2 \\ y_3^* \end{bmatrix}}_{\triangleq \mathbf{y}} = \sqrt{P_{eNB}} \underbrace{\begin{bmatrix} h_{eNB} & 0 \\ \eta h_{RN_1} & h_{eNB} \\ h_{eNB}^* & -\eta h_{RN_2}^* \end{bmatrix}}_{\triangleq \mathbf{H}} \underbrace{\begin{bmatrix} s_1 \\ \\ s_2 \end{bmatrix}}_{\triangleq \mathbf{s}} + \underbrace{\begin{bmatrix} w_1 \\ w_2 \\ w_3^* \end{bmatrix}}_{\triangleq \mathbf{w}} \tag{3.6}$$

where $\mathbf{y} \in \mathbb{C}^{3\times 1}$ is the received signal vector, $\mathbf{H} \in \mathbb{C}^{3\times 2}$ is the channel matrix, $\mathbf{s} \in \mathbb{C}^{2\times 1}$ is the information code vector, and $\mathbf{w} \in \mathbb{C}^{3\times 1}$ is the noise vector. It is clearly seen that the E-DF scheme provides a transmission of two ST-coded symbols over three phases, or signaling intervals, and provides diversity for both transmitted symbols. Therefore, the transmission rate is improved from ½ in the conventional ST-coded DF to ⅔ at the cost of an extra relay. Adding another relay increases the diversity order, and consequently increases the communication reliability. However, it has been seen that the improvement in communication reliability when using more than two relays is not significant [58]. In turn, this increases the complexity of coordinating the relays, its cost, ST code design, and the generated interference between relays.

In the following, we propose a modified maximum-likelihood (ML) decoder to decode $\mathbf{y}$ over quasi-static flat fading channels. The modified ML decoder is motivated by the work of Tran & Sesay [105].

3.2.2 *Modified* ML *Decoder of* E-DF *Over Quasi-Static Fading Channel*

Under the assumption of perfect channel state information (CSI) at the receiver, the conventional ML decoder selects the code vector $\hat{\mathbf{s}} \triangleq \begin{bmatrix} \hat{s}_1 & \hat{s}_2 \end{bmatrix}^T$ according to [106]

$$\hat{\mathbf{s}} = \arg\min_{\mathbf{s}} \left\| \mathbf{y} - \mathbf{H}\mathbf{s} \right\|^2 \tag{3.7}$$

where $\left\| .. \right\|^2$ is the norm-squared operation. This is conventionally performed by multiplying the received signals in Equation (3.6) by the conjugate transpose of the channel matrix to decouple the received symbols if the product of $\mathbf{H}^H$ and $\mathbf{H}$ is a diagonal matrix, i.e.

$$\mathbf{H}^H\mathbf{H} = \left(\lambda_1, \lambda_2\right)\mathbf{I}_2, \tag{3.8}$$

According to the conventional Alamouti ST coding [73], the product of $\mathbf{H}^H\mathbf{H}$ is diagonal when the amplitudes of fading from each transmit antenna to each receive antenna are mutually uncorrelated Rayleigh distributed, and time-invariant over two signaling periods. Also, the transmitted symbol at each antenna (or the code word) is chosen such that the $\mathbf{H}$'s channel vectors are orthogonal. Having establish these two conditions, the product of $\mathbf{H}^H$ and $\mathbf{H}$ is now a diagonal matrix,

$$\underbrace{\mathbf{H}^H\mathbf{y}}_{\triangleq\hat{\mathbf{y}}} = \mathbf{H}^H\mathbf{H}\mathbf{s} + \underbrace{\mathbf{H}^H\mathbf{w}}_{\triangleq\hat{\mathbf{w}}}$$

and consequently, conventional ML decoding is used by computing the decision statistic vector $\hat{\mathbf{y}} \triangleq \begin{bmatrix} \hat{y}_1 & \hat{y}_2 \end{bmatrix}^T$ as

$$\hat{\mathbf{y}} \triangleq \mathbf{H}^H\mathbf{y} = \left(\lambda_1, \lambda_2\right)\mathbf{I}_2\mathbf{s} + \hat{\mathbf{w}} \tag{3.9}$$

where λ_1 and λ_2 are complex-valued coefficients, and $\mathbf{I}_2$ is a 2×2 identity matrix. Equation (3.9) can be simplified as

$$\hat{\mathbf{s}} = \arg\min_{\mathbf{s}} \left\| \hat{\mathbf{y}} - \left(\lambda_1, \lambda_2\right)\mathbf{I}_2\mathbf{s} \right\|^2 \tag{3.10}$$

Consider the channel matrix $\mathbf{H}$ in Equation (3.6). Assuming the channel to be time-invariant over three consecutive signaling periods, multiplying $\mathbf{H}$ by its conjugate transpose $\mathbf{H}^H$ yields,

$$\begin{aligned}\mathbf{H}^H\mathbf{H} &= \begin{bmatrix} h_{eNB}^* & \eta h_{RN_1}^* & h_{eNB} \\ 0 & h_{eNB}^* & -\eta h_{RN_2} \end{bmatrix} \begin{bmatrix} h_{eNB} & 0 \\ \eta h_{RN_1} & h_{eNB} \\ h_{eNB}^* & -\eta h_{RN_2}^* \end{bmatrix} \\ &= \begin{bmatrix} 2|h_{eNB}|^2 + \eta^2 |h_{RN_1}|^2 & \eta h_{eNB}\left(h_{RN_1}^* - h_{RN_2}^*\right) \\ \eta h_{eNB}^*\left(h_{RN_1} - h_{RN_2}\right) & |h_{eNB}|^2 + \eta^2 |h_{RN_2}|^2 \end{bmatrix}\end{aligned} \tag{3.11}$$

The matrix in Equation (3.11) is not diagonal. Therefore, ML decoding of the received signals is degraded due to the non-zero off-diagonal terms. In this case, the conventional ML decoder in Equation (3.10) is no longer valid. In this dissertation, we propose a modified ML method similar to the method in [105], where a matrix is constructed such that its product with $\mathbf{H}$ is a diagonal matrix. i.e.

$$\boldsymbol{\varphi}\mathbf{H} = diag\left(\lambda_1, \lambda_2\right) \triangleq \boldsymbol{\Lambda} \tag{3.12}$$

where λ_1 and λ_2 are in general complex-valued coefficients that are specified later in this section. Define a 3×2 matrix $\boldsymbol{\varphi}$

$$\boldsymbol{\varphi} \triangleq \begin{bmatrix} \varphi_1 & \varphi_2 & \varphi_3 \\ 0 & \varphi_4 & \varphi_5 \end{bmatrix}$$

Multiplying $\mathbf{H}$ by $\boldsymbol{\varphi}$ yields

$$\begin{aligned}\boldsymbol{\varphi}\mathbf{H} &= \begin{bmatrix} \varphi_1 & \varphi_2 & \varphi_3 \\ 0 & \varphi_4 & \varphi_5 \end{bmatrix} \begin{bmatrix} h_{eNB} & 0 \\ \eta h_{RN_1} & h_{eNB} \\ h_{eNB}^* & -\eta h_{RN_2}^* \end{bmatrix} \\ &= \begin{bmatrix} \varphi_1 h_{eNB} + \eta\varphi_2 h_{RN_1} + \varphi_3 h_{eNB}^* & \varphi_2 h_{eNB} - \eta\varphi_3 h_{RN_2}^* \\ \eta\varphi_4 h_{RN_1} + \varphi_5 h_{eNB}^* & \varphi_4 h_{eNB} - \eta\varphi_5 h_{RN_2}^* \end{bmatrix}\end{aligned} \tag{3.13}$$

In order to diagonalize the product, the elements of $\boldsymbol{\varphi}$ are selected to annihilate the off- diagonal terms. That is,

$$\varphi_2 h_{eNB} - \eta\varphi_3 h^*_{RN_2} = 0 \tag{3.14}$$

and

$$\eta\varphi_4 h_{RN_1} + \varphi_5 h^*_{eNB} = 0 \tag{3.15}$$

A set of values of φ_2 and φ_3 that satisfy Equation (3.14) can be obtained intuitively as,

$$\varphi_2 = \eta h^*_{RN_2} \quad \text{and} \quad \varphi_3 = h_{eNB}\,.$$

Also, a set of values of φ_4 and φ_5 that satisfy Equation (3.15) is given by,

$$\varphi_4 = h^*_{eNB} \quad \text{and} \quad \varphi_5 = -\eta h_{RN_1}\,.$$

Using the above four values, $\boldsymbol{\varphi}$ is written as

$$\boldsymbol{\varphi} = \begin{bmatrix} \varphi_1 & \eta h^*_{RN_2} & h_{eNB} \\ 0 & h^*_{eNB} & -\eta h_{RN_1} \end{bmatrix}$$

To find a suitable value of φ_1, we substitute $\boldsymbol{\varphi}$ into Equation (3.13), which yields

$$\begin{aligned} \boldsymbol{\varphi}\mathbf{H} &= \begin{bmatrix} \varphi_1 & \eta h^*_{RN_2} & h_{eNB} \\ 0 & h^*_{eNB} & -\eta h_{RN_1} \end{bmatrix} \begin{bmatrix} h_{eNB} & 0 \\ \eta h_{RN_1} & h_{eNB} \\ h^*_{eNB} & -\eta h^*_{RN_2} \end{bmatrix} \\ &= \begin{bmatrix} \varphi_1 h_{eNB} + |h_{eNB}|^2 + \eta^2 h^*_{RN_2} h_{RN_1} & 0 \\ 0 & |h_{eNB}|^2 + \eta^2 h^*_{RN_2} h_{RN_1} \end{bmatrix} \end{aligned} \tag{3.16}$$

Here, φ_1 can take any arbitrary value. A suitable value of φ_1 is h^*_{eNB}, which yields $\varphi_1 h^*_{eNB} = |h_{eNB}|^2$, and increases the diversity. The desired matrix is therefore given by,

$$\boldsymbol{\varphi} = \begin{bmatrix} h^*_{eNB} & \eta h^*_{RN_2} & h_{eNB} \\ 0 & h^*_{eNB} & -\eta h_{RN_1} \end{bmatrix}$$

Using the above matrix, Equation (3.12) reduces to

$$\mathbf{\Lambda} \triangleq diag\left(\lambda_1, \lambda_2\right) = \boldsymbol{\varphi}\mathbf{H} = \begin{bmatrix} 2\left|h_{eNB}\right|^2 + \eta^2 h_{RN_2}^* h_{RN_1} & 0 \\ 0 & \left|h_{eNB}\right|^2 + \eta^2 h_{RN_2}^* h_{RN_1} \end{bmatrix}$$

Denote the diagonal terms by λ_1 and λ_2, respectively. That is,

$$\lambda_1 = 2\left|h_{eNB}\right|^2 + \eta^2 h_{RN_2}^* h_{RN_1} \quad \text{and} \quad \lambda_2 = \left|h_{eNB}\right|^2 + \eta^2 h_{RN_2}^* h_{RN_1} \tag{3.17}$$

The decision statistic vector $\hat{\mathbf{y}}$ for the modified ML decoder is given by

$$\underbrace{\begin{bmatrix} \hat{y}_1 \\ \hat{y}_2 \end{bmatrix}}_{\hat{\mathbf{y}}} = \sqrt{P_{eNB}} \underbrace{\begin{bmatrix} \lambda_1 & 0 \\ 0 & \lambda_2 \end{bmatrix}}_{\mathbf{\Lambda}} \underbrace{\begin{bmatrix} s_1 \\ s_2 \end{bmatrix}}_{\mathbf{s}} + \underbrace{\begin{bmatrix} \hat{w}_1 \\ \hat{w}_2 \end{bmatrix}}_{\hat{\mathbf{w}}} \tag{3.18}$$

where $\hat{\mathbf{y}} \triangleq \boldsymbol{\varphi}\mathbf{y}$ and $\hat{\mathbf{w}} \triangleq \boldsymbol{\varphi}\mathbf{w}$. The decoding of $\hat{\mathbf{s}}$ is then performed

$$\hat{\mathbf{s}} = \arg\min_{\mathbf{s}} \left\| \hat{\mathbf{y}} - \mathbf{\Lambda}\mathbf{s} \right\|^2 \tag{3.19}$$

3.3 Performance Analysis

In this section, we present the analysis of *SER* for the proposed E-DF protocol when *M*-ary phase shift keying (MPSK) modulation is employed. Furthermore, we provide a *SER* upper-bound as well as an approximated *SER* expressions for the proposed E-DF cooperation scheme.

3.3.1 *Signal-to-Noise Ratio* (*SNR*) *Analysis*

3.3.1.1 Instantaneous SNR

In this section, an instantaneous *SNR* expression is derived for the proposed E-DF scheme. According to Equation (3.18), the noise vector $\hat{\mathbf{w}}$ is expressed as

$$\hat{\mathbf{w}} = \underbrace{\begin{bmatrix} h_{eNB}^* & \eta h_{RN_2}^* & h_{eNB} \\ 0 & h_{eNB}^* & -\eta h_{RN_1} \end{bmatrix}}_{\boldsymbol{\varphi}} \underbrace{\begin{bmatrix} w_1 \\ w_2 \\ w_3^* \end{bmatrix}}_{\mathbf{w}} = \begin{bmatrix} w_1 h_{eNB}^* + \eta w_2 h_{RN_2}^* + w_3^* h_{eNB} \\ w_2 h_{eNB}^* - \eta w_3^* h_{RN_1} \end{bmatrix} \triangleq \begin{bmatrix} \hat{w}_1 \\ \hat{w}_2 \end{bmatrix}$$

where $\hat{w}_1$ and $\hat{w}_2$ are modeled as a zero-mean, conditionally complex Gaussian random variables with variances (assuming h_{eNB}, h_{RN_1} and h_{RN_2} are fixed)

$$\sigma_{\hat{w}_1}^2(\mathbf{H}) = \sigma_{w_1}^2\left(2|h_{eNB}|^2 + \eta^2|h_{RN_2}|^2\right) \text{ and } \sigma_{\hat{w}_2}^2(\mathbf{H}) = \sigma_{w_2}^2\left(|h_{eNB}|^2 + \eta^2|h_{RN_1}|^2\right),$$

respectively. With knowledge of the channel coefficients h_{eNB}, h_{RN_1} and h_{RN_2} at the receiver, and $P_{RN} = \eta P_{eNB}$, $0 < \eta < 1$, the conditional *SNRs* , γ_1 and γ_2, at the output of the decoder are given by

$$\gamma_1(\mathbf{H}) = \frac{|\lambda_1|^2}{\sigma_{\hat{w}_1}^2(\mathbf{H})} = \frac{P_{eNB}\left|2|h_{eNB}|^2 + \eta^2 h_{RN_2}^* h_{RN_1}\right|^2}{\sigma_{w_1}^2\left(2|h_{eNB}|^2 + \eta^2|h_{RN_2}|^2\right)}$$

and (3.20)

$$\gamma_2(\mathbf{H}) = \frac{|\lambda_2|^2}{\sigma_{\hat{w}_2}^2(\mathbf{H})} = \frac{P_{eNB}\left||h_{eNB}|^2 + \eta^2 h_{RN_2}^* h_{RN_1}\right|^2}{\sigma_{w_2}^2\left(|h_{eNB}|^2 + \eta^2|h_{RN_1}|^2\right)}$$

respectively, and the instantaneous overall (exact) conditional *SNR* is given by

$$SNR(\mathbf{H}) = \gamma_1(\mathbf{H}) + \gamma_2(\mathbf{H}) \tag{3.21}$$

3.3.1.2 Conditional SNR Upper Bound

In this section, we use vector analysis to further simplify the overall *SNR* expression in Equation (3.21). Define α and β as $|\alpha|^2 \triangleq \left|2|h_{eNB}|^2\right|^2$ and $|\beta|^2 \triangleq \left|\eta^2 h_{RN_1} h_{RN_2}^*\right|^2$ are lengths of two sides of a triangle. Then, the length of the third side (i.e. $|\alpha+\beta|^2$) is less than or equal the sum of the two sides ($|\alpha|^2 + |\beta|^2$). i.e. $|\alpha+\beta|^2 \le |\alpha|^2 + |\beta|^2$. This is called Triangle Inequality found in [106]. In this inequality, the term $|\alpha+\beta|^2$ equals $|\alpha|^2 + |\beta|^2$ only when $\alpha = \beta$.

Recalling the values of α and β, the numerators in Equation (3.20) are upper bounded as

$$\left|2\left|h_{eNB}\right|^2+\eta^2 h_{RN_1}h_{RN_2}^*\right|^2 \le \left|2\left|h_{eNB}\right|^2\right|^2+\left|\eta^2 h_{RN_1}h_{RN_2}^*\right|^2 = 4\left|h_{eNB}\right|^4+\eta^4\left|h_{RN_1}\right|^2\left|h_{RN_2}\right|^2$$

and

$$\left|\left|h_{eNB}\right|^2+\eta^2 h_{RN_1}h_{RN_2}^*\right|^2 \le \left|\left|h_{eNB}\right|^2\right|^2+\left|\eta^2 h_{RN_1}h_{RN_2}^*\right|^2 = \left|h_{eNB}\right|^4+\eta^4\left|h_{RN_1}\right|^2\left|h_{RN_2}\right|^2$$

Then the conditional *SNR* upper bounds are

$$\gamma_1^u(\mathbf{H}) = \frac{4P_{eNB}\left|h_{eNB}\right|^4+\eta^4 P_{eNB}\left|h_{RN_1}\right|^2\left|h_{RN_2}\right|^2}{\sigma_{w_1}^2\left(2\left|h_{eNB}\right|^2+\eta^2\left|h_{RN_2}\right|^2\right)}$$

and (3.22)

$$\gamma_2^u(\mathbf{H}) = \frac{P_{eNB}\left|h_{eNB}\right|^4+\eta^4 P_{eNB}\left|h_{RN_1}\right|^2\left|h_{RN_2}\right|^2}{\sigma_{w_2}^2\left(\left|h_{eNB}\right|^2+\eta^2\left|h_{RN_1}\right|^2\right)}$$

The overall conditional *SNR* upper bound is given by

$$SNR^u(\mathbf{H}) = \gamma_1^u(\mathbf{H})+\gamma_2^u(\mathbf{H}) \tag{3.23}$$

3.3.1.3 Approximate Conditional SNR Upper Bound

The LTE-A standard specifies the transmit power of the RN to be approximately 10 times less than the transmit power of the base station [104]. Under such conditions, we can neglect the component η^4 and obtain an approximate conditional upper bound for *SNR*'s $\gamma_1(\mathbf{H})$ and $\gamma_2(\mathbf{H})$ are given by

$$\gamma_1^a(\mathbf{H}) = \frac{4P_{eNB}\left|h_{eNB}\right|^4}{\sigma_{w_1}^2\left(2\left|h_{eNB}\right|^2+\eta^2\left|h_{RN_2}\right|^2\right)} \quad \text{and} \quad \gamma_2^a(\mathbf{H}) = \frac{P_{eNB}\left|h_{eNB}\right|^4}{\sigma_{w_2}^2\left(\left|h_{eNB}\right|^2+\eta^2\left|h_{RN_1}\right|^2\right)} \tag{3.24}$$

The overall approximate conditional upper bound is

$$SNR^a(\mathbf{H}) = \gamma_1^a(\mathbf{H})+\gamma_2^a(\mathbf{H}) \tag{3.25}$$

Figure 3.7 shows Monte-Carlo simulation results for the exact *SNR*, the *SNR* upper-bound, and approximate *SNR* upper bound as a function of the power ratio η. At values of η below 0.3, all three curves match. However above $\eta = 0.3$, the approximate *SNR* and the *SNR* upper bound deviate from the exact *SNR*. For LTE-A where $\eta \leq 0.1$, the *SNR* upper bound and the approximate *SNR* are accurate representations of the exact *SNR*.

3.3.2 *Symbol Error Rate (SER) Analysis*

3.3.2.1 Instantaneous *SER* for MPSK

For an MPSK-modulated system ($M = 2^i$, $i = 1,2,\ldots$), the *SER* is given by [106]

$$SER \triangleq 2Q\left[\sqrt{2SNR}\sin\left(\frac{\pi}{M}\right)\right] \tag{3.26}$$

where

$$Q\left[\varsigma\right] = \int_{\varsigma}^{\infty} \frac{\exp\left(-t^2/2\right)}{2\pi}\,\mathrm{d}t$$

is the Q-function. Here, the exact instantaneous *SER* is obtained by using the actual *SNR* in Equation (3.21). The average *SER* is obtained by averaging the instantaneous *SER* over the distribution of *SNR*. Since the distribution of the exact *SNR* is difficult to evaluate, and the approximate *SNR* upper bound (SNR^a) is an accurate representation of the exact *SNR*, SNR^a is used to obtain the average *SER*.

In the following, the average *SER* is derived for the proposed E-DF cooperative relaying scheme based on the approximate conditional *SNR* upper bound (SNR^a) found in Equation (3.24). First, the probability density functions (*PDFs*) are obtained for $\gamma_1^a(\mathbf{H})$ and $\gamma_2^a(\mathbf{H})$. Then, the *PDFs* are used to obtain the associated moment generating function (*MGF*) expressions. Based on the *MGF* expressions, the overall approximate average *SER* expression is obtained for the proposed E-DF

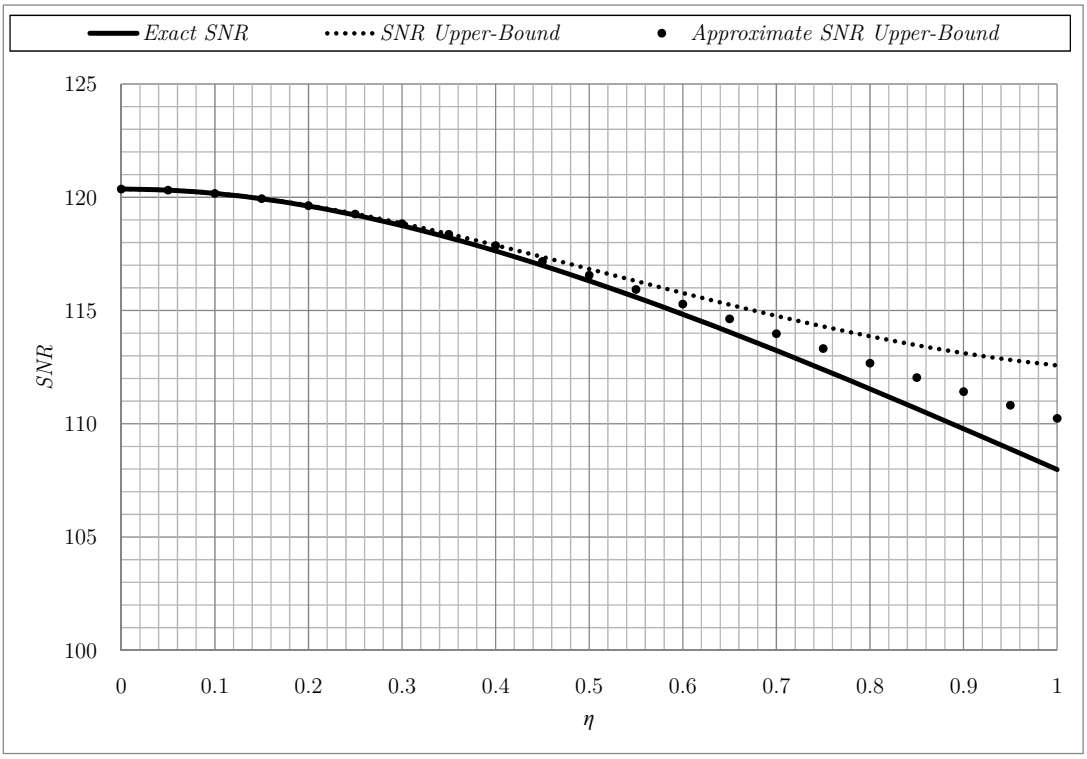

Figure 3.7: Exact, upper bound and approximate *SNR* upper bound profile versus η

cooperation systems. Finally, a worse-case and approximate worse-case average *SERs* are derived.

3.3.2.2 *SER* Analysis via *MGF*

The moment-generating function (*MGF*) of a random variable ψ is defined as [108]

$$MGF\left(s\right) = \int_{-\infty}^{\infty} f_{\Psi}\left[\psi\right] \exp\left(-\psi s\right) d\psi \tag{3.27}$$

for any real number s, where $f_{\Psi}\left[\psi\right]$ is the probability density function of ψ. Denote the *MGF* for data symbols s_1 and s_2 by MGF_1 and MGF_2, respectively. For MPSK modulation, the *SER* is determined in terms of the associated $MGF_1\left(s\right)$ and $MGF_2\left(s\right)$ as

$$SER = \frac{1}{\pi} \int_{0}^{\frac{\pi(M-1)}{M}} MGF_1\left(-\frac{\tau_{MPSK} SNR}{\sin^2(\theta)}\right) \quad MGF_2\left(-\frac{\tau_{MPSK} SNR}{\sin^2(\theta)}\right) d\theta \tag{3.28}$$

where $\tau_{MPSK} = \sin^2\left(\pi/M\right)$. This method of evaluating average *SER* was first introduced in [109], then in [110], and generalized later as an alternative way to evaluate average *SER*. We now proceed to the derivation of the moment generating functions $MGF_1(s)$ and $MGF_2(s)$.

Consider the approximate *SNR* upper bound provided in Equation (3.24), and define the variables $x \triangleq |h_{eNB}|^2$, $y \triangleq |h_{RN_2}|^2$ and $z \triangleq |h_{RN_1}|^2$, respectively. For derivation simplicity, let the noise variances $\sigma_w^2 \triangleq \sigma_{w_1}^2 = \sigma_{w_2}^2$ are equal. The channels h_{eNB}, h_{RN_2} and h_{RN_1} are modeled as zero-mean, complex random variables with variances σ_{eNB}^2, $\sigma_{RN_2}^2$ and $\sigma_{RN_1}^2$, respectively. Since all channels are Rayleigh fading channels, the associated probability density functions for the random variables x, y and z given as

$$f_X[x] = \begin{cases} \dfrac{\exp\left(\dfrac{-x}{2\sigma_{eNB}^2}\right)}{2\sigma_{eNB}^2} & x > 0 \\ 0 & \text{else where} \end{cases}, \quad f_Y[y] = \begin{cases} \dfrac{\exp\left(\dfrac{-y}{2\sigma_{RN_2}^2}\right)}{2\sigma_{RN_2}^2} & y > 0 \\ 0 & \text{else where} \end{cases} \text{ and}$$

$$f_Z[z] = \begin{cases} \dfrac{\exp\left(\dfrac{-z}{2\sigma_{RN_1}^2}\right)}{2\sigma_{RN_1}^2} & z > 0 \\ 0 & \text{else where} \end{cases}$$

respectively. The components $\gamma_1^a(\mathbf{H})$ and $\gamma_2^a(\mathbf{H})$ in Equation (3.24) may be rewritten as

$$\gamma_1^a(x,y) = \frac{4\gamma x^2}{2x + \eta^2 y} \quad \text{and} \quad \gamma_2^a(x,z) = \frac{\gamma x^2}{x + \eta^2 z},$$

where $\gamma = P_{eNB}/\sigma_w^2$. To derive the probability density functions, consider first $\gamma_1^a(x,y)$. We define two variables

$$u \triangleq 4\gamma x \quad \text{and} \quad v \triangleq \frac{x}{2x+\eta^2 y}.$$

Then, the probability density function of $\gamma_1^a(x,y)$ is the joint PDF $f_{U,V}[u,v]$ of the product $\Gamma_1 = UV$.

Two conditions for the PDF $f_{U,V}[u,v]$ to exist [108]. The first condition is that a unique set of solution exists for x and y in terms of u and v. In this case, the unique solutions for x and y are

$$x = \frac{u}{4\gamma} \quad \text{and} \quad y = \frac{u}{2\eta^2\gamma}\left(\frac{1-2v}{v}\right),$$

respectively. The second condition is that the Jacobian of x and y not equal to zero, i.e. $J(x,y) \neq 0$, where

$$J(x,y) = Det\begin{vmatrix} \dfrac{\partial(4\gamma x)}{\partial x} & \dfrac{\partial(4\gamma x)}{\partial y} \\ \dfrac{\partial\left(\dfrac{x}{2x+\eta^2 y}\right)}{\partial x} & \dfrac{\partial\left(\dfrac{x}{2x+\eta^2 y}\right)}{\partial y} \end{vmatrix}$$

It can be easily shown that,

$$J(x,y) = Det\begin{vmatrix} 4\gamma & 0 \\ \dfrac{1}{2x+\eta^2 y} - \dfrac{x}{(2x+\eta^2 y)^2} & \dfrac{-x}{(2x+\eta^2 y)^2} \end{vmatrix} = \frac{-4\gamma x}{\left(2x+\eta^2 y\right)^2} \neq 0$$

Hence, both conditions are satisfied. Since the random variables x and y are independent, the joint probability density function of x and y is the product of the $PDFs$ of x and y, i.e.

$$f_{XY}[x,y] = f_X[x] f_Y[y] = \begin{cases} \dfrac{\exp\left(\dfrac{-x}{2\sigma_{eNB}^2} + \dfrac{-y}{2\sigma_{RN_2}^2}\right)}{4\sigma_{eNB}^2\sigma_{RN_2}^2} & x,y > 0 \\ 0 & \text{else where} \end{cases}$$

The joint pdf $f_{U,V}\left[u,v\right]$ is given by [108],

$$f_{U,V}\left[u,v\right] = J\left(\tfrac{u}{4\gamma},\tfrac{u}{2\eta^2\gamma}\left(\tfrac{1-2v}{v}\right)\right)^{-1} f_{XY}\left[\tfrac{u}{4\gamma},\tfrac{u}{2\eta^2\gamma}\left(\tfrac{1-2v}{v}\right)\right]$$
$$= \begin{cases} \dfrac{-u\,\exp\left(\dfrac{-u}{4\gamma\sigma_{eNB}^2}+\dfrac{u\left(2v-1\right)}{4\eta^2\gamma v\sigma_{RN_2}^2}\right)}{32\eta^2\gamma^2v^2\sigma_{eNB}^2\sigma_{RN_2}^2} & u>0, v<\dfrac{1}{2} \\ 0 & \text{else where} \end{cases} \tag{3.29}$$

where for $x>0,\ u>0$ and for $y>0,\ v<\frac{1}{2}$. The result in Equation (3.29) is used to determine the *PDF* of $\Gamma_1 = UV$, which is the product of two random variables u and v. The *PDF* of Γ_1 is defined as [108]

$$f_{\Gamma_1}\left[\gamma_1^a\right] = \int_0^\infty f_{UV}\left[u,\frac{\gamma_1^a}{u}\right]\mathrm{d}u = \int_0^\infty \frac{-u^3\exp\left(\dfrac{-u}{4\gamma\sigma_{eNB}^2}+\dfrac{u\left(2\gamma_1^a-u\right)}{4\eta^2\gamma\gamma_1^a\sigma_{RN_2}^2}\right)}{32\left(\eta\gamma\gamma_1^a\right)^2\sigma_{eNB}^2\sigma_{RN_2}^2}\mathrm{d}u \tag{3.30}$$

where we have used $v=\dfrac{\gamma_1^a}{u}$. Using the table of integrals [111], we obtain

$$f_{\Gamma_1}\left[\gamma_1^a\right] = \begin{cases} \dfrac{\left(16\gamma\eta^2\sigma_{eNB}^4\sigma_{RN_2}^2+\gamma_1^a\left(2\sigma_{eNB}^2-\eta^2\sigma_{RN_2}^2\right)^2\right)}{128\,\sigma_{eNB}^6\sqrt{\dfrac{2\gamma_1^a\gamma^3\eta^2\sigma_{RN_2}^2}{\pi}}}\times\ldots \\ \ldots\times\dfrac{erfc\left[\dfrac{2\sigma_{eNB}^2+\eta^2\sigma_{RN_2}^2}{\sqrt{\dfrac{32\gamma\eta^2\sigma_{RN_2}^2}{\gamma_1^a}}\sigma_{eNB}^2}\right]}{\exp\left(\dfrac{\gamma_1^a(\eta^2\sigma_{RN_2}^2-2\sigma_{eNB}^2)^2}{32\,\gamma\,\eta^2\,\sigma_{eNB}^4\,\sigma_{RN_2}^2}\right)}+.. & ,\ \gamma_1^a>0 \\ ..+\dfrac{6\sigma_{eNB}^2-\eta^2\sigma_{RN_2}^2}{32\,\gamma\,\sigma_{eNB}^4\exp\left(\dfrac{\gamma_1^a}{4\gamma\sigma_{eNB}^2}\right)} & \\ 0 & ,\ \text{else where} \end{cases} \tag{3.31}$$

where *erfc*[.] is the complementary error function given as

$$erfc\left[\varsigma\right]=\int_{\varsigma}^{\infty}\frac{2\exp\left(-t^{2}\right)}{\sqrt{\pi}}\mathrm{d}t\,.$$

Using similar steps for $\gamma_2^a\left(x,z\right)=\dfrac{\gamma x^2}{x+\eta^2 z}$, we obtain the *PDF* $f_{\Gamma_2}\left[\gamma_2^a\right]$ for γ_2^a as

$$f_{\Gamma_2}\left[\gamma_2^a\right]=\begin{cases}\dfrac{\left(4\gamma\eta^2\sigma_{eNB}^4\sigma_{RN_1}^2+\gamma_2^a\left(\sigma_{eNB}^2-\eta^2\sigma_{RN_1}^2\right)^2\right)}{16\sigma_{eNB}^6\sqrt{\dfrac{2\gamma_2^a\gamma^3\eta^2\sigma_{RN_1}^2}{\pi}}}\times\ldots \\ \ldots\times\dfrac{erfc\left[\dfrac{\sigma_{eNB}^2+\eta^2\sigma_{RN_1}^2}{\sqrt{\dfrac{8\gamma\eta^2\sigma_{RN_1}^2}{\gamma_2^a}}\sigma_{eNB}^2}\right]}{\exp\left(\dfrac{\gamma_2^a\left(\eta^2\sigma_{RN_1}^2\sigma_{eNB}^2\right)^2}{8\gamma\eta^2\sigma_{eNB}^4\sigma_{RN_1}^2}\right)}+\ldots & ,\gamma_2^a>0 \\ \ldots+\dfrac{3\sigma_{eNB}^2-\eta^2\sigma_{RN_1}^2}{8\gamma\sigma_{eNB}^4\exp\left(\dfrac{\gamma_2^a}{2\gamma\sigma_{eNB}^2}\right)} & \\ 0 & ,\quad \text{else where}\end{cases} \tag{3.32}$$

The associated moment generating functions are calculated using the relations,

$$MGF_1\left(s\right)=\int_0^{\infty}f_{\Gamma_1}\left[\gamma_2^a\right]\exp\left(-\gamma_1^a s\right)d\gamma_1^a \quad \text{and} \quad MGF_2\left(s\right)=\int_0^{\infty}f_{\Gamma_2}\left[\gamma_2^a\right]\exp\left(-\gamma_2^a s\right)d\gamma_2^a$$

The moment generating functions for the approximate *SNR* upper bound can be shown to be given by

$$\begin{aligned}MGF_1\left(s\right)=&-\frac{\left(2\sigma_{eNB}^2-\eta^2\sigma_{RN_2}^2\right)^2+4s\gamma\eta^2\sigma_{eNB}^2\sigma_{RN_2}^2\left(6\sigma_{eNB}^2-\eta^2\sigma_{RN_2}^2\right)}{\left(4\gamma s\sigma_{eNB}^2-1\right)\left(\left(2\sigma_{eNB}^2-\eta^2\sigma_{RN_2}^2\right)^2+32\eta^2\gamma s\sigma_{eNB}^4\sigma_{RN_2}^2\right)}-\ldots \\ &\ldots-\frac{32\eta^4\gamma s\sigma_{eNB}^4\sigma_{RN_2}^4\tan^{-1}\left(\dfrac{\sqrt{-32\eta^2\gamma s\sigma_{eNB}^4\sigma_{RN_2}^2-\left(2\sigma_{eNB}^2-\eta^2\sigma_{RN_2}^2\right)^2}}{2\sigma_{eNB}^2+\eta^2\sigma_{RN_2}^2}\right)}{\left(-32\gamma s\eta^2\sigma_{eNB}^4\sigma_{RN_2}^2-\left(2\sigma_{eNB}^2-\eta^2\sigma_{RN_2}^2\right)^2\right)^{3/2}}\end{aligned} \tag{3.33}$$

and

$$MGF_2\left(s\right) = -\frac{\left(\sigma_{eNB}^2 - \eta^2\sigma_{RN_1}^2\right)^2 + 2\eta^2\gamma s\sigma_{eNB}^2\sigma_{RN_1}^2\left(3\sigma_{eNB}^2 - \eta^2\sigma_{RN_1}^2\right)}{\left(2\gamma s\sigma_{eNB}^2 - 1\right)\left(\left(\sigma_{eNB}^2 - \eta^2\sigma_{RN_1}^2\right)^2 + 8\eta^2\gamma s\sigma_{eNB}^4\sigma_{RN_1}^2\right)} - ..$$
$$.. - \frac{8\eta^4 s\gamma\sigma_{eNB}^4\sigma_{RN_1}^4 \tan^{-1}\left(\frac{\sqrt{-8s\gamma\eta^2\sigma_{eNB}^4\sigma_{RN_1}^2 - \left(\sigma_{eNB}^2 - \eta^2\sigma_{RN_1}^2\right)^2}}{\sigma_{eNB}^2 + \eta^2\sigma_{RN_1}^2}\right)}{\left(-8\eta^2\gamma s\sigma_{eNB}^4\sigma_{RN_1}^2 - \left(\sigma_{eNB}^2 - \eta^2\sigma_{RN_1}^2\right)^2\right)^{3/2}} \quad , \quad (3.34)$$

respectively. To evaluate the *SER* for MPSK, we set $s = -\tau_{MPSK}\big/\sin^2\left(\theta\right)$ into Equation (3.33) and Equation (3.34) and integrate over the interval $0 < \theta < \frac{\pi(M-1)}{M}$, that is,

$$SER = \frac{1}{\pi}\int_0^{\frac{\pi(M-1)}{M}} MGF_1\left(\frac{-\tau_{MPSK}}{\sin^2\left(\theta\right)}\right) \quad MGF_2\left(\frac{-\tau_{MPSK}}{\sin^2\left(\theta\right)}\right)\mathrm{d}\theta \quad (3.35)$$

Numerical integration is used to evaluate the expression in Equation (3.35).

3.3.2.3 Worse-Case *SER* Upper Bound

Evaluation of the integral in Equation (3.35) may be simplified by considering a worse-case situation. Consider the *MGF* expressions for $s = -\tau_{MPSK}\big/\sin^2\left(\theta\right)$,

$$MGF_1\left(\frac{-\tau_{MPSK}}{\sin^2(\theta)}\right) = \frac{\left(2\sigma_{eNB}^2 - \eta^2\sigma_{RN_2}^2\right)^2 - \frac{4\eta^2\gamma\tau_{MPSK}\sigma_{eNB}^2\sigma_{RN_2}^2\left(6\sigma_{eNB}^2 - \eta^2\sigma_{RN_2}^2\right)}{\sin^2\left(\theta\right)}}{\left(\frac{4\gamma\tau_{MPSK}\sigma_{eNB}^2}{\sin^2\left(\theta\right)} + 1\right)\left(\left(2\sigma_{eNB}^2 - \eta^2\sigma_{RN_2}^2\right)^2 - \frac{32\eta^2\gamma\tau_{MPSK}\sigma_{eNB}^4\sigma_{RN_2}^2}{\sin^2\left(\theta\right)}\right)} + ..$$
$$.. + \frac{32\eta^4\gamma\tau_{MPSK}\sigma_{eNB}^4\sigma_{RN_2}^4 \tan^{-1}\left(\frac{\sqrt{\frac{32\eta^2\gamma\tau_{MPSK}\sigma_{eNB}^4\sigma_{RN_2}^2}{\sin^2\left(\theta\right)} - \left(2\sigma_{eNB}^2 - \eta^2\sigma_{RN_2}^2\right)^2}}{2\sigma_{eNB}^2 + \eta^2\sigma_{RN_2}^2}\right)}{\sin^2\left(\theta\right)\left(\frac{32\eta^2\gamma\tau_{MPSK}\sigma_{eNB}^4\sigma_{RN_2}^2}{\sin^2\left(\theta\right)} - \left(2\sigma_{eNB}^2 - \eta^2\sigma_{RN_2}^2\right)^2\right)^{3/2}} \quad (3.36)$$

and

$$MGF_2\left(\frac{-\tau_{MPSK}}{\sin^2(\theta)}\right)=\frac{\left(\sigma_{eNB}^2-\eta^2\sigma_{RN_1}^2\right)^2-\dfrac{2\eta^2\gamma\tau_{MPSK}\sigma_{eNB}^2\sigma_{RN_1}^2\left(3\sigma_{eNB}^2-\eta^2\sigma_{RN_1}^2\right)}{\sin^2(\theta)}}{\left(\dfrac{2\gamma\tau_{MPSK}\sigma_{eNB}^2}{\sin^2(\theta)}+1\right)\left(\left(\sigma_{eNB}^2-\eta^2\sigma_{RN_1}^2\right)^2-\dfrac{8\eta^2\gamma\tau_{MPSK}\sigma_{eNB}^4\sigma_{RN_1}^2}{\sin^2(\theta)}\right)}+..$$
$$..+\frac{8\eta^4\gamma\tau_{MPSK}\sigma_{eNB}^4\sigma_{RN_1}^4\tan^{-1}\left(\dfrac{\sqrt{\dfrac{8\eta^2\gamma\tau_{MPSK}\sigma_{eNB}^4\sigma_{RN_1}^2}{\sin^2(\theta)}-\left(\sigma_{eNB}^2-\eta^2\sigma_{RN_1}^2\right)^2}}{\sigma_{eNB}^2+\eta^2\sigma_{RN_1}^2}\right)}{\sin^2(\theta)\left(\dfrac{8\eta^2\gamma\tau_{MPSK}\sigma_{eNB}^4\sigma_{RN_1}^2}{\sin^2(\theta)}-\left(\sigma_{eNB}^2-\eta^2\sigma_{RN_1}^2\right)^2\right)^{3/2}} \quad (3.37)$$

Figure 3.8 illustrates *SER* curves versus angle θ for various *SNR* values obtained by using Equations (3.36) and (3.37). It is seen that $\theta=\frac{\pi}{2}$ produces the worse-case *SER* for M = 4, 8, and 16. Therefore, setting $\theta=\frac{\pi}{2}$, we obtain a worse-case upper

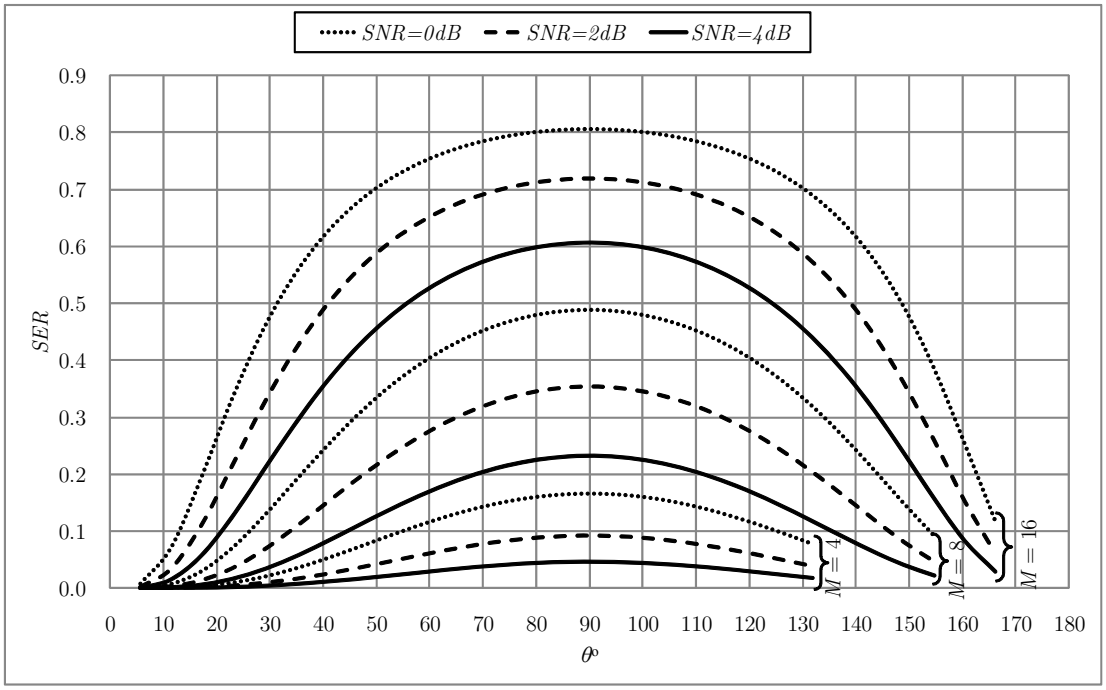

Figure 3.8: The effect of varying θ on the *SER* for different *SNR* values.

bound on *SER*. The justification behind such result is that the function $\sin^2\left(\theta\right)$ achieves its maximum value at $\theta=\frac{\pi}{2}$. Since the term $\sin^2\left(\theta\right)$ is found in all *MGFs* terms and *MGFs* represent the *SER*, therefore the number error reach its maximum rate when $\theta=\frac{\pi}{2}$. The benefit here is that evaluation of the integral in Equation (3.35) is avoided. With $\theta=\frac{\pi}{2}$, the integral in Equation (3.35) reduces to the following,

$$SER \le \frac{(M-1)\pi \;\; MGF_1\left(-\tau_{MPSK}\right) \;\; MGF_2\left(-\tau_{MPSK}\right)}{M} \tag{3.38}$$

3.3.2.4 Approximate *SER* worse-case for MPSK

In the following, an approximation is provided to simplify the calculations for the worse-case *SER*. Consider the worse-case *MGF* expressions in Equation (3.36) and Equation (3.37). For sufficiently large signal-to-noise ratio (γ), the terms with the structure $\xi\gamma \pm 1$ can be approximated by $\xi\gamma$, (i.e. $\xi\gamma \pm 1 \approx \xi\gamma$). Thus, the worse-case MGF_1 and MGF_2 are approximated as

$$MGF_1 \approx \frac{6\sigma_{eNB}^2 - \eta^2\sigma_{RN_2}^2 + \sigma_{eNB}^2\sqrt{32\eta^2\gamma\tau_{MPSK}\sigma_{RN_2}^2}\,\tan^{-1}\left(\dfrac{\sigma_{eNB}^2\sqrt{32\eta^2\gamma\tau_{MPSK}\sigma_{RN_2}^2}}{\left(2\sigma_{eNB}^2+\eta^2\sigma_{RN_2}^2\right)}\right)}{32\gamma\tau_{MPSK}\sigma_{eNB}^4} \tag{3.39}$$

and

$$MGF_2 \approx \frac{3-\eta^2\dfrac{\sigma_{RN_1}^2}{\sigma_{eNB}^2}+\sqrt{8\eta^2\gamma\tau_{MPSK}\sigma_{RN_1}^2}\,\tan^{-1}\left(\dfrac{\sqrt{8\eta^2\gamma\tau_{MPSK}\sigma_{eNB}^4\sigma_{RN_1}^2}}{\left(\sigma_{eNB}^2+\eta^2\sigma_{RN_1}^2\right)}\right)}{8\gamma\tau_{MPSK}\sigma_{eNB}^2} \tag{3.40}$$

respectively. Therefore, the worse-case *SER* for the E-DF scheme is approximated as

$$SER \approx \frac{(M-1)\,MGF_1\ MGF_2}{M}$$

$$= \frac{\pi(M-1)}{256\gamma^2\tau_{MPSK}^2\sigma_{eNB}^4 M}\left(\left(6+\sqrt{32\eta^2\gamma\tau_{MPSK}\sigma_{RN_2}^2}\ \tan^{-1}\left(\frac{\sigma_{eNB}^2\sqrt{32\eta^2\gamma\tau_{MPSK}\sigma_{RN_2}^2}}{\left(2\sigma_{eNB}^2+\eta^2\sigma_{RN_2}^2\right)}\right)\right)-\eta^2\frac{\sigma_{RN_2}^2}{\sigma_{eNB}^2}\right)\times .. \quad (3.41)$$

$$..\times\left(\left(3+\sqrt{8\eta^2\gamma\tau_{MPSK}\sigma_{RN_1}^2}\ \tan^{-1}\left(\frac{\sigma_{eNB}^2\sqrt{8\eta^2\gamma\tau_{MPSK}\sigma_{RN_1}^2}}{\left(\sigma_{eNB}^2+\eta^2\sigma_{RN_1}^2\right)}\right)\right)-\eta^2\frac{\sigma_{RN_1}^2}{\sigma_{eNB}^2}\right)$$

Figure 3.9 illustrates plots for the *SER* in Equation (3.35), the worse-case *SER* in Equation (3.38) and the approximate worse-case *SER* in Equation (3.41) for the E-DF protocol. The curves are obtained for systems employing QPSK modulation (M=4). The channel coefficients, h_{eNB}, h_{RN_1}, and h_{RN_2}, are modeled as zero-mean, complex Gaussian random variables with variances of $\sigma_{eNB}^2 = 1$, $\sigma_{RN_1}^2 = 0.9$, and $\sigma_{RN_2}^2 = 0.8$. Also, the ratio between the relay power and the base station power is

Figure 3.9: Comparison of the actual, the worse-case, and the approximate *SER* worse-case for the E-DF cooperation scheme with QPSK signals assuming

set to $\eta = 0.1$. The approximate worse-case *SER* matches the worse-case *SER* for γ values above 15dB but, however, deviate below 15dB γ values. This result is due to the assumption made in deriving the approximate worse-case *SER*, for sufficiently high γ. The highest deviation of the worse-case *SER* from the exact *SER* is approximately 1.5dB.

In order to demonstrate the benefits of employing the E-DF over the conventional DF and the non-relay schemes, the analytical and simulated *SER* versus γ are plotted for the three schemes as shown in Figures 3.10. The analytical curves are obtained for systems employing QPSK modulation ($M = 4$). The channel coefficients, h_{eNB}, h_{RN_1}, and h_{RN_2}, are modeled as zero-mean, complex Gaussian random variables with variances of $\sigma^2_{eNB} = 1$, $\sigma^2_{RN_1} = 0.9$, and $\sigma^2_{RN_2} = 0.8$, respectively. Also, the ratio between the relay power and the base station power is

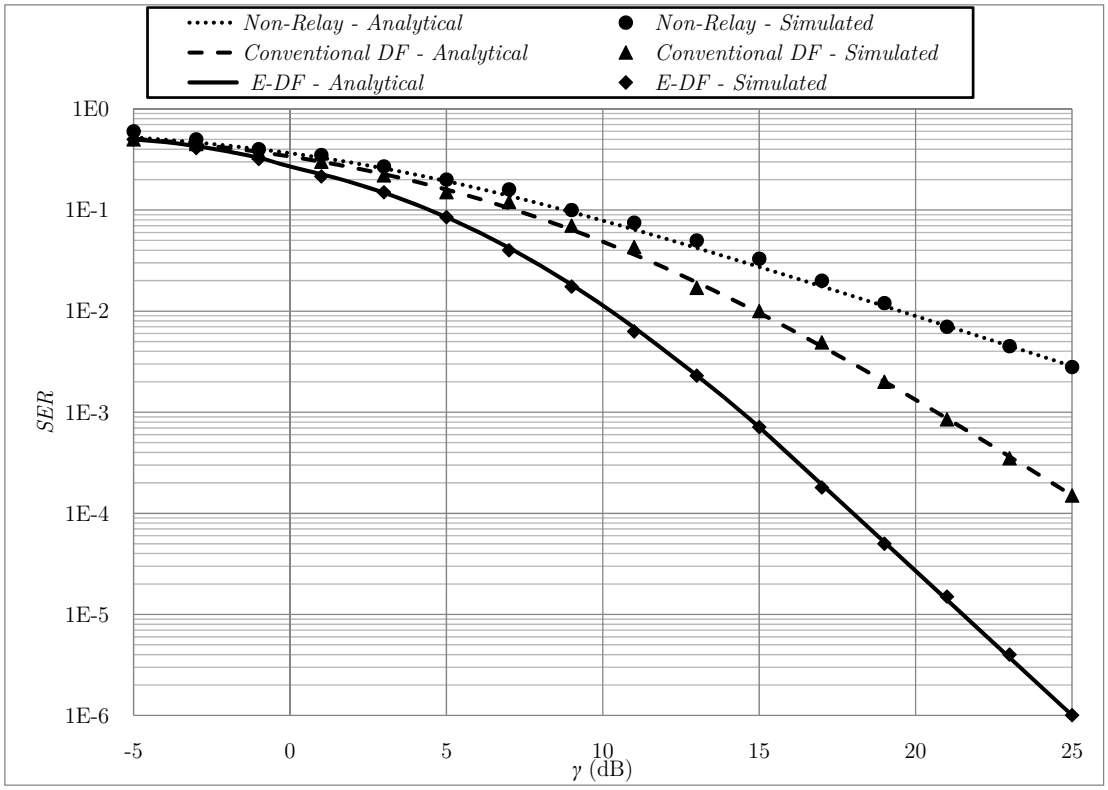

Figure 3.10: *SER* comparison for the E-DF, the conventional DF and the non-relay schemes.

set to $\eta = 0.1$. For each channel realization, the instantaneous *SNR* is calculated using Equation (3.21) and averaged over the number of channel realizations. Then, Equation (3.26) is used to find the analytical average *SER*. On the other hand, the simulated curves are obtained by generating 1×10^7 Rayleigh fading channel realizations for h_{eNB}, h_{RN_1} and h_{RN_2} with variances of $\sigma^2_{eNB}= 1$, $\sigma^2_{RN_1}= 0.9$, and $\sigma^2_{RN_2}= 0.8$, respectively. Also, 1×10^7 data symbols are generated, mapped and transmitted according to E-DF scheme. The received symbols are then decoded according to the modified ML decoder. Finally, the symbol error rate is calculated by counting the number of corrupted symbols and comparing it to the total number of transmitted symbols. Figure 3.10 shows that the E-DF scheme significantly outperforms the conventional DF and the non-relay scheme. For example, for $SER = 4\times10^{-3}$, the γ requirement of the E-DF is approximately 5dB lower than for the conventional DF and approximately 10dB lower than for the non-relay scheme. Moreover, the simulated *SER* curves match the analytical curves very well.

3.3.3 *Other Performance Measures – Mutual Information, Achieved Rate, and Outage Probability*

In this section, the mutual information, the achieved channel rate, and the outage probability are derived for the proposed E-DF.

The mutual information is a measure of the reliability of communications between communicating terminals. The mutual information for the E-DF scheme in terms of the channel fades can be given as [106]

$$I_{E-DF}\left(\mathbf{H}\right) = \frac{1}{2}\log_2\left(1 + SNR\left(\mathbf{H}\right)\right) \tag{3.42}$$

where $SNR\left(\mathbf{H}\right)$ is the instantaneous signal-to-noise ratio. Using the expression of the overall $SNR\left(\mathbf{H}\right)$ in Equation (3.21) yields,

$$I_{E-DF}\left(\mathbf{H}\right)=\frac{1}{2}\log_2\left(1+\gamma_1\left(\mathbf{H}\right)+\gamma_2\left(\mathbf{H}\right)\right)$$
$$=\frac{1}{2}\log_2\left(1+\gamma\left(\frac{\left|\left|h_{eNB}\right|^2+\eta^2h_{RN_2}^*h_{RN_1}\right|^2}{\left(\left|h_{eNB}\right|^2+\eta^2\left|h_{RN_1}\right|^2\right)}+\frac{\left|2\left|h_{eNB}\right|^2+\eta^2h_{RN_2}^*h_{RN_1}\right|^2}{\left(2\left|h_{eNB}\right|^2+\eta^2\left|h_{RN_2}\right|^2\right)}\right)\right) \quad (3.43)$$

The outage probability for the E-DF relay scheme is defined as the probability that the mutual information between terminals is less than the channel rate $\mathfrak{R}$ [106]. Hence, the outage event is equivalent to

$$\Pr\left[I_{E-DF}\left(\mathbf{H}\right)<\mathfrak{R}\right]=\Pr\left[\frac{1}{2}\log_2\left(1+\gamma\left(\frac{\left|\left|h_{eNB}\right|^2+\eta^2h_{RN_2}^*h_{RN_1}\right|^2}{\left(\left|h_{eNB}\right|^2+\eta^2\left|h_{RN_1}\right|^2\right)}+\frac{\left|2\left|h_{eNB}\right|^2+\eta^2h_{RN_2}^*h_{RN_1}\right|^2}{\left(2\left|h_{eNB}\right|^2+\eta^2\left|h_{RN_2}\right|^2\right)}\right)\right)<\mathfrak{R}\right]$$

or

$$\Pr\left[I_{E-DF}\left(\mathbf{H}\right)<\mathfrak{R}\right]=\Pr\left[\gamma\left(\frac{\left|\left|h_{eNB}\right|^2+\eta^2h_{RN_2}^*h_{RN_1}\right|^2}{\left(\left|h_{eNB}\right|^2+\eta^2\left|h_{RN_1}\right|^2\right)}+\frac{\left|2\left|h_{eNB}\right|^2+\eta^2h_{RN_2}^*h_{RN_1}\right|^2}{\left(2\left|h_{eNB}\right|^2+\eta^2\left|h_{RN_2}\right|^2\right)}\right)<2^{2\mathfrak{R}}-1\right] \quad (3.44)$$

3.4 Special Scenarios

In the following, we consider two special scenarios when some of the channel links in the E-DF network are not available. One scenario represents the conventional DF scheme and another scenario represents the non-relay scheme. For each scenario we derive the mutual information, the achieved channel rate, and the outage probability measures and use it for comparison with the E-DF scheme.

3.4.1 *Scenario One*: *The Conventional DF Scheme*

In this scenario, the link between the base station and one of the assistant relays is blocked by, for example, an obstacle as seen in Figure 3.11 (a) when RN_1 is unavailable and in Figure 3.11 (b) when RN_2 is unavailable. In this scenario, the unavailable relay is unable to perform any signal relaying to the mobile station,

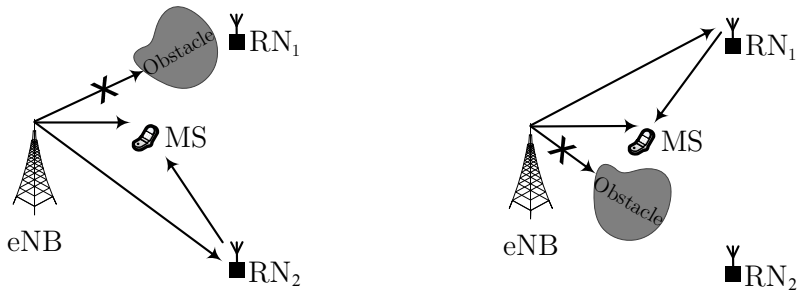

(a) $\sigma^2_{RN_1} = 0$ **(b)** $\sigma^2_{RN_2} = 0$

Figure 3.11: Demonstration of the conventional DF when either one of the relays is not available due to obstacles.

therefore, the transmission to the mobile station is achieved by the base station and the available relay. This scenario represents the conventional DF scheme.

In this scenario, the overall instantaneous SNR is given as

$$SNR(\mathbf{H})\big|_{DF} = \begin{cases} \dfrac{P_{eNB}\left|h_{eNB}\right|^2}{\sigma^2_{w_1}} + \dfrac{P_{RN}\left|h_{RN_2}\right|^2}{\sigma^2_{w_3}}, & \sigma^2_{RN_1} = 0 \\ \dfrac{P_{eNB}\left|h_{eNB}\right|^2}{\sigma^2_{w_1}} + \dfrac{P_{RN}\left|h_{RN_1}\right|^2}{\sigma^2_{w_2}}, & \sigma^2_{RN_2} = 0 \end{cases}$$

and the mutual information is obtained as

$$I_{DF}\left(\mathbf{H}\right) = \frac{1}{2}\log_2\left(1 + SNR(\mathbf{H})\big|_{DF}\right) = \begin{cases} \dfrac{1}{2}\log_2\left(1 + \dfrac{P_{eNB}\left|h_{eNB}\right|^2}{\sigma^2_{w_1}} + \dfrac{P_{RN}\left|h_{RN_2}\right|^2}{\sigma^2_{w_3}}\right), & \sigma^2_{RN_1} = 0 \\ \dfrac{1}{2}\log_2\left(1 + \dfrac{P_{eNB}\left|h_{eNB}\right|^2}{\sigma^2_{w_1}} + \dfrac{P_{RN}\left|h_{RN_1}\right|^2}{\sigma^2_{w_2}}\right), & \sigma^2_{RN_2} = 0 \end{cases}$$

Hence, the outage probability is equivalent to

$$\Pr\left[I_{DF}\left(\mathbf{H}\right)<\Re\right]=\begin{cases}\Pr\left[\left(\dfrac{P_{eNB}\left|h_{eNB}\right|^2}{\sigma_{w_1}^2}+\dfrac{P_{RN}\left|h_{RN_2}\right|^2}{\sigma_{w_3}^2}\right)<2^{2\Re}-1\right], & \sigma_{RN_1}^2=0\\ \Pr\left[\left(\dfrac{P_{eNB}\left|h_{eNB}\right|^2}{\sigma_{w_1}^2}+\dfrac{P_{RN}\left|h_{RN_1}\right|^2}{\sigma_{w_2}^2}\right)<2^{2\Re}-1\right], & \sigma_{RN_2}^2=0\end{cases} \tag{3.45}$$

3.4.2 *Scenario Two: Non-Relay Scheme*

In this scenario, the links between the base station and the two potential relays are blocked as shown in Figure 3.12. In this scenario, the relay nodes are unable to forward any information from the base station to the mobile station, therefore, the transmission to the mobile station is achieved by the base station only. This scenario represents the conventional direct transmission or non-relay scheme.

In this scenario, the instantaneous *SNR* for non-relay scheme is given as

$$SNR\left(\mathbf{H}\right)\Big|_{Non-relay}=\frac{P_{eNB}\left|h_{eNB}\right|^2}{\sigma_{w_1}^2}$$

and the associated mutual information is given as

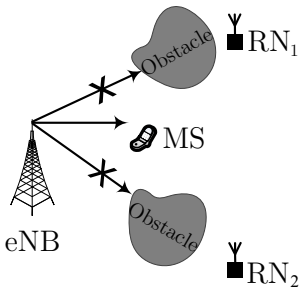

Figure 3.12: Demonstration of direct transmission or non-relay scheme when $\sigma_{RN_1}^2=\sigma_{RN_2}^2=0$.

$$I_{Non-relay}\left(\mathbf{H}\right)=\frac{1}{2}\log_2\left(1+SNR\left(\mathbf{H}\right)\Big|_{Non-relay}\right)=\frac{1}{2}\log_2\left(1+\frac{P_{eNB}\left|h_{eNB}\right|^2}{\sigma_{w_1}^2}\right)$$

Hence, the outage event is equivalent to

$$\Pr\left[I_{Non-relay}\left(\mathbf{H}\right)<\Re\right]=\Pr\left[\frac{P_{eNB}\left|h_{eNB}\right|^2}{\sigma_{w_1}^2}<2^{2\Re}-1\right] \tag{3.46}$$

Figure 3.13 illustrates the outage probability versus γ for the E-DF, the conventional DF and non-relay schemes. The outage probability is evaluated for each scenario as a function of the γ at a fixed spectrum efficiency of 2bps/Hz. The results are obtained by generating 1×10^7 channel realizations for h_{eNB}, h_{RN_1} and

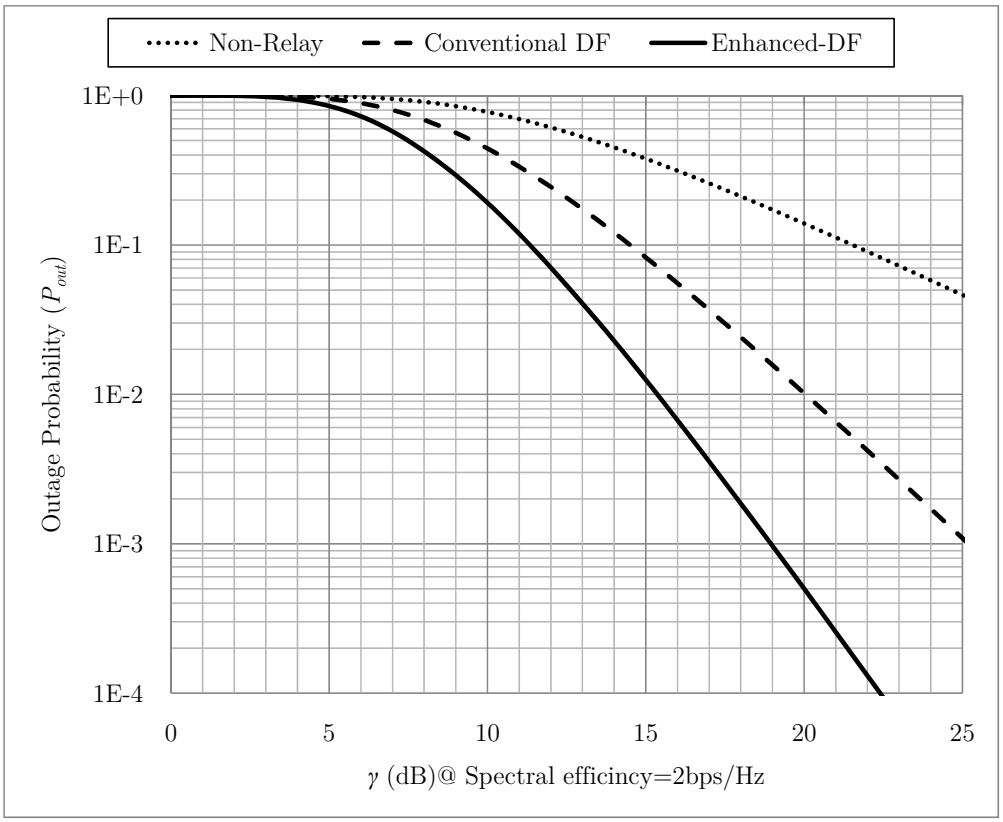

Figure 3.13: P_{out} versus γ for the E-DF, the conventional DF and the non-relay schemes assuming spectral efficiency = 2bps/Hz, $\sigma_{eNB}^2=1$, $\sigma_{RN_1}^2=0.9$ and $\sigma_{RN_2}^2=0.8$.

h_{RN_2} with variances of $\sigma^2_{eNB} = 1$, $\sigma^2_{RN_1} = 0.9$, and $\sigma^2_{RN_2} = 0.8$, respectively. For each channel realization, Equations (3.44), (3.45), and (3.46) are used to evaluate the outage probability for the E-DF, the conventional DF and the non-relays schemes, respectively. The figure shows that the outage probability is high for poor link strength and decays for all scenarios whenever the link strength improves. The E-DF scheme shows the lowest outage probability followed by the conventional DF while the worst of all is the non-relay scheme. For example, at 20 dB *SNR*, the outage probability for E-DF scheme is 5×10^{-4}, for conventional DF is 1×10^{-2} and for non-relay scheme is 0.14. This is an improvement of approximately 2 orders of magnitude over the conventional DF. This low outage probability is due to the high overall *SNR* comes from diversity when utilizing the E-DF compared to the conventional DF and the non-relay schemes.

Figure 3.14 illustrates the outage probability versus spectral efficiency (bps/Hz) for the E-DF, the conventional DF and direct transmission schemes. The outage probability is evaluated for each scenario as a function of the spectral efficiency at $\gamma = 20$dB. The results are obtained by generating 1×10^7 channel realizations for h_{eNB}, h_{RN_1}, and h_{RN_2} with variances of $\sigma^2_{eNB} = 1$, $\sigma^2_{RN_1} = 0.9$, and $\sigma^2_{RN_2} = 0.8$, respectively. For each channel realization, Equations (3.44), (3.45) and (3.46) are used to evaluate the P_{out} for the E-DF, the conventional DF, and the non-relays schemes, respectively. The figure shows that the outage probability increases with the spectral efficiency. The proposed E-DF scheme shows the least outage probability when increasing the spectral efficiency.

The analytical results show that the proposed E-DF cooperative relaying protocol outperforms the conventional DF protocol and the non-relay scheme in terms of error rate performance and outage probability performance.

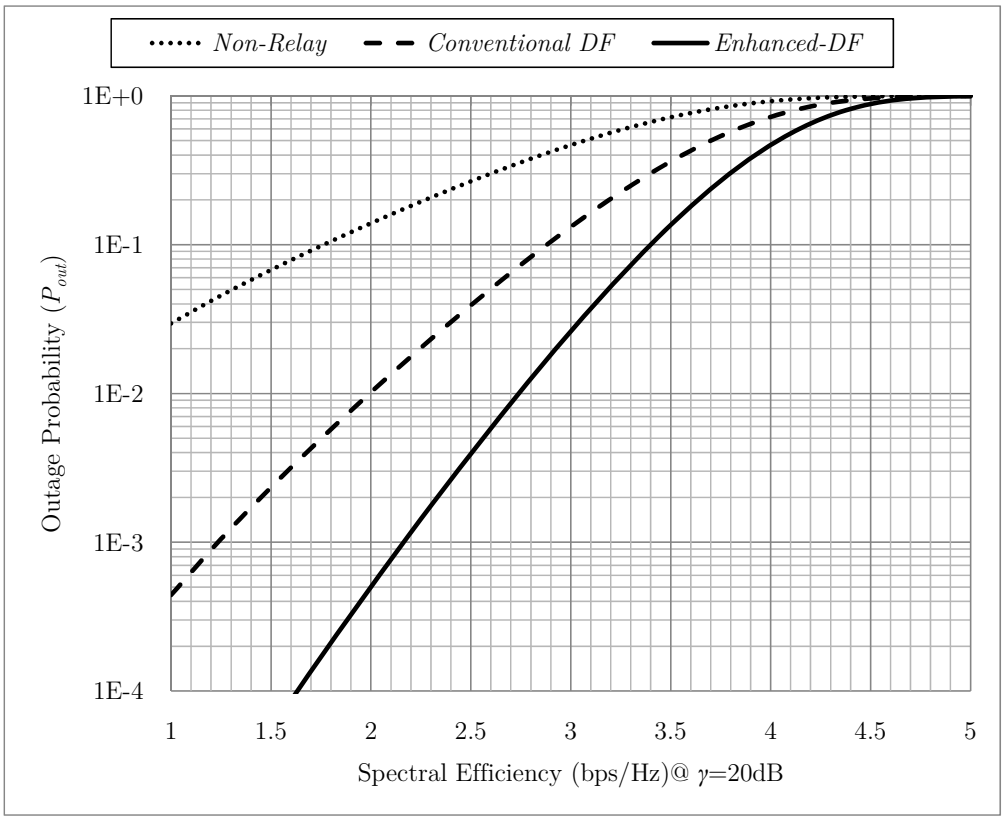

Figure 3.14: P_{out} versus spectral efficiency for the E-DF, the conventional DF and the non-relay schemes assuming: $\gamma = 20dB$, $\sigma^2_{eNB}=1$, $\sigma^2_{RN_1}=0.9$ and $\sigma^2_{RN_2}=0.8$.

3.5 Chapter Summary

In this chapter, the conventional decode-and-forward relaying protocol is enhanced to achieve higher data rate with diversity. The system model for the proposed enhanced-DF (E-DF) was presented by showing the input-output relation. Also, a modified maximum likelihood decoder is proposed for decoding the received signals over a quasi-static fading channel. In order to study the performance of the proposed protocol and the decoder, the average symbol error rate expression is derived from the moment generating function by averaging the signal-to-noise ratio

for the decoder over Rayleigh fading channel. Based on the average *SNR* expression, a worse-case *SER* and its approximate expressions were obtained for the E-DF. In addition, other information theoretic measures such as mutual information, the achieved channel rate and the outage probability were also derived. Finally, simulations were conducted to validate the E-DF scheme. The simulations showed significant improvement for the proposed E-DF protocol over the conventional DF and the non-relay schemes.

Chapter Four: Omni-Relay (OR) Scheme-Aided LTE-A Communication Systems

4.1 Introduction

Cellular systems are considered advanced technologies that offer very high capacity in a limited spectral allocation. This is achieved by reusing the available frequencies in a regular pattern of areas, called *cells*, each covered by one base station. To ensure that the interference from other cells, or inter-cell interference (ICI), stays below a destructive level, it is essential to allocate different frequency bands or channels to adjacent cells so that their coverage can overlap slightly without causing harmful interference. In this way cells can be grouped together in what is termed a *cluster*.

In cellular systems, the number of distinct frequency sets used per cluster is called *frequency reuse factor* (*FRF*) [112]. *FRF* is chosen such that the effect of ICI is reduced to minimum. Figure 4.1 shows three examples of *FRF* patterns, where $FRF = 1$, 3 and 7. For $FRF = 1$, Figure 4.1 (a), the available frequencies allocated to each cell are the same in each cell. For $FRF = 3$, the available frequencies are divided into 3 sets, namely f_1, f_2 and f_3, each set is allocated to one cell such that the surrounding cells carry different sets of frequencies, as shown in Figure 4.1 (b). Similarly, in pattern $FRF = 7$, the available frequencies are divided into 7 sets, f_i, $i = 1,2,\ldots 7$, and allocated as shown in Figure 4.1 (c).

There is a strong relationship between *FRF* and the effect of ICI. Utilizing a high value of *FRF* results in increased separation between adjacent or nearest co-channel cells and hence reduction in ICI. Higher *FRF* would mean less number of available channels per cell, lower spectral efficiency, but reduced ICI due to increased distance between co-channel cells.

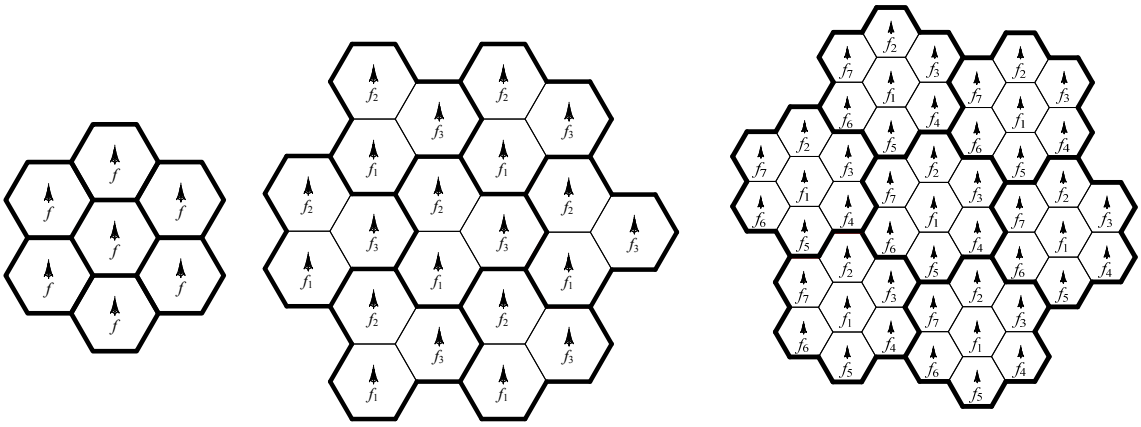

(a) $FRF = 1$ **(b)** $FRF = 3$ **(c)** $FRF = 7$

Figure 4.1: Examples of frequency reuse factor (FRF).

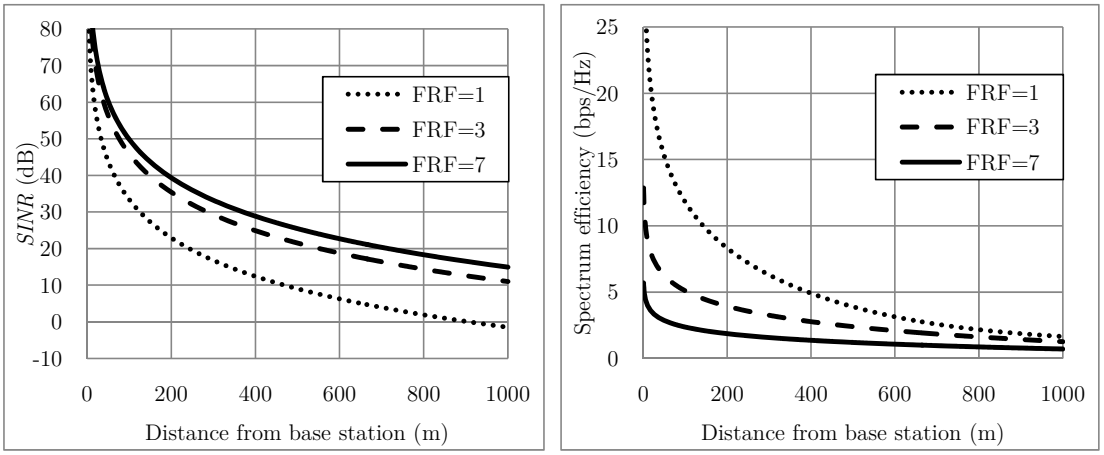

(a) $SINR$ vs distance (b) Spectrum efficiency vs distance

Figure 4.2: The effect of frequency reuse factor on $SINR$ and spectrum efficiency.

In order to illustrate the effect of FRF on the ICI and the cell spectral efficiency, the theoretical downlink signal to interference plus noise ratio ($SINR$) and spectral efficiency performances are demonstrated in Figure 4.2 (a) and (b) for a mobile station (MS) that moves from the base station (BS) toward the edge of the cell. The graphs are obtained for systems with $FRF = 1$, 3 and 7. In Figure 4.2 (a), the signal to interference plus noise ratio ($SINR$ (dB)) is plotted when varying the

distance (m) from the base station, and in Figure 4.2 (b) the spectral efficiency (bps/Hz) is plotted versus distance (m). The distance represents the movement of the MS from BS to the cell edge. As observed in Figure 4.2 (a), for systems utilizing $FRF = 1$, 3 and 7, the *SINR* is reduced as the distance between the BS and the MS increases. This is due to the reduction in the received power as the distance increases and the increase in the interference from the co-channel cells. However, the system with $FRF = 7$ provides the highest *SINR*, followed by $FRF = 3$ and $FRF = 1$. This is due to the increased separation between the adjacent co-channel cells. Figure 4.2 (b), shows the corresponding cell spectrum efficiency for the systems. The figure shows that the system with $FRF = 1$ provides the highest spectral efficiency. This is because the system with $FRF = 1$ utilizes the entire available download bandwidth, while $FRF = 3$ and $FRF = 7$ utilize $\frac{1}{3}$ and $\frac{1}{7}$ of the available bandwidth, respectively.

Hence, the spectral efficiency of a cellular system is limited by two main factors – the ICI in a wireless propagation channel and the *FRF* of a system.

4.1.1 *Motivation*

Future wireless systems promise very high data rates per user over high bandwidth channels. An example is the long term evolution-advanced (LTE-A) system that requires high peak rate for uplink and downlink as well as high spectral efficiency as shown in Table 4.1 [109].

Claude Shannon [113] and *Ralph Hartley* [114] provided the following relationship between capacity, bandwidth, *FRF* and *SINR*

$$C = \left(\frac{\text{Total Bandwidth}}{FRF} \right) \log_2 \left(1 + SINR\right) \tag{4.1}$$

According to Equation (4.1), channel capacity is increased by increasing the total available bandwidth, and/or *SINR*. Increasing *FRF*, on the other hand, decreases

Table 4.1: LTE-A requirements.

		Downlink	**Uplink**
Peak data rate		1 Gbps	500 Mbps
Spectral efficiency (4 antennas eNB, 2 antennas MS)	**Peak**	30 bps/Hz	15 bps/Hz
	Average	2.6 bps/Hz	2.0 bps/Hz
	Cell-edge	0.09 bps/Hz	0.07 bps/Hz

the capacity. For $FRF = 1$, the *SINR* degrades due to propagation path loss, while ICI increases as the MS moves closer to an adjacent base station that employs the same frequencies as in the serving base station. The issue becomes critical when the mobile station approaches the cell-edge region where the received signal strength is low and the ICI is high.

Based on these issues, we propose the use of relay terminals at the cell edge. Each relay terminal is equipped with an omni-directional antenna. Our objectives are to reduce the effect of interference stemming from adjacent cells and increase the desired signal level. In addition, we propose a data frame structure for the edge relay terminals that is compatible with the LTE-A standard. To validate the performance of the proposed structure, we conduct analyses of the average *SINR* and the average capacity, and compare with the conventional universal frequency reuse factor (UFRF) scheme.

Chapter 4 is organized as follows. Section 4.2 focuses on the conventional universal frequency reuse factor (UFRF) scheme. It discusses the system model and analyses of the average *SINR* and the average capacity. Section 4.3 presents the proposed topology for the LTE-A system. It includes a description of the system model, a proposed frame structure that is compatible with LTE-A standard, and analyses of the average *SINR* and the average capacity. Finally, Section 4.4 provides analytical and simulation performance results for the conventional UFRF and the proposed topology.

4.2 Universal Frequency Reuse Factor (UFRF) Scheme

The universal frequency reuse factor scheme, or simply UFRF scheme, is a scheme that utilizes $FRF = 1$ in allocating the frequency resources. This scheme is included in the 3GPP standard [104] in order to meet the LTE-A system requirement. In the following, the UFRF system model is presented together with an analysis of the average *SINR* and the average capacity.

4.2.1 *System Model*

The UFRF scheme is illustrated in Figure 4.3 for a 7-cell reuse cluster. In the UFRF the entire available frequency resources are allocated to each cell. In other words, each base station utilizes the same frequency resources as its neighboring base stations for uplink and downlink transmission. In the LTE-A standard, the base station is referred to as evolved-node base station (eNB).

During the downlink transmission, the MS users suffer from strong ICI signals from the co-channel eNBs particularly MS users at the edge of the cell where the desired signal level is low and the interference level is high.

When the MS is moving from one cell to another, service is switched from the

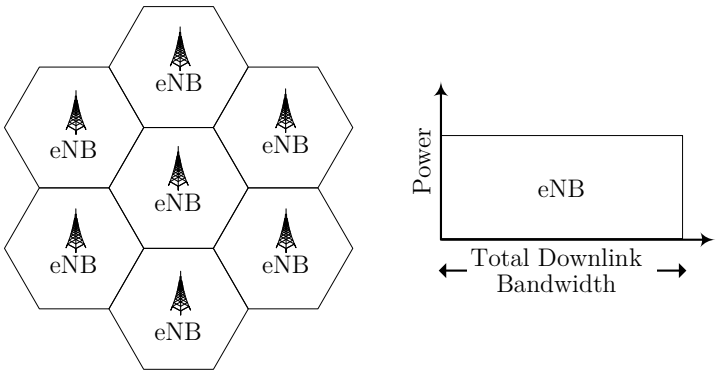

Figure 4.3: Universal frequency reuse factor (UFRF) system model.

serving eNB to a new host or 'target' eNB by performing handover without interruption in service. Handover in LTE-A standard, according to [115,116], is initiated by the MS. The MS periodically performs downlink radio channel measurements for link power. If the received power at the mobile station drops below certain threshold, the MS sends the corresponding measurement. Based on these measurement, the serving eNB initiates handover preparation that involves exchanging of signaling between serving and target eNB. Upon successful handover preparation, the handover decision is made and consequently the handover command is sent to the MS and the connection between MS and the serving cell is released.

4.2.2 *Performance Analysis*

In this section, we provide analyses for the signal to interference plus noise ratio (*SINR*) and the capacity for UFRF scheme. The analyses are carried out under the following assumptions.

1. Only downlink *SINR* and capacity analyses are considered. The uplink performance has received much attention in many researches.

2. The path loss model is given by [106]

$$PL(d) = d^{\upsilon}\left(\frac{4\pi f_c}{c_o}\right)^2 \tag{4.2}$$

   where d is the distance between the eNB and the MS in kilometers, υ is the path loss factor, f_c the carrier frequency in MHz and c_o is the speed of light.

3. The channel between any two terminals is modeled as Rayleigh flat fading channel.

4. For analytical convenience, mobile users are distributed uniformly within a cell. This assumption was considered in [63] when deriving area spectral efficiency of cellular mobile radio systems.

5. The case where the MS is receiving interference from all co-channel cells in the first two tiers is considered as the *worse-case*.

6. Based on the 3GPP standard, *M*-ary phase shift keying (MPSK) is chosen to be the modulation scheme for the system.

7. The noise is modeled as additive white Gaussian noise (AWGN) with zero-mean and variance σ_w^2.

4.2.2.1 Average *SINR* Analysis for the UFRF Scheme

Analysis of the average *SINR* for UFRF scheme only takes into account interference from the first two tiers co-channel eNBs. This is because the first two tiers of co-channel eNBs contribute significant interference. The average *SINR* analysis includes obtaining the instantaneous *SINR* and then averaging over the distance and the channel realizations.

Figure 4.4 shows 6 interferers in tier 1 and 6 interferers in tier 2. Interference from these two tiers shall be referred to as the worse-case. The worse-case instantaneous *SINR* for the UFRF scheme is defined as

$$SINR_{UFRF} \triangleq \frac{P_r}{I+N} \tag{4.3}$$

where P_r is the received signal power from the desired serving eNB, I is total instantaneous interference power from other eNBs and N is the noise power. P_r can be written as

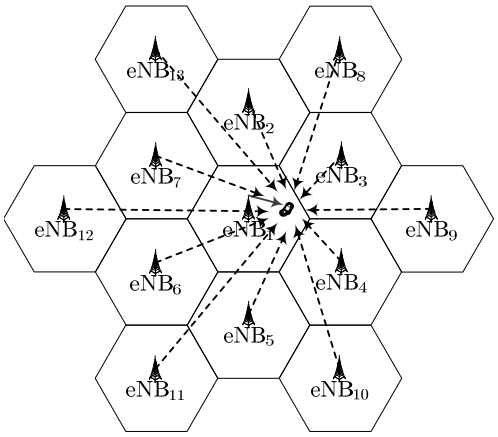

Figure 4.4: Illustration of ICI from co-channel eNBs.

$$P_r\left(\chi_{MS}, h_{MS}, d_{MS}\right) = \frac{\sqrt{P_{eNB}}\left|h_{MS}\right|^2}{\chi_{MS}\ PL\left(d_{MS}\right)} \tag{4.4}$$

where P_{eNB} is the transmitted power at the base station, h_{MS} is the small-scale fading channel coefficient between eNB and MS, χ_{MS} is a log-normal shadow coefficient, and $PL\left(d_{MS}\right)$ is the path loss function provided in Equation (4.2) for a mobile station located at distance d_{MS} (km) from eNB. In Equation (4.4), h_{MS} is modeled as a complex Gaussian random variable with zero-mean and variance σ^2_{MS}, and the log-normal shadow coefficient χ_{MS} has zero-mean and variance σ^2_{χ}. The term $I+N$ is the summation of the interference level from each interfering eNB plus noise power, when the mobile station is located at the cell edge, and is expressed as

$$I\left(\chi_i, h_i\right) + N = \sum\nolimits_{i=1}^{12}\left(\frac{\sqrt{P_{eNB}}\left|h_i\right|^2}{\chi_i\ PL\left(d_i\right)}\right) + \frac{BD}{U} \tag{4.5}$$

where d_i is the distance from the i^{th} interfering eNB (i =1,2,…,12) to a MS located at the edge of the cell, h_i is a channel coefficient between the i^{th} interfering eNB and MS, χ_i is a log-normal shadow coefficient, B (MHz) is the entire available downlink bandwidth, D (watt.user/Hz) is the per-user noise power spectral density

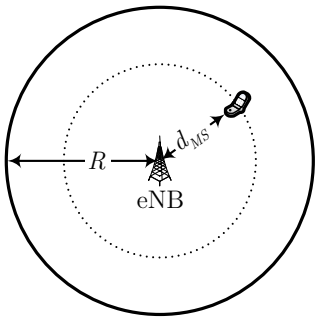

Figure 4.5: MS being at a distance of d_{MS} from *eNB*.

level and U is the average number of MSs users in each cell. For the worse-case interference, d_i is given as [65]

$$d_i = \left\{ \underbrace{R, R, 2R, 2R, \sqrt{7}R, \sqrt{7}R}_{First\ Tier}, \underbrace{2R, 4R, \sqrt{7}R, \sqrt{7}R, \sqrt{13}R, \sqrt{13}R}_{Second\ Tier} \right\}$$

In Equation (4.5), each instantaneous interference power level depends only on the random channel coefficients and the log-normal shadow coefficients. The instantaneous *SINR* is obtained by substituting Equations (4.4) and (4.5) into Equation (4.3) which yields,

$$SINR_{UFRF}(\chi, h, d_{MS}) = \frac{\dfrac{\sqrt{P_{eNB}}|h_{MS}|^2}{\chi_{MS} PL(d_{MS})}}{\sum_{i=1}^{12}\left(\dfrac{\sqrt{P_{eNB}}|h_i|^2}{\chi_i PL(d_i)}\right) + \dfrac{BD}{U}} = \frac{d_{MS}^{-\upsilon}}{a_{UFRF}(\chi, h)} \tag{4.6}$$

where

$$a_{UFRF}(\chi, h) = \frac{\chi_{MS}}{|h_{MS}|^2}\left(\sum_{i=1}^{12}\left(\frac{|h_i|^2 d_i^{-\upsilon}}{\chi_i}\right) + \frac{BD}{U\sqrt{P_{eNB}}}\left(\frac{4\pi f_c}{c_o}\right)^2\right)$$

is conditioned on random channel gains $h = \{h_{MS}, h_i\}$ and log-normal shadowing coefficients $\chi = \{\chi_{MS}, \chi_i\}$. In the following, we shall average over d_{MS} and consider the *SINR* conditioned on χ and h.

Since the MSs are assumed to be randomly distributed within a cell in a ring-like pattern (Figure 4.5), the probability density function (*PDF*) for an MS being at a distance of d_{MS} from eNB may be defined as [108]

$$f\left[d_{MS}\right] \triangleq \frac{\text{The circumference of a circle with diameter } d_{MS}}{\text{Total area of the cell}} = \frac{2\pi d_{MS}}{\pi R^2} = \frac{2d_{MS}}{R^2}, \quad 0 \le d_{MS} \le R \tag{4.7}$$

where R is the cell radius in km. The average of $SINR_{UFRF}$ conditioned on χ and h is defined as,

$$\overline{SINR}_{UFRF}\left(\chi,h\right) = E\left[SINR_{UFRF}\right] \triangleq \int_0^R SINR_{UFRF}\left(\chi,h,d_{MS}\right)\ f\left[d_{MS}\right]\ \mathrm{d}d_{MS}$$

Using the expression in Equation (4.7) for $f\left[d_{MS}\right]$ and integrating, we obtain

$$\overline{SINR}_{UFRF}\left(\chi,h\right) = \int_0^R \frac{2d_{MS}^{1-\upsilon}}{R^2\ a_{UFRF}\left(\chi,h\right)}\ \mathrm{d}d_{MS} = \frac{2R^{-\upsilon}}{\left|2-\upsilon\right|\ a_{UFRF}\left(\chi,h\right)} \tag{4.8}$$

Due to the difficulty in averaging the above expression over the channel and the shadowing parameters χ and h, we resort to Monte-Carlo method.

4.2.2.2 Average Capacity Analysis for UFRF

To determine the average capacity, we first need to find the relation between the capacity and d_{MS}. In the UFRF scheme, the instantaneous capacity, conditioned on channel coefficients, shadowing coefficients, and distance d_{MS}, can be expressed as [113,114]

$$C_{UFRF}\left(\chi,h,d_{MS}\right) = B\log_2\left(1+SINR_{UFRF}\left(\chi,h,d_{MS}\right)\right) = BQ_{UFRF}\left(\chi,h,d_{MS}\right) \tag{4.9}$$

where

$$Q_{UFRF}\left(\chi,h,d_{MS}\right)=\log_2\left(1+SINR_{UFRF}\left(\chi,h,d_{MS}\right)\right) \tag{4.10}$$

is the instantaneous spectral efficiency in bps/Hz. Using the expression for $SINR_{UFRF}\left(\chi,h,d_{MS}\right)$ in Equation (4.6), Equation (4.10) becomes

$$Q_{UFRF}\left(\chi,h,d_{MS}\right)=\log_2\left(1+\frac{d_{MS}^{-\upsilon}}{a_{UFRF}\left(\chi,h\right)}\right)$$

The average spectral efficiency $\overline{Q}_{UFRF}\left(\chi,h\right)$, conditioned on χ and h, for the UFRF scheme is obtained by using $f\left[d_{MS}\right]$ in Equation (4.7) and integrating as

$$\begin{aligned}\overline{Q}_{UFRF}\left(\chi,h\right)&=E\left[Q_{UFRF}\right]\triangleq\int_0^R Q_{UFRF}\left(\chi,h,d_{MS}\right)f\left[d_{MS}\right]\mathrm{d}d_{MS}\\&=\frac{2\left(R^{-\gamma}+a_{UFRF}\right)^{\frac{\upsilon-2}{\upsilon}}-2a_{UFRF}^{\frac{\upsilon-2}{\upsilon}}\left(\chi,h\right)}{\left|\upsilon-2\right|R^2\log\left(2\right)a_{UFRF}\left(\chi,h\right)}\end{aligned} \tag{4.11}$$

The conditional average capacity is given by

$$\overline{C}_{UFRF}\left(\chi,h\right)=B\overline{Q}_{UFRF}\left(\chi,h\right)=\frac{2B\left(R^{-\upsilon}+a_{UFRF}\right)^{\frac{\upsilon-2}{\upsilon}}-2Ba_{UFRF}^{\frac{\upsilon-2}{\upsilon}}\left(\chi,h\right)}{\left|\upsilon-2\right|R^2\log\left(2\right)a_{UFRF}\left(\chi,h\right)} \tag{4.12}$$

Due to the difficulty in averaging the above over the channel and the shadowing parameters, we resort to Monte-Carlo simulation.

In general, *SINR* and C_{UFRF} degrade as the MS approaches the cell edge. The following section presents a proposed communication scheme that is designed to improve the desired signal quality at cell edges, reduce interference, and increase capacity.

4.3 The Omni-Relay (OR) Scheme

4.3.1 *Introduction*

In the UFRF scheme, the system suffers severely from ICI particularly at the cell edges. The high ICI together with the weak received signal have significant impact on the *SINR* and, consequently, the capacity. One technique to improve signal reception in the cell-edge region is to create smaller and simpler transmit/receive terminals, called relay nodes (RN), that are placed at the edges of the cell. These nodes are connected to the host base station by, for example, cables. RN can capture the signal from the host eNB and relay it to cell-edge users. Here, each relay is assumed to be equipped with an omni-directional antenna. *We shall refer to this as Omni-Relay* (*OR*) *scheme*. Following is a description of the OR system model together with a proposed frame structure design for relay nodes. Finally, the analyses of the average *SINR* and the average capacity are conducted for the OR scheme.

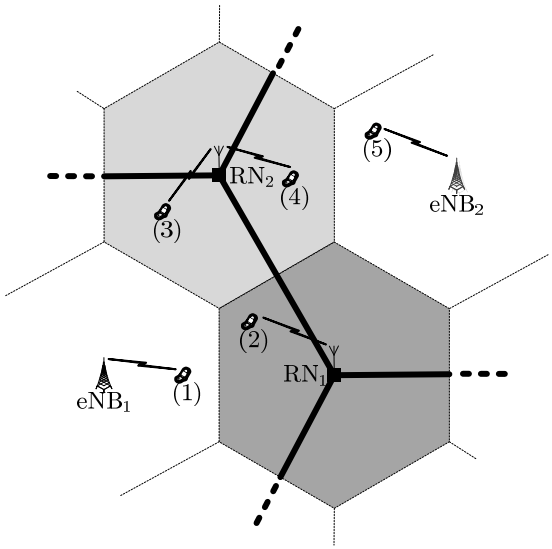

Figure 4.7: Examples of handover scenarios.

4.3.2 *System Model*

The omni-relay (OR) scheme is illustrated in Figure 4.6. The model assumes that the entire available downlink bandwidth is divided into three segments, namely, f_1, f_2, and f_3. Segment f_1 is allocated to each eNB, whereas f_2 and f_3 are assigned to the relay terminals as illustrated in Figure 4.6. Each cell is surrounded by six-Type I relay nodes each being equipped with an omni-directional antenna. According to the LTE-A standard [91], Type I relays are assigned different frequency resources from the host eNB and have their own reference signals and control information. The frequency resources, f_2 and f_3, at each relay are assigned such that, for each two consecutive relays, different frequency segments are used. The assignment of frequency resources in this way reduces interference resulting from the use of omni-directional antennas.

In Figure 4.6, we shall refer to unshaded areas as *inner regions* and shaded areas as *outer regions*. Consequently, users of the OR scheme shall be classified into *inner MSs* and *outer MSs*. Inner MS users are located within the eNB transmission range

and are served directly by one of the eNBs. On the other hand, outer MS users are located within RN transmission ranges and are served by one of the RNs at the cell edges.

The serving terminal in the OR scheme is either the eNB or one of the RNs at the cell edges. A serving terminal can be determined based on the link power between the MS and the eNB or the MS and one of candidate relays. When the link power drops below a certain threshold, the MS initiates the handover. Figure 4.7 shows several scenarios when MS is moving from one cell to another traversing two relays. Let an MS be located within the transmission range of eNB_1 as shown at location **(1)**. When the MS moves toward the RN_1 transmission range, location **(2)**, the MS informs eNB_1 that RN_1 is the future serving terminal. Therefore, eNB_1 starts transmitting to RN_1 instead of MS while RN_1 relays to MS. When MS moves to location **(3)**, where RN_2 provides stronger link power, eNB_1 stops transmitting to RN_1 and switches to RN_2 which in turn relays to MS. At locations, **(1)**, **(2)** and **(3)**, eNB_1 is the serving base station for MS, RN_1, and RN_2, respectively. The procedure is similar for location **(4)** where eNB_2 transmits to RN_1 and RN_2 forwards to MS, while eNB_2 transmits directly to MS in location **(5)**.

4.3.3 *Frame Structure Design for Relay Transmission*

The LTE-A standard provides seven frame pattern configurations for the downlink eNB to MS and the uplink MS to eNB but not for the RN [103]. In this section, we propose a frame structure for relay terminals. The frame structure is designed to be fully compatible with TD-LTE systems, as shown in Figure 4.8 using the *Configuration* 2 *Frame Pattern* [117]. The justification behind using the *Configuration* 2 *Frame Pattern* is that the frame pattern supports more downlink sub-frames than other configurations, therefore, we can achieve higher downlink data.

For the *Configuration* 2 *Frame Pattern*, each radio frame consists of two half-frames with length $T_f = 153600\ T_s = 5ms$. Each half-frame consists of eight slots and three special fields, namely, downlink pilot timeslot (DwPTS), Guard period (GP), and uplink pilot timeslot (UpPTS). For the proposed RN frame, we combine two time slots into one sub-frame, i.e., for any sub-frame ξ, it consists of slots 2ξ and 2ξ +1. This combining is originally used for the conventional eNB and MS frame. Sub-frames 0, 5 and DwPTS are always reserved for the downlink transmissions. As seen in Figure 4.8, most sub-frames are reserved for downlink channels, where six sub-frames are reserved for downlink and two sub-frames are reserved for uplink. It is noted that there are two sub-frames for DwPTS, GP, and UpPTS. Every sub-frame has one long arrow and one short arrow, where the long one indicates the link between eNBs and the inner MSs, while the short one represents the link between eNBs and RNs, or the link between RNs and outer MSs. Since the relays in the OR scheme are Type I, eNB and RN can communicate with their own MSs simultaneously.

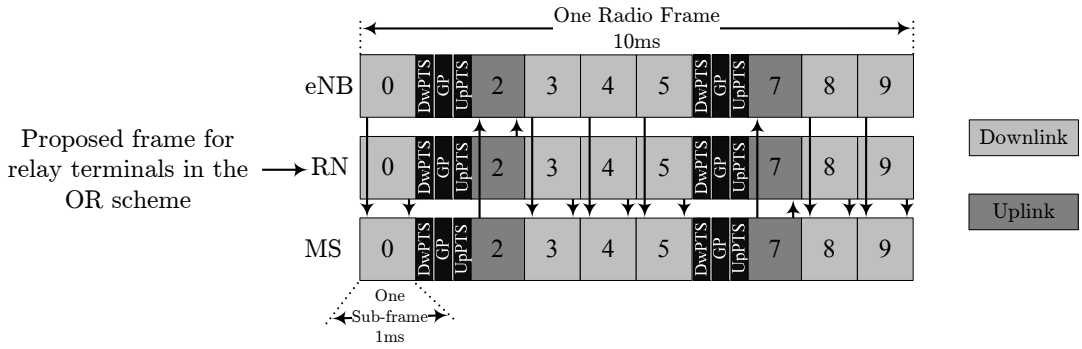

Figure 4.8: *Configuration* 2 *Frame Pattern* and proposed frame for relay terminals in the OR scheme.

4.3.4 *Performance Analysis*

In this section, the average SINR and the average capacity are analyzed for the OR scheme. The analyses are carried out for the two categories of MS users; the inner MSs and the outer MSs. The average SINR and the average capacity are used later for comparison between the conventional UFRF and the OR scheme.

Throughout the analysis, the worse-case is assumed, where during transmission from eNB to the inner MSs, there is interference from all the co-channel eNBs in the first two eNB tiers, and when the desired relay is transmitting, there is interference from all the co-channel relays in the first two relay tiers.

4.3.4.1 Average Number of Inner and Outer Users per Cell

In order to carry out the analyses of the average *SINR* and the average capacity, the average number of inner users (U_{inner}) and outer users (U_{outer}) are needed. In the following, the radius of the inner region is derived with respect to the cell radius and the ratio of RN and eNB transmitted power. The derived inner radius is

then used to determine the average number of inner and the average number of outer mobile users.

Let the transmit power be denoted by P_{eNB} for all eNBs and P_{RN} for all RNs. Also, let R denote the eNB cell radius and r the relay cell radius. Using the expression for path loss in Equation (4.2), the received instantaneous signal power from eNB at the boundary of the inner region equals

$$P_{r_{eNB}} = \frac{\sqrt{P_{eNB}}\left|h_{eNB}\right|^2}{\chi_{eNB} PL(R)} = \frac{\sqrt{P_{eNB}}\left|h_{eNB}\right|^2}{\chi_{eNB} R^{\upsilon}\left(\frac{4\pi f_c}{c_o}\right)^2} \tag{4.13}$$

where h_{RN} and χ_{eNB} are the small-scale fading channel and the log-normal shadowing coefficients, respectively. Also, the instantaneous received power from RN in the outer region equals

$$P_{r_{RN}} = \frac{\sqrt{P_{RN}}\left|h_{RN}\right|^2}{\chi_{RN} PL(r)} = \frac{\sqrt{P_{RN}}\left|h_{RN}\right|^2}{\chi_{RN} r^{\upsilon}\left(\frac{4\pi f_c}{c_o}\right)^2} \tag{4.14}$$

The power transmitted at eNB and at all RNs are set such that the received signal power at the cell boundaries of eNB and RN is the same. Therefore, equating the expressions in Equations (4.13) and (4.14), the following relation is obtained,

$$P_{r_{eNB}} = P_{r_{RN}} \rightarrow \frac{\sqrt{P_{eNB}}\left|h_{eNB}\right|^2}{\chi_{eNB} R^{\upsilon}\left(\frac{4\pi f_c}{c_o}\right)^2} = \frac{\sqrt{P_{RN}}\left|h_{RN}\right|^2}{\chi_{RN} r^{\upsilon}\left(\frac{4\pi f_c}{c_o}\right)^2} \rightarrow \left(\frac{r}{R}\right)^{\upsilon} = \frac{\sqrt{P_{RN}}\left|h_{RN}\right|^2 \chi_{eNB}}{\sqrt{P_{eNB}}\left|h_{eNB}\right|^2 \chi_{RN}} \tag{4.15}$$

Let η denote the ratio of P_{RN} and P_{eNB} as defined in Chapter 3, and let R_o denote the inner region radius, which is defined as $R_o \triangleq R - r$, as shown in Figure 4.9, therefore,

$$\left(\frac{R - R_o}{R}\right)^{\upsilon} = \sqrt{\eta}\frac{\left|h_{RN}\right|^2 \chi_{eNB}}{\left|h_{eNB}\right|^2 \chi_{RN}} \tag{4.16}$$

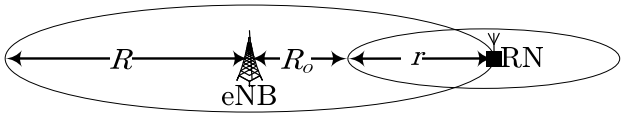

Figure 4.9: eNB and RN transmission range.

Equation (4.16) can be rewritten as

$$R_o = R\left(1-\left(\sqrt{\eta}\,\frac{|h_{RN}|^2\,\chi_{eNB}}{|h_{eNB}|^2\,\chi_{RN}}\right)^{\frac{1}{\upsilon}}\right) \tag{4.17}$$

From Equation (4.17), the radius of the inner region is a function of the power ratio η, the cell radius, and channel and shadowing coefficients. In order to proceed to find the average number of inner and outer mobile users, the probability density functions (*PDF*) for the inner and outer mobile users and their associated cumulative distribution functions (*CDF*) are needed. We now proceed to deriving average number of inner and outer mobile users.

Let the MSs be distributed uniformly throughout the cell. This assumption is made to simplify the calculations for the the average inner and outer users per cell. The *PDF* of the inner users is obtained similar to Equation (4.7) as

$$f\left[R_o\right] \triangleq \frac{2R_o}{R^2}, \quad 0 \le R_o \le R \tag{4.18}$$

and its associated *CDF* is obtained by integrating $f\left[R_o\right]$ as,

$$f\left[R_o\right] = \int f\left(R_o\right)\mathrm{d}R_o = \int \frac{2R_o}{R^2}\,\mathrm{d}R_o = \frac{R_o^2}{R^2}, \quad 0 \le R_o \le R \tag{4.19}$$

The *CDF* of the outer users is the complement of the *CDF* of the inner users. That is

$$F\left[r\right] = 1 - F\left[R_o\right] = 1 - \frac{R_o^2}{R^2} = 1 - \frac{\left(R - r\right)^2}{R^2}, \quad R_o \le r \le R \tag{4.20}$$

$F\left[R_o\right]$ and $F\left[r\right]$ can be written in terms of the power ratio η and the channel and the shadowing coefficients by substituting the expression for R_o in Equation (4.17) into Equations (4.19) and (4.20) as

$$F_{inner}\left[\eta, h, \chi\right] = \frac{1}{R} - \frac{1}{R}\left(\sqrt{\eta}\frac{\left|h_{RN}\right|^2 \chi_{eNB}}{\left|h_{eNB}\right|^2 \chi_{RN}}\right)^{\frac{1}{\upsilon}}, \quad 0 \le R_o \le R$$

and

$$F_{outer}\left[\eta, h, \chi\right] = 1 - \frac{1}{R} + \frac{1}{R}\left(\sqrt{\eta}\frac{\left|h_{RN}\right|^2 \chi_{eNB}}{\left|h_{eNB}\right|^2 \chi_{RN}}\right)^{\frac{1}{\upsilon}}, \quad R_o \le r \le R,$$

respectively. If the average number of MSs per cell is U, the average number of inner MSs (U_{inner}) and the average outer MSs (U_{outer}) are obtained by multiplying each *CDF* with the total average number of users. That is,

$$U_{inner} = \frac{U}{R} - \frac{U}{R}\left(\sqrt{\eta}\frac{\left|h_{RN}\right|^2 \chi_{eNB}}{\left|h_{eNB}\right|^2 \chi_{RN}}\right)^{\frac{1}{\upsilon}} \quad \text{and} \quad U_{outer} = U - \frac{U}{R} + \frac{U}{R}\left(\sqrt{\eta}\frac{\left|h_{RN}\right|^2 \chi_{eNB}}{\left|h_{eNB}\right|^2 \chi_{RN}}\right)^{\frac{1}{\upsilon}} \tag{4.21}$$

respectively. This average number of inner and outer users will be used in the analysis of per-cell capacity in later sections.

4.3.4.2 Average *SINR* Analysis for Inner MSs

In this section, the average *SINR* is derived for the inner MSs. The derivation involves finding the instantaneous *SINR* and then averaging it over the distance, the channel realizations, and the log-normal shadowing coefficients. The averaging

over the distance is obtained by using the probability density function for the inner users being at distance d_{MS} from the cell base station.

Figure 4.10 illustrates the co-channel eNBs for the downlink for the inner MSs. The first two tiers of interfering eNBs are assumed the main source of ICI. The figure shows 6 eNBs interferers in the first tier and 6 eNBs interferers in the second tier. The worse-case instantaneous *SINR* for the OR schemes' inner users is

$$SINR_{inner} \triangleq \frac{P_r}{I+N} \tag{4.22}$$

where P_r is the instantaneous received signal power from the desired serving eNB, I is total instantaneous interference power from other eNBs and N is the noise power.

P_r can be written as

$$P_r\left(\chi_{MS}, h_{MS}, d_{MS}\right) = \frac{\sqrt{P_{eNB}}\left|h_{MS}\right|^2}{\chi_{MS} PL\left(d_{MS}\right)} \tag{4.23}$$

where P_{eNB} is the transmitted power at the base station, h_{MS} is the eNB–MS small-scale fading channel coefficient, χ_{MS} is the log-normal shadow coefficient and $PL\left(d_{MS}\right)$ is the path loss function provided in Equation (4.2) for MS locate at a distance of d_{MS} from the base station. In Equation (4.23), h_{MS} is a complex Gaussian random variable with zero-mean and variance σ_{MS}^2, and the log-normal shadow coefficient χ_{MS} has zero-mean and variance σ_{χ}^2. Each received instantaneous power level depends on the random channel, the log-normal shadow coefficients and the path loss that depends mainly on the distance between eNB and MS. The term $I+N$ is the summation of the interference from each interfering eNB plus the noise power when the mobile station locates at the cell edge. That is,

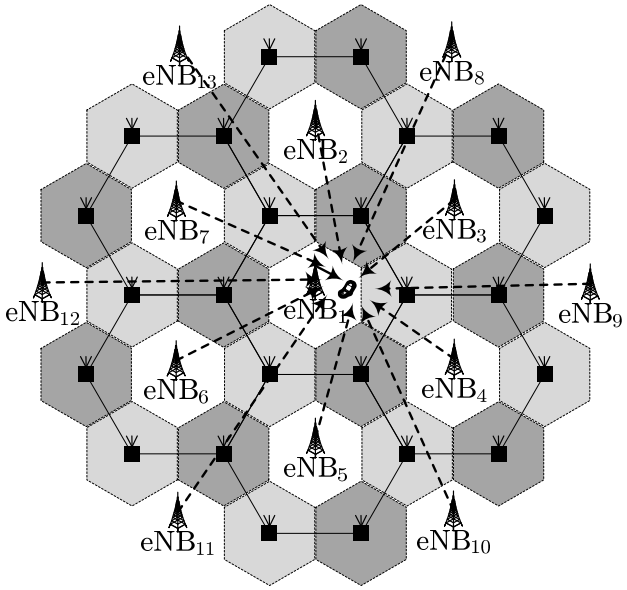

Figure 4.10: Illustration of the inner ICI caused by co-channel eNBs.

$$I(\chi_i, h_i) + N = \sum_{i=1}^{12} \left(\frac{\sqrt{P_{eNB}}|h_i|^2}{\chi_i PL(d_i)} \right) + \frac{BD}{U_{inner}} \tag{4.24}$$

where d_i is the distance from the i^{th} interfering eNB (i =1,2,…,12) to a MS, h_i is a channel coefficient between the i^{th} interfering eNB and MS, χ_i is a log-normal shadow coefficient, B (MHz) is the entire available downlink bandwidth, D (*watt.user*/Hz) is the per-user noise power spectral density level and U_{inner} is the average number of MSs users in the inner region. For the worse-case interference, d_i is given as

$$d_i = \left\{ \underbrace{R, 2R, \frac{\sqrt{7}}{2}R, \frac{\sqrt{7}}{2}R, \frac{\sqrt{13}}{2}R, \frac{\sqrt{13}}{2}R}_{First\ Tier}, \underbrace{\frac{5}{2}R, \frac{5}{2}R, 3R, 3R, \frac{7}{2}R, \frac{7}{2}R}_{Second\ Tier} \right\}$$

Assume the transmitted power from the base station is adjusted to just cover an area of radius R_o ($R_o < R$). The adjusted transmitted power equals

$$P'_{eNB} = P_{eNB}\left(\frac{R_o}{R}\right)^{2\nu} \tag{4.25}$$

Since all eNBs transmit using equal power P'_{eNB} and the number of interferers for the worse-case is 12, the instantaneous *SINR* experienced by the inner mobile stations, $SINR_{inner}(\chi, h, d_{MS})$, is obtained by using the expressions in Equations (4.23) and (4.24). That is,

$$SINR_{inner}(\chi, h, d_{MS}) = \frac{\dfrac{\sqrt{P'_{eNB}}\,|h_{MS}|^2}{\chi_{MS} PL(d_{MS})}}{\sum_{i=1}^{12}\left(\dfrac{\sqrt{P'_{eNB}}\,|h_i|^2}{\chi_i PL(d_i)}\right) + \dfrac{B\,D}{U_{inner}}} = \frac{d_{MS}^{-\nu}}{a_{inner}(\chi, h)} \tag{4.26}$$

where

$$a_{inner}(\chi, h) = \frac{\chi_{MS}}{|h_{MS}|^2}\sum_{i=1}^{12}\left(\frac{|h_i|^2}{\chi_i\, d_i^{-\nu}}\right) + \frac{\chi_{MS} B\,D}{|h_{MS}|^2 U_{inner}\sqrt{P'_{eNB}}}\left(\frac{4\pi f_c}{c_o}\right)^2$$

is conditioned on the channel gains $h = \{h_{MS}, h_i\}$ and the log-normal shadowing coefficients $\chi = \{\chi_{MS}, \chi_i\}$. In the following, we consider the conditional average *SINR.* That is, the average *SINR* is conditioned on knowledge of χ and *h*.

Since the mobile users are assumed to be randomly distributed within a cell in a ring-like pattern, the probability density function (*PDF*) for a mobile user being at a distance of d_{MS} (KM) from eNB may be defined as [108]

$$\begin{aligned} f\left[d_{MS}\right] &\triangleq \frac{\text{The circumference of a circle with diameter } d_{MS}}{\text{Total area of } R_o} \\ &= \frac{2\pi d_{MS}}{\pi R_o^2} = \frac{2d_{MS}}{R_o^2}, \quad 0 \le d_{MS} \le R_o \end{aligned} \tag{4.27}$$

The average *SINR* conditioned on χ and *h* is defined as [108]

$$\overline{SINR}_{inner}\left(\chi,h\right)=E\left[SINR_{inner}\right]\triangleq\int_{0}^{R_o}SINR_{inner}\left(\chi,h,d_{MS}\right)\;\;f\left[d_{MS}\right]\;\;\mathrm{d}\,d_{MS}$$

Using the expression in Equation (4.27) for $f\left[d_{MS}\right]$ and integrating, we obtain

$$\overline{SINR}_{inner}\left(\chi,h\right)=\int_{0}^{R_o}\frac{2d_{MS}^{1-\gamma}}{R_o^2\;a_{inner}\left(\chi,h\right)}\mathrm{d}\,d_{MS}=\frac{2R_o^{-\upsilon}}{\left|2-\upsilon\right|a_{inner}\left(\chi,h\right)}\tag{4.28}$$

Due to difficulty in averaging the above over channel and shadowing parameters h and χ, we resort to a Monte-Carlo method.

4.3.4.3 Average *SINR* Analysis for Outer MSs

In this section, the average *SINR* for the outer MSs is analyzed. Figure 4.11 shows the 6 interferers in the first tier and 6 interferers in the second tier.

Following similar steps used in the analysis for the inner users, we obtain the probability density function of d_{MS} as

$$f\left[d_{MS}\right]=\frac{2\pi d_{MS}}{\pi\left(R^2-R_o^2\right)}=\frac{2d_{MS}}{\left(R^2-R_o^2\right)},\qquad R_o\le d_{MS}\le R$$

Therefore, the conditional average $SINR_{outer}$ for the outer MSs is calculated as

$$\begin{aligned}\overline{SINR}_{outer}\left(\chi,h\right)&=\int_{R_o}^{R}SINR_{outer}\left(\chi,h,d_{MS}\right)\;\;f\left[d_{MS}\right]\mathrm{d}\,d_{MS}\\&=\frac{2\left(R^{2-\upsilon}-R_o^{2-\upsilon}\right)}{\left|2-\upsilon\right|\left(R^2-R_o^2\right)a_{outer}\left(\chi,h\right)}\end{aligned}\tag{4.29}$$

where

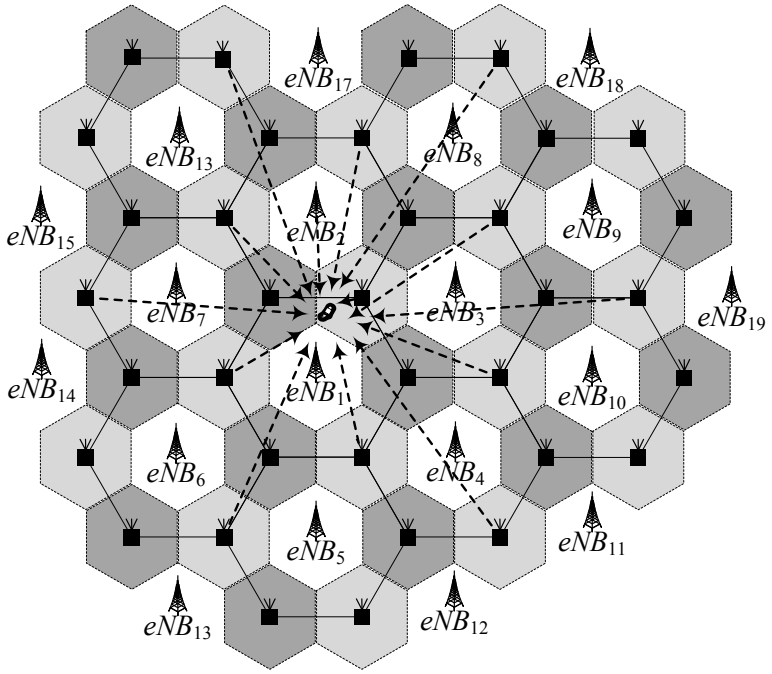

Figure 4.11: Illustration of the outer ICI caused by neighboring *RNs.*

$$a_{outer}\left(\chi,h\right)=\frac{\chi_{MS}}{\left|h_{MS}\right|^2}\sum\nolimits_{j=1}^{12}\left(\frac{\left|h_j\right|^2}{\chi_j\, d_j^{-\upsilon}}\right)+\frac{\chi_{MS}BD}{\left|h_{MS}\right|^2 U_{outer}\sqrt{P_{RN}}}\left(\frac{4\pi f_c}{c_o}\right)^2$$

is conditioned on the random channel gains $h=\left\{h_{MS},h_j\right\}$ and the log-normal shadowing coefficients $\chi=\left\{\chi_{MS},\chi_j\right\}$, P_{RN} is the transmitted power at the relay station, d_j is a distance from the j^{th} interfering RN (j =1,2,…,12) to the MS being located at the edge of the relay covering area, h_j is the channel coefficient between the j^{th} interfering RN and MS, χ_j is the log-normal shadow coefficient and U_{outer} is the average number of users in the outer region. For the worse-case interference, d_j is given as

$$d_j=\left\{\underbrace{R,2R,\frac{\sqrt{7}}{2}R,\frac{\sqrt{7}}{2}R,\frac{\sqrt{13}}{2}R,\frac{\sqrt{13}}{2}R}_{First\ Tier},\underbrace{\frac{5}{2}R,\frac{5}{2}R,3R,3R,\frac{7}{2}R,\frac{7}{2}R}_{Second\ Tier}\right\}$$

Similarly, the unconditional average *SINR* for outer users is obtained by averaging the expression in Equation (4.29) over h and χ using a Monte-Carlo simulation.

4.3.4.4 Average Capacity Analysis for OR Scheme

Analysis of the average capacity for the OR scheme is now considered. The average cell capacity is obtained by adding the average capacities for inner and outer users. The average capacity for each user category is obtained by evaluating the probability density function of the instantaneous spectral efficiency and averaging over the distance between the base station and the mobile user.

In the OR scheme, the overall per-cell capacity is the sum of the capacities provided to the inner and the outer MSs. The radio bandwidth resources is allocated among the inner and the outer MSs using a radio resource allocation factor Φ, which is defined as

$$\Phi \triangleq \frac{B_{outer}}{B_{inner}}$$

where B_{outer} and B_{inner} are the bandwidth resources allocated to the outer and inner MSs respectively. Since the total available bandwidth is the summation of B_{outer} and B_{inner} (i.e. $B = B_{outer} + B_{inner}$), and $B_{outer} = \Phi B_{inner}$, the total available resources allocated for all inner users is

$$\begin{aligned} B &= B_{outer} + B_{inner} \\ B &= \Phi B_{inner} + B_{inner} \\ B &= (1+\Phi) B_{inner} \rightarrow B_{inner} = \frac{B}{(1+\Phi)} \end{aligned}$$

and the total available resources allocated to all outer users is

$$B_{outer} = \Phi B_{inner} = \frac{\Phi B}{(1+\Phi)}$$

The link bandwidth for each inner and outer user is calculated by dividing the total allocated bandwidth for each region by its associated number of users. i.e. the total bandwidth resources allocated to each outer MS is $\Phi\, B/(1+\Phi)\, U_{outer}$, and to each inner MS is $B/(1+\Phi)\, U_{inner}$ for an available bandwidth B, where U_{inner} is the number of users within the inner region and U_{outer} is the number of users within the outer region. Therefore, the total average capacity is obtained as

$$\begin{aligned} E\left[C\left(\chi,h,d_{MS}\right)\right] &= E\left[C_{inner}\left(\chi,h,d_{MS}\right)\right]+E\left[C_{outer}\left(\chi,h,d_{MS}\right)\right] \\ &= \frac{B}{(1+\Phi)}\,E\left[Q_{inner}\left(\chi,h,d_{MS}\right)\right]+\frac{\Phi\, B}{(1+\Phi)}\,E\left[Q_{outer}\left(\chi,h,d_{MS}\right)\right] \end{aligned} \tag{4.30}$$

where $Q_{inner}\left(\chi,h,d_{MS}\right)=\log_2\left(1+SINR_{inner}\left(\chi,h,d_{MS}\right)\right)$ is the instantaneous spectral efficiency for the inner users and $Q_{outer}\left(\chi,h,d_{MS}\right)=\log_2\left(1+SINR_{outer}\left(\chi,h,d_{MS}\right)\right)$ is the instantaneous spectral efficiency for the outer users. In order to find the average spectral efficiency for the inner and outer mobile users, $Q_{inner}\left(\chi,h,d_{MS}\right)$ and $Q_{outer}\left(\chi,h,d_{MS}\right)$ must be written as a function of d_{MS}. That is,

$$Q_{inner}\left(\chi,h,d_{MS}\right)=\log_2\left(1+\frac{d_{MS}^{-\upsilon}}{a_{inner}\left(\chi,h\right)}\right) \quad \text{and} \quad Q_{outer}\left(\chi,h,d_{MS}\right)=\log_2\left(1+\frac{d_{MS}^{-\upsilon}}{a_{outer}\left(\chi,h\right)}\right).$$

The average spectral efficiency for the inner MSs equals

$$\overline{Q}_{inner}\left(\chi,h\right)=\int_0^{R_o} Q_{inner}\left(\chi,h,d_{MS}\right) f\left[d_{MS}\right]\mathrm{d}\,d_{MS}=\frac{2R_o^{2-\upsilon}\left(R_o^{\upsilon}a_{inner}\left(\chi,h\right)+1\right)^{1-\frac{2}{\upsilon}}-2a_{inner}^{1-\frac{2}{\upsilon}}\left(\chi,h\right)}{|2-\upsilon|\log\left(2\right)R_o^2\;a_{inner}\left(\chi,h\right)} \tag{4.31}$$

Similarly, the average spectral efficiency for the outer MSs equals

$$\overline{Q}_{outer}\left(\chi,h\right)=\int_{R_o}^{R} Q_{outer}\left(\chi,h,d_{MS}\right) f\left[d_{MS}\right]\mathrm{d}\,d_{MS}=\frac{2\left(a_{outer}\left(\chi,h\right)+1\right)^{1-\frac{2}{\upsilon}}\left(\frac{1}{R^{\upsilon-2}}-\frac{1}{R_o^{\upsilon-2}}\right)}{|2-\upsilon|\left(R^2-R_o^2\right)\log\left(2\right)a_{outer}\left(\chi,h\right)} \tag{4.32}$$

Table 4.2: System parameters.

Parameter	**Value**
Carrier frequency (f_c)	2 GHz
Frequency bandwidth (B)	10 MHz
eNBs' transmission power (P_{eNB})	46 dBm
Relays transmission power (P_{RN})	40dBm
eNB antenna pattern	Omni-directional
Relay antenna pattern	Omni-directional
Noise power density (D)	-174 dBm.user/Hz
Cell radius (R)	1000 m
Relay radius (r)	500 m
Modulation type	QPSK
Number of relays per cell	6
Path loss exponent (υ)	3.5
Path loss model	$PL(dB) = 35.46 + 35 \log(d)$
Rayleigh fading variance (σ_h^2)	1
Log-normal shadowing variance (σ_χ^2)	6.31

After obtaining the average spectral efficiencies for inner and outer MSs, the total conditional average capacity, conditioned on χ and h, is calculated by substituting Equations (4.31) and (4.32) into Equation (4.30). That is,

$$\overline{C}(\chi,h) = E\left[C(\chi,h)\right] = \frac{B}{(1+\Phi)}\overline{Q}_{inner}(\chi,h) + \frac{\Phi B}{(1+\Phi)}\overline{Q}_{outer}(\chi,h) \qquad (4.33)$$

Due to difficulty in averaging the above over the channel and shadowing parameters, we resort to Monte-Carlo simulation.

4.4 Numerical Results and Discussion

In this section, the performances of the conventional UFRF and the proposed OR schemes are compared. Semi-analytical results for the average *SINR* and the average capacity are obtained from the derived expressions in Sections 4.2.2 and 4.3.4. The parameters for the OR scheme are shown in Table 4.2, which are consistent with the LTE-A standard [116]. The results for the inner MSs are obtained when inner users are served by eNB and are located at distances 0m to 500m from eNB, and the results for the outer MSs are obtained when outer users are served by distributed relay terminals at distances 500m to 1000m.

4.4.1 *The Effect of Using RN at Cell Edge on Average SINR*

Figure 4.12 shows 3D plots for analytical attainable *SINR* at a mobile station at different locations within the cell for the conventional UFRF and the proposed OR scheme. The *SINR* is averaged over Rayleigh fading channel realizations and log-normal shadowing coefficients. For each MS location, several instantaneous *SINRs* are obtained for 1×10^6 channel realizations and 1×10^6 shadowing coefficients.

Figure 4.12 (a) illustrates the *SINR* profile versus the distance from the base station for conventional UFRF scheme. The figure shows that high *SINR* is achieved when the mobile station is close to the base station, and decays as the mobile station moves towards the edge of the cell. This is due to the strong received signal strength and low interference in areas close to the base station, and low received signal strength and high interference from co-channel base stations in areas close to the edge of the cell. Figure 4.12 (b) illustrates the *SINR* profile versus the distance from the base station for the proposed OR scheme. The figure shows seven, high-*SINR* peaks representing the attainable *SINR* from the base station (middle peak) and for the signals from the six distributed relays. The figure illustrates that when the mobile station moves from the base station toward the cell edge, it encounters high signal strength from one of the distributed relays.

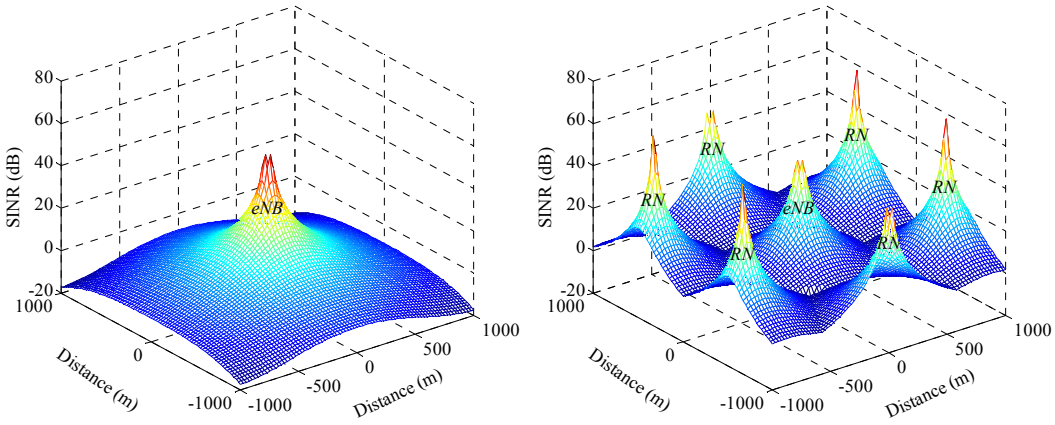

(a) The UFRF scheme **(b)** The OR scheme

Figure 4.12: Analytical *SINR* 3D records.

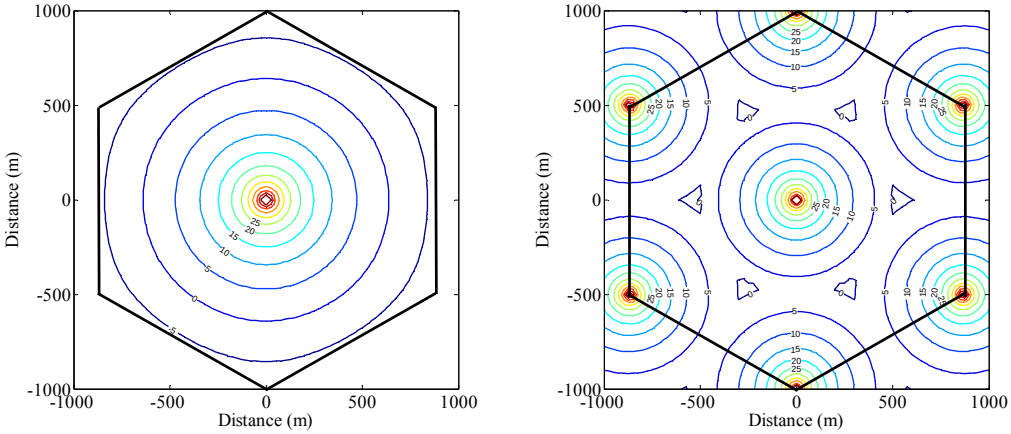

(a) The UFRF scheme **(b)** The OR scheme

Figure 4.13: Analytical *SINR* contours.

For better demonstration, Figure 4.13 shows the recorded *SINR* contours across the cell for the UFRF and the OR schemes. For both schemes, the *SINR* is decaying when the mobile station moves away from the serving terminal. For example, in Figure 4.13 (a), the *SINR* at 100m from the eNB is 30dB and decays to less than 0dB at a distance greater than 650m. However, in Figure 4.13 (b) where OR relays are employed, the *SINR* at inner MSs is always greater than 2dB for distances

between 0m and 500m, and the *SINR* at outer MSs is always greater than 2dB for distances between 500m and 1000m. Therefore, when OR relays are employed, the *SINR* at the outer mobile users is significantly improved. This significant improvement is due to the strong signal strength from the distributed relays as well as the reduction in ICI due to the physical separation of interferers.

Table 4.3 provides comparisons for the UFRF and the OR schemes in terms of semi-analytical and simulated average *SINR*. The table shows the average *SINR* for inner and outer OR relay users. Considering the analytical *SINR*, UFRF users achieve an average *SINR* of 8.6186dB, whereas the inner and outer OR relay users achieve higher average *SINR* of 17.1594dB and 17.3175dB, respectively. This is due to the signal strength gain provided by the relay terminals for outer users. The table also shows that the analytical and the simulated results have small differences. The differences between results are due to the averaging over the shadowing and channel realization, such that increasing the number of realizations results in reducing the difference between the analytical and simulated results.

Figure 4.14 illustrates semi-analytical *SINR* results for the UFRF and the OR schemes as the MS moves from the cell center (Distance=0m) to the cell edge (Distance=1000m). The results are obtained by averaging over channel coefficients (fading and shadowing) at each mobile user location. It is observed that the average *SINR* decreases exponentially when the MS moves away from the base station due to the decrease in received signal strength and increase in ICI. However, the decrease in the average *SINR* occurs only until the inner MS reaches the boundary of the outer region after which the *SINR* increases exponentially as the MS approaches the relay. Therefore, the average *SINR* at the cell-edge is improved remarkably with the assistance of the relay nodes. Despite the remarkable improvement at cell edge area, the users in the OR scheme suffer from poor signal strength and high interference at distances 300m to 700m when average *SINR* drops to values less than 10dB. In the following chapter, this issue will be solved by employing a different transmission scheme that helps to improve this region.

Table 4.3: Semi-analytical and simulated average *SINR* over distance and channel coefficients

		Average ***SINR*** **(dB)**	
		Semi-analytical	**Simulated**
The UFRF scheme		8.6186	8.5564
The OR scheme	**inner users**	17.1594	16.9884
	outer users	17.3175	17.2635

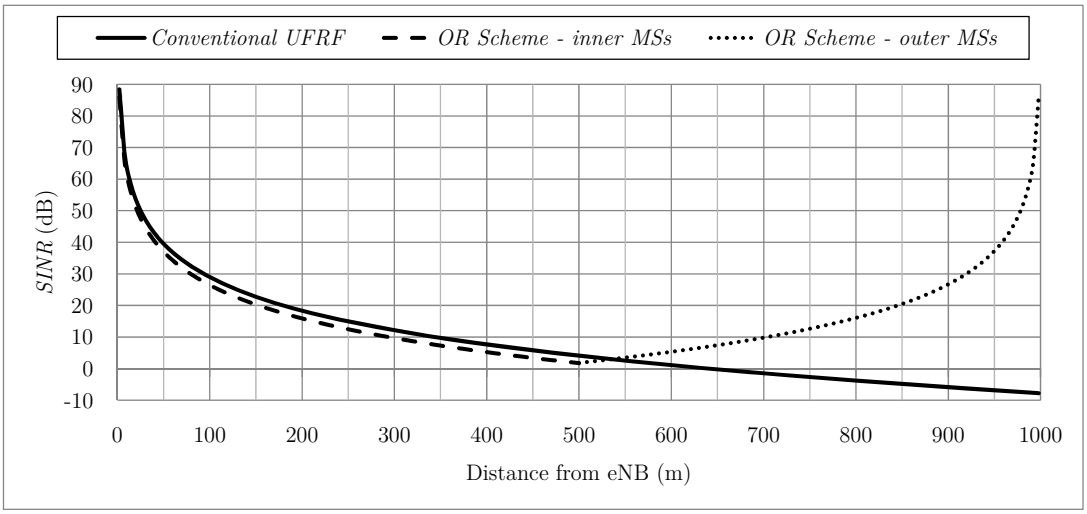

Figure 4.14: Semi-analytical *SINR* profiles for the UFRF and the OR schemes.

To make a fair comparison of the *SINR* distributions for different schemes, the *CDF* curves of average *SINR* obtained from the semi-analytical results are shown in Figure 4.15. In the conventional UFRF scheme, about 40 percent of the MS users experience a *SINR* less than 10dB, which means that they have to resort to other signal processing techniques to recover useful signals from overwhelming interference and noise. On the contrary, when utilizing the OR scheme, both the outer and inner MS users have good transmission quality, where more that 85 percent of MSs experience a *SINR* higher than 10dB.

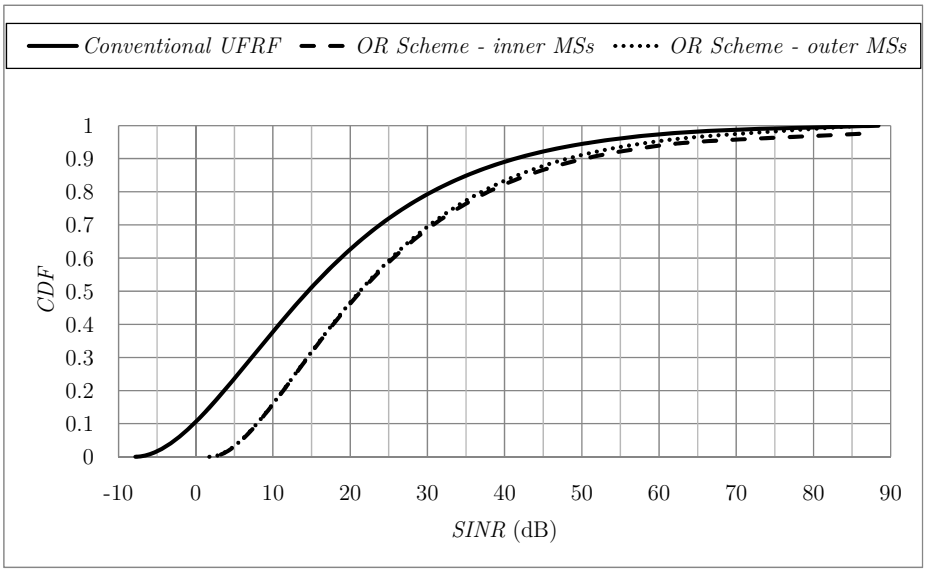

Figure 4.15: *CDF* of *SINR*.

Table 4.4: Average capacity over distance and channel coefficients

		Average Capacity (bps/Hz)	
		Semi-analytical	**Simulated**
The UFRF scheme		3.6979	3.5827
The OR scheme	**inner users**	5.8826	5.8255
	outer users	5.9316	5.8919

4.4.2 *The Effect of Using* RN *at Cell Edge on Average Capacity Profile*

Table 4.4 shows the average semi-analytical and simulated capacity comparisons for the conventional UFRF and the proposed OR schemes. The table also shows the results for inner and outer OR relay users when the radio resource allocation factor Φ is set to 0.5 (i.e. inner and outer users are allocated the same size of bandwidth resources). The UFRF users achieve an average capacity of 3.6979bps/Hz, whereas the inner and outer OR relay users achieve higher average capacity of

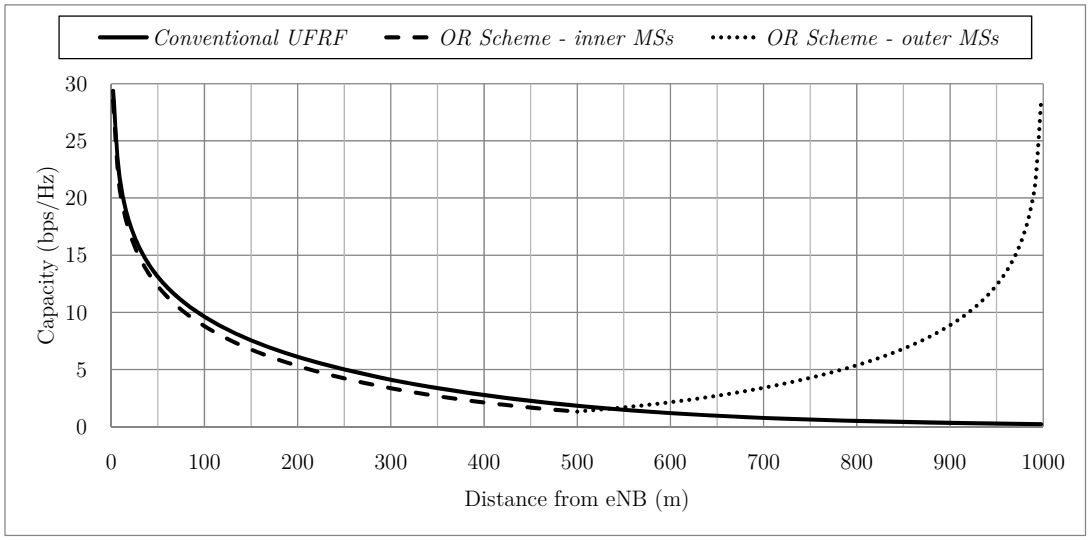

Figure 4.16: Average capacity profiles for the UFRF and the OR schemes.

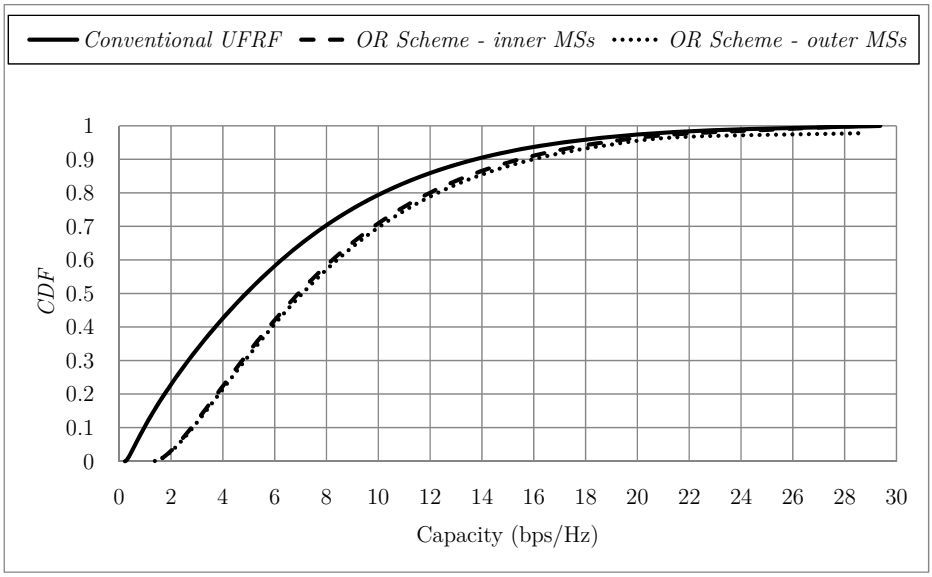

Figure 4.17: *CDF* of capacity.

5.8826bps/Hz and 5.9316bps/Hz, respectively. This is due to the signal improvements at cell-edge regions and the ICI reduction from the use of the relays.

Figure 4.16 illustrates average capacity profiles for the two schemes, where the MS is moving from the cell center to the cell edge. The results are obtained when

averaging over channel coefficients (fading and shadowing) at each MS location. The average capacity for the UFRF is shown to decrease exponentially with increasing distance. However, for the OR scheme, the mobile users experience an exponential increase in capacity when they move across the eNB's serving boundary into the region served by the RNs. It is observed also that OR users experience drop in capacity at distances 300m to 700m when average *SINR* drops to values less than 3bps/Hz. This issue will be solved in the following chapter.

To make a fair comparison of the average capacity distributions for different schemes, the *CDF* curves of average capacity are illustrated in Figure 4.17. The figure shows that utilizing the proposed OR scheme, 50 percent of MS users result in an average capacity higher than 7bps/Hz. On the other hand, 50 percent of UFRF users result in an average capacity higher than 5bps/Hz.

From all previously provided results, the average *SINR* and the average capacity of cell-edge users are improved remarkably compared with the conventional scheme. The improvement is due to the assistance of distributed relay nodes that improve the desired signal level and reduce the interference by increasing the separation distance between co-channel interferers. This improvement however brings new cost for relay terminals in each cell and requires coordination between terminals.

4.5 Chapter Summary

In this chapter, the use of omni-directional antennas at relay terminals has been proposed to overcome the issues of inter-cell interference and weak received signal that arise when employing the conventional universal frequency reuse factor (UFRF) scheme. The omni-relay (OR) has been proposed to be compatible with LTE-A standard in aspects of relay deployment, transmission power, frequency resources allocation and frame structure. The chapter discussed the system model for the UFRF together with the analysis of average *SINR* and capacity. Similarly, average *SINR* and capacity analysis were conducted for the OR user categories; the inner and outer MSs. The chapter also provided analytical and simulated results

for the UFRF and the OR schemes. The results included – the *SINR* experienced by users across the cell, average *SINR*, *SINR* distributions, capacity across the cell, average capacity, and capacity distributions. The simulation results show that utilizing the OR scheme provides significant *SINR* improvement and capacity gain compared with the UFRF scheme. Such remarkable results are due to the increase in the desired signal power at the cell edge when distributing relay nodes, and the reduction of the interference from other interferes when increase the distance between co-channel interferers.

Despite the remarkable improvement, the OR scheme users experience poor signal strength, high interference and low capacity in some regions inside the cell. The following chapter aims to solve such issues.

Chapter Five: Directional Relay (DR) Scheme-Aided LTE-A Communication Systems

5.1 Introduction

In Chapter Four, the omni-relay (OR) scheme shows a significant improvement compared to the conventional UFRF scheme in terms of desired signal enhancement, interference reduction and spectral efficiency improvement. This is due to the setup of the OR network that increases the distance between the inter-cell interfering cells and improves the signal at the edge of the cell when utilizing the distributed relays.

Despite the remarkable improvement, the OR scheme users suffer from two main issues; frequent handover and poor signal strength in areas between any two consecutive relays. In the OR scheme, the base station and the distributed relays operate in different frequency resources. Therefore, when mobile users roam inside one cell or move from one cell to another, the service is switched from one serving terminal to another. The switching between serving terminals or handover may increase the probability of call drop and increase the required processing load for the serving terminal and the user itself. Since the network structure for the OR scheme consists of many regions that utilize different resources, the possibility of having handover is high. Figure 5.1 illustrates an example of an OR cell when a mobile station moves from location a to location b. In this example, the service is switched between three serving terminals; from eNB to RN_1, from RN_1 to RN_2 and from RN_2 to RN_3.

In the OR scheme, performance improvement of the outer users is significant when the user is located close to the relay. However, performance decays when the user is located between two relays. Since the benefit of relay nodes is to boost the desired signal in areas of weak signal strength, placing another set of relays in such areas is

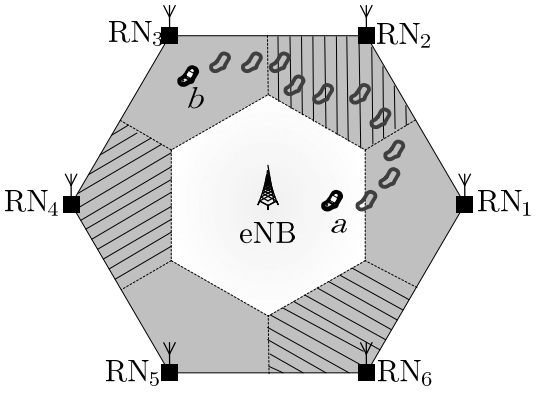

Figure 5.1: Illustrates the frequent handover problem in the OR scheme.

a valid solution but develops issues of cost, implementation complexity, and interference.

Based on these two issues, we propose the use of directional antennas at the relay terminals in LTE-A cellular system. We aim to reduce the effect of interference from co-channel relays, reduce the frequent handover, and improve the desired signal level. To validate the performance of the proposed structure, we conduct analyses of the average *SINR* and the average capacity, and compare it with the omni-relay scheme discussed in Chapter 4.

Chapter 5 is organized as follows. Section 5.2 focuses on the new scheme. It discusses the system model and analyses of the average *SINR* and the average capacity. The section also provides numerical results and discussions for such analysis compared to the OR scheme. Section 5.3 presents a modification in the transmission between terminals for the proposed scheme. It includes a description of the transmission algorithm and its effect on the network performance. Finally, Section 5.3 provides analytical and simulation performance results for the proposed structure and its modified transmission algorithm.

5.2 The Directional Relay (DR) Scheme

In the omni-relay scheme, the system suffers from frequent handover and low desired signal level particularly in areas between two consecutive relays. Such issues may be solved by reducing the interference from co-channel interfering cells and improve the signal from the relay terminals. This is obtained by changing the antenna pattern of the relays in the previous OR scheme from omni-directional antenna to directional antenna pattern. *We shall refer to this as Directional Relay (DR) scheme*. Following is a description of the DR system model together with the analyses of the average *SINR* and the average capacity.

5.2.1 *System Model*

The directional relay (DR) scheme is illustrated in Figure 5.2. The model assumes that the entire available download bandwidth is divided into four segments, namely, f_1, f_2, f_3 and f_4. Segment f_1 is allocated to each eNB, whereas f_2, f_3 and f_4 are assigned to the relay terminals as illustrated in Figure 5.2. Each cell is surrounded by six-Type I relay nodes each being equipped with a 120° directional antenna. The frequency resources for each sector are selected from f_2, f_3 and f_4

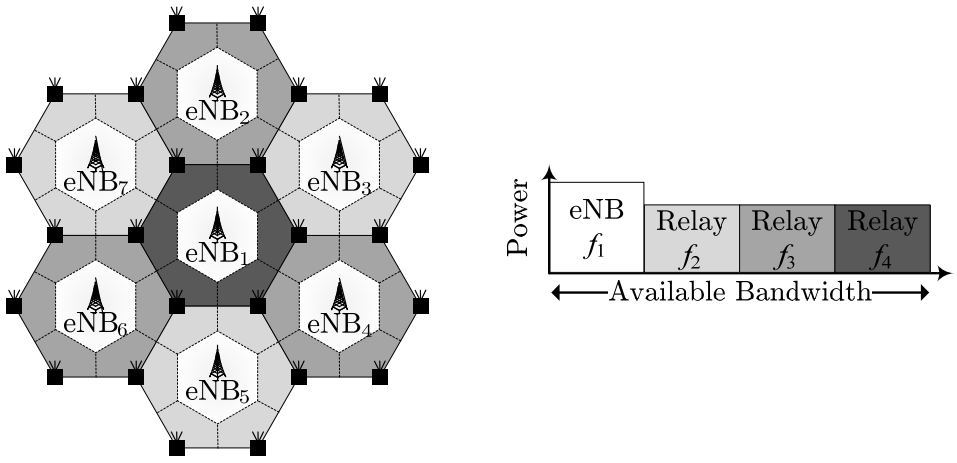

Figure 5.2: The DR network topology and power / frequency allocation.

such that, the six sectors jointly cover the same cell utilize the same frequency resources. The use of the directional antennas and the assignment of frequency resources in this way may increase the interference within one cell but reduce the interference from other cells.

Similar to the OR scheme, we shall refer to the unshaded areas as *inner region* and shaded areas as *outer region*. Consequently, users of the DR scheme shall be classified into *inner MSs* and *outer MSs*. Inner MS users are located within the eNB transmission range and are served directly by one of the eNBs. On the other hand, outer MS users are located within RN transmission ranges and are served by one of the RNs at the cell edges.

5.2.2 *Performance Analysis*

In this section, we perform the analysis of the average *SINR* and the average capacity for the DR scheme. Through the analyses, we consider the two categories of MS users; the inner MSs and the outer MSs. We will use the average *SINR* and the average capacity later for comparison between the OR and the DR scheme.

Throughout the analysis, the worse-case is assumed, where during transmission from eNB to the inner MSs, there is interference from all the co-channel eNBs in the first two eNB tiers, and when the desired relay is transmitting, there is interference from all the co-channel relays in the first two relay tiers.

5.2.2.1 Average Number of Inner and Outer Users per cell

In order to carry out the analyses of the average *SINR* and the average capacity, the average number of inner users (U_{inner}) and outer users (U_{outer}) are needed. Referring to the analyses of the average number of inner and outer users for the OR scheme in Chapter 4, similar expressions are obtained for the average number

of inner and outer users for the DR scheme. Hence, for the inner region cell radius of

$$R_o = R\left(1-\left(\sqrt{\eta}\,\frac{\left|h_{RN}\right|^2 \chi_{eNB}}{\left|h_{eNB}\right|^2 \chi_{RN}}\right)^{\frac{1}{\upsilon}}\right),$$

the average number of inner and outer users are given as

$$U_{inner} = \frac{U}{R} - \frac{U}{R}\left(\sqrt{\eta}\,\frac{\left|h_{RN}\right|^2 \chi_{eNB}}{\left|h_{eNB}\right|^2 \chi_{RN}}\right)^{\frac{1}{\upsilon}} \quad \text{and} \quad U_{outer} = U - \frac{U}{R} + \frac{U}{R}\left(\sqrt{\eta}\,\frac{\left|h_{RN}\right|^2 \chi_{eNB}}{\left|h_{eNB}\right|^2 \chi_{RN}}\right)^{\frac{1}{\upsilon}},$$

respectively. This average number of inner and outer users will be used in the analysis of per-cell capacity in later sections.

5.2.2.2 Average *SINR* Analysis for Inner MSs

In this section, the average *SINR* is derived for the inner MSs. The derivation involves finding the instantaneous *SINR* and then averaging it over the distance, the channel realizations, and the log-normal shadowing coefficients. The averaging over the distance is obtained by using the probability density function for the inner users being at distance d_{MS} from the cell base station.

Figure 5.3 illustrates the co-channel eNBs for the downlink inner MSs. The first two tiers of interfering eNBs are assumed the main source of ICI. The figure shows 6 eNBs interferers in the first tier and 6 eNBs in the second tier. The worse-case instantaneous *SINR* for the DR schemes' inner users is

$$SINR_{inner} \triangleq \frac{P_r}{I+N} \tag{5.1}$$

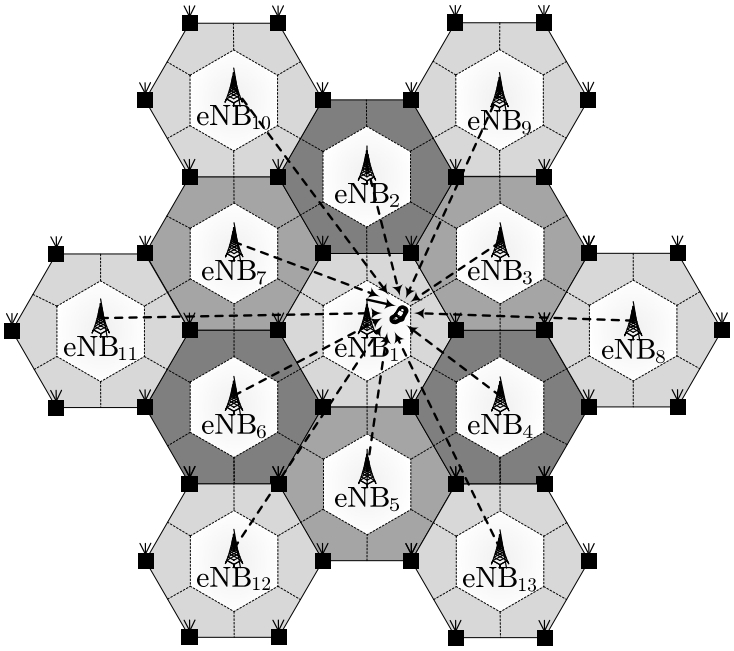

Figure 5.3: Illustration of the inner ICI caused by co-channel eNBs.

where P_r is the instantaneous received signal power from the desired serving eNB, I is the total instantaneous interference power from other eNBs, and N is the noise power. P_r can be written as

$$P_r\left(\chi_{MS}, h_{MS}, d_{MS}\right) = \frac{\sqrt{P_{eNB}}\left|h_{MS}\right|^2}{\chi_{MS} PL\left(d_{MS}\right)} \tag{5.2}$$

where P_{eNB} is the transmitted power at the base station, h_{MS} is the eNB–MS small-scale fading channel coefficient, χ_{MS} is the log-normal shadow coefficient and $PL\left(d_{MS}\right)$ is the path loss function provided in Equation (4.2) for MS located at a distance of d_{MS} from the base station. In Equation (5.2), h_{MS} is a complex Gaussian random variable with zero-mean and variance σ_{MS}^2, and the log-normal shadow coefficient χ_{MS} has zero-mean and variance σ_{χ}^2. Each received instantaneous power level depends on the random channel, the log-normal shadow coefficients, and the path loss that depends mainly on the distance between eNB

and MS. The term $I+N$ is the summation of the interference from each interfering eNB plus the noise power when the mobile station locates at the cell edge. That is

$$I(\chi_i, h_i) + N = \sum_{i=1}^{12} \left(\frac{\sqrt{P_{eNB}} |h_i|^2}{\chi_i PL(d_i)} \right) + \frac{BD}{U_{inner}} \tag{5.3}$$

where d_i is the distance from the i^{th} interfering eNB (i =1,2,…,12) to a MS located at the edge of the cell, h_i is a small-scale fading channel coefficient between the i^{th} interfering eNB and MS, χ_i is a log-normal shadow coefficient, B (MHz) is the entire available downlink bandwidth, D (watt.user/Hz) is the per-user noise power spectral density level, and U_{inner} is the average number of MSs users in the inner region. For the worse-case interference, d_i is given as

$$d_i = \left\{ \underbrace{R, 2R, \frac{\sqrt{7}}{2}R, \frac{\sqrt{7}}{2}R, \frac{\sqrt{13}}{2}R, \frac{\sqrt{13}}{2}R}_{First\ Tier}, \underbrace{\frac{5}{2}R, \frac{5}{2}R, 3R, 3R, \frac{7}{2}R, \frac{7}{2}R}_{Second\ Tier} \right\}$$

Assume the transmitted power from the base station is adjusted to just cover an area of radius R_o ($R_o < R$). The adjusted transmitted power equals

$$P'_{eNB} = P_{eNB} \left(\frac{R_o}{R} \right)^{-2\upsilon} \tag{5.4}$$

Since all eNBs transmit using equal power P'_{eNB} and the number of interferers for the worse-case is 12, the instantaneous $SINR$ experienced by the inner mobile stations is obtained by using the expressions in Equations (5.2) and (5.3). That is,

$$SINR_{inner}(\chi, h, d_{MS}) = \frac{\dfrac{\sqrt{P'_{eNB}} |h_{MS}|^2}{\chi_{MS} PL(d_{MS})}}{\displaystyle\sum_{i=1}^{12} \left(\frac{\sqrt{P'_{eNB}} |h_i|^2}{\chi_i PL(d_i)} \right) + \frac{BD}{U_{inner}}} = \frac{d_{MS}^{-\upsilon}}{a_{inner}(\chi, h)} \tag{5.5}$$

where

$$a_{inner}(\chi,h)=\frac{\chi_{MS}}{|h_{MS}|^2}\sum_{i=1}^{12}\left(\frac{|h_i|^2}{\chi_i\, d_i^{-\upsilon}}\right)+\frac{\chi_{MS}B\,D}{|h_{MS}|^2\,U_{inner}\sqrt{P'_{eNB}}}\left(\frac{4\pi f_c}{c_o}\right)^2$$

is conditioned on the channel gains $h=\{h_{MS},h_i\}$ and the log-normal shadowing coefficients $\chi=\{\chi_{MS},\chi_i\}$. In the following, we consider the conditional average *SINR*. That is, the average *SINR* is conditioned on knowledge of χ and h.

Since the mobile users assumed to be randomly distributed within a cell in a ring-like pattern, the probability density function (*PDF*) for a mobile user being at a distance of d_{MS} (KM) from eNB may be written as

$$f[d_{MS}]=\frac{2\pi d_{MS}}{\pi R_o^2}=\frac{2d_{MS}}{R_o^2},\quad 0\le d_{MS}\le R_o \tag{5.6}$$

The average *SINR* conditioned on χ and h is defined as

$$\overline{SINR}_{inner}(\chi,h)=E[SINR_{inner}]\triangleq\int_0^{R_o}SINR_{inner}(\chi,h,d_{MS})\,f[d_{MS}]\,\mathrm{d}d_{MS}$$

Using the expression in Equations (5.5) and (5.6) and integrating, we obtain

$$\overline{SINR}_{inner}(\chi,h)=\int_0^{R_o}\frac{2d_{MS}^{1-\gamma}}{R_o^2\;a_{inner}(\chi,h)}\mathrm{d}SINR_{inner}=\frac{2R_o^{-\upsilon}}{|2-\upsilon|a_{inner}(\chi,h)} \tag{5.7}$$

which is the conditional average *SINR* for the inner mobile users. The unconditional average *SINR* for inner users is obtained by averaging the expression in Equation (5.7) over χ and h using a Monte-Carlo simulation.

5.2.2.3 *SINR* Analysis for Outer MSs

In this section, the average *SINR* for the outer MSs is analyzed. Figure 5.4, shows the 5 interferers in the first tier from co-channel relays in the same cell and 6 interferers in the second tier from co-channel relays in other cells.

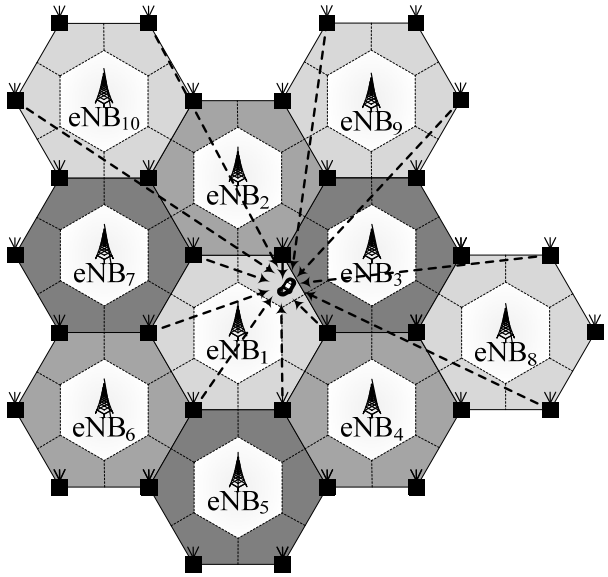

Figure 5.4: Illustration of the outer ICI cause by co-channel RNs.

Following similar steps used in the analysis for the inner users, we obtain the probability density function of d_{MS} as

$$f\left[d_{MS}\right]=\frac{2\pi d_{MS}}{\pi\left(R^2-R_o^2\right)}=\frac{2d_{MS}}{\left(R^2-R_o^2\right)},\quad R_o\le d_{MS}\le R \tag{5.8}$$

Therefore, the conditional average $SINR_{outer}$ for the outer MSs is calculated as

$$\overline{SINR}_{outer}\left(\chi,h\right)=\int_{R_o}^{R}SINR_{outer}\left(\chi,h,d_{MS}\right)\,f\left[d_{MS}\right]\mathrm{d}\,d_{MS}=\frac{2R^{2-\upsilon}-2R_o^{2-\upsilon}}{|2-\upsilon|\left(R^2-R_o^2\right)a_{outer}\left(\chi,h\right)} \tag{5.9}$$

where

$$a_{outer}\left(\chi,h\right)=\frac{\chi_{MS}}{\left|h_{MS}\right|^2}\sum\nolimits_{j=1}^{11}\left(\frac{\left|h_j\right|^2}{\chi_j\,d_j^{-\upsilon}}\right)+\frac{\chi_{MS}BD}{\left|h_{MS}\right|^2\sqrt{P_{RN}}U_{outer}}\left(\frac{4\pi f_c}{c_o}\right)^2$$

is conditioned on the random channel gains $h=\left\{h_{MS},h_j\right\}$ and the log-normal shadowing coefficients $\chi=\left\{\chi_{MS},\chi_j\right\}$, P_{RN} is the transmitted power at the relay station, d_j is a distance from the j^{th} interfering RN (j = 1,2,…,11) to the MS being

located at the edge of the relay covering area, h_j is the channel coefficient between the j^{th} interfering RN and MS, χ_j is the log-normal shadow coefficient, and U_{outer} is the average number of users in the outer region. For the worse-case interference, d_j is given as

$$d_j = \left\{ \underbrace{R, R, \sqrt{3}R, \sqrt{3}R, 2R}_{First\ Tier}, \underbrace{\sqrt{7}R, \sqrt{7}R, \sqrt{7}R, 3R, 3R, 3R}_{Second\ Tier} \right\}$$

Similarly, the unconditional average *SINR* for outer users is obtained by averaging the expression in Equation (5.9) over χ and h using a Monte-Carlo simulation.

5.2.2.4 Average Capacity Analysis for DR Scheme

The analysis of the average capacity for the DR scheme is now considered. The average cell capacity is obtained by adding the average capacities for inner and outer users. The average capacity for each user category is obtained by evaluating the probability density function of the instantaneous spectral efficiency and averaging over the distance between the base station and the mobile station.

Consider the same predefined radio resource allocation factor (Φ) in Chapter 4, the total average capacity is given as

$$E[C] = E[C_{outer}] + E[C_{inner}] = \frac{\Phi B}{(1+\Phi)} E[Q_{outer}] + \frac{B}{(1+\Phi)} E[Q_{inner}] \qquad (5.10)$$

where $Q_{inner}(\chi, h, d) = \log_2(1 + SINR_{inner}(\chi, h, d))$ is the instantaneous spectral efficiency for the inner users and $Q_{outer}(\chi, h, d) = \log_2(1 + SINR_{outer}(\chi, h, d))$ is the instantaneous spectral efficiency for the outer users. The average spectral efficiency for the inner MSs equals

$$\overline{Q}_{inner}(\chi,h)=\int_{0}^{R_o} Q_{inner}(\chi,h,d_{MS})\, f[d_{MS}]\,\mathrm{d}d_{MS}=\frac{2\left(R_o^{\upsilon}\left(R_o^{\upsilon}a_{inner}+1\right)^{1-\frac{2}{\upsilon}}-a_{inner}^{1-\frac{2}{\upsilon}}(\chi,h)\right)}{|2-\upsilon|R_o^2\log(2)a_{inner}(\chi,h)} \quad (5.11)$$

and the average spectral efficiency for the outer MSs equals

$$\overline{Q}_{outer}(\chi,h)=\int_{R_o}^{R} Q_{outer}(\chi,h,d_{MS})\, f[d_{MS}]\,\mathrm{d}d_{MS}=\frac{2\left|R^{2-\upsilon}-R_o^{2-\upsilon}\right|\left(a_{outer}(\chi,h)+1\right)^{1-\frac{2}{\upsilon}}}{|2-\upsilon|\left(R^2-R_o^2\right)\log(2)a_{outer}(\chi,h)} \quad (5.12)$$

After obtaining the average spectral efficiencies for inner and outer MSs, the total conditional average capacity, conditioned on χ and h, is calculated by substituting Equations (5.11) and (5.12) into Equation (5.10). That is,

$$\overline{C}(\chi,h)=\frac{B}{(1+\Phi)}\overline{Q}_{inner}(\chi,h)+\frac{\Phi\, B}{(1+\Phi)}\overline{Q}_{outer}(\chi,h)$$

Due to the difficulty in averaging the above over the channel and shadowing parameters, we resort to Monte-Carlo simulation.

5.2.3 *Numerical Results and Discussion*

In this section, the performance of the DR scheme is compared to the OR scheme discussed in Chapter 4. Semi-analytical results for the average *SINR* and the average capacity are obtained from the derived expressions in Section 5.2.2. The parameters for the DR scheme are shown in Table 5.1, which are consistent with the LTE-A standard. The results for inner MSs are obtained when inner users are served by eNB and are located in distance from 0m to 500m from eNB, and the results for outer MSs are obtained when outer users are served by distributed relay terminals from the distance 500m to 1000m.

Moreover, the semi-analytical results are conducted when the mobile station is moving in two paths as shown in Figure 5.5. Path (a) for MS is moving from the

Table 5.1: System parameters.

Parameter	**Value**
Carrier frequency (f_c)	2 GHz
Frequency bandwidth (B)	10 MHz
eNBs' transmission power (P_{eNB})	46 dBm
Relays transmission power (P_{RN})	40dBm
eNB antenna pattern	Omni-directional antenna
Relay antenna pattern	120^o directional antenna
Noise power density (D)	-174 dBm.user/Hz
Cell radius (R)	1000 m
Relay radius (r)	500 m
Modulation type	QPSK
Number of relays per cell	6
Path loss exponent (υ)	3.5
Path loss model	$PL(dB) = 35.46 + 35 \log(d)$, d in km
Rayleigh fading variance (σ_h^2)	1
Log-normal shadowing variance (σ_χ^2)	6.31

base station towards the relay station, crossing the inner and outer regions, and Path (b) for MS is moving from one relay to another in the same cell. Both paths illustrate the effect of relay deployment in regions between the base station and the relay, and the region between two consecutive relays.

Figure 5.6 shows the *SINR* profile for the OR and the DR schemes when the MS is taking Path (a). The mobile station is assumed to move from the cell center (Distance=0m) to the cell edge (Distance=1000m). The semi-analytical results were obtained for a MS taking steps away from the base station, each is 10m long. For each step, 10^6 small-scale fading channel coefficients and shadowing coefficients were generated and used in the expressions in Equations (5.7) and (5.9) for inner

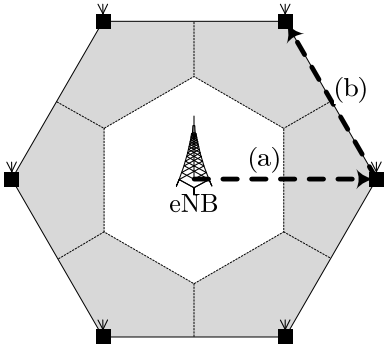

Figure 5.5: Moving paths for the mobile station

and outer average *SINR*, respectively. The average *SINR* for each step is then calculated by averaging this several *SINRs* over 10^6. It is noticed that the *SINR* decreases exponentially when the MS moves away from the base station due to the decrease in received signal strength and the increase in ICI. However, the *SINR* decreases exponentially until the inner MS reaches the bounds of the outer region and increase exponentially as it approaches the relay. Since inner users in both schemes have similar conditions (the number of eNB interferes, distances, and eNB transmit power), the curves for both scheme from 0m to 500m match. The figure also shows that, in the worse-case, the OR scheme performs better than the DR in terms of *SINR* by about 8dB. This is due to the strong ICI from the relays within the cell in the DR.

For a mobile station taking Path (b), the *SINR* at the mobile station is obtained in Figure 5.7. The mobile station is receiving from the first relay from distance 0m to 500m, and then it starts receiving from the second relay from distance 500m to 1000m. It is noticed that the *SINR* decreases exponentially when the MS moves away from the first relay due to the decrease in received signal strength and the increase in ICI. However, the *SINR* decreases exponentially only until the MS reaches the boundary between the two relays and increase exponentially as it approaches the second relay. The figure also shows that the OR scheme performs better than the DR at cell-edge areas due to relatively weak ICI from the relays

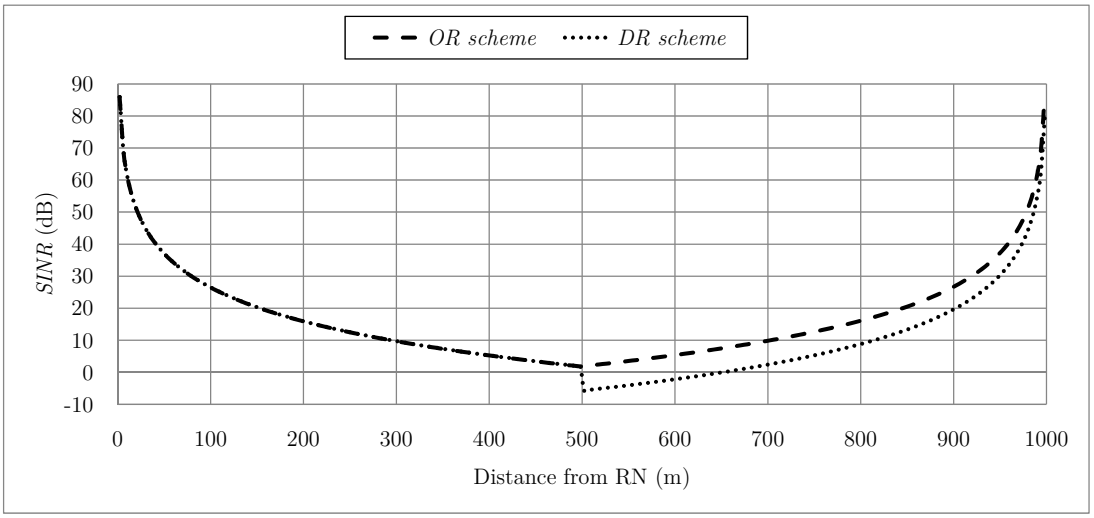

Figure 5.7: *SINR* performance comparison for the DR and the OR schemes.

within the cell in the OR scheme. For example, at distance from 400m to 600m, the *SINR* difference between the two curves is about 10dB.

It is noticed from Figure 5.7 that the *SINR* is dropping to very small values when the mobile station locates between two consecutive relays. This is due to the strong

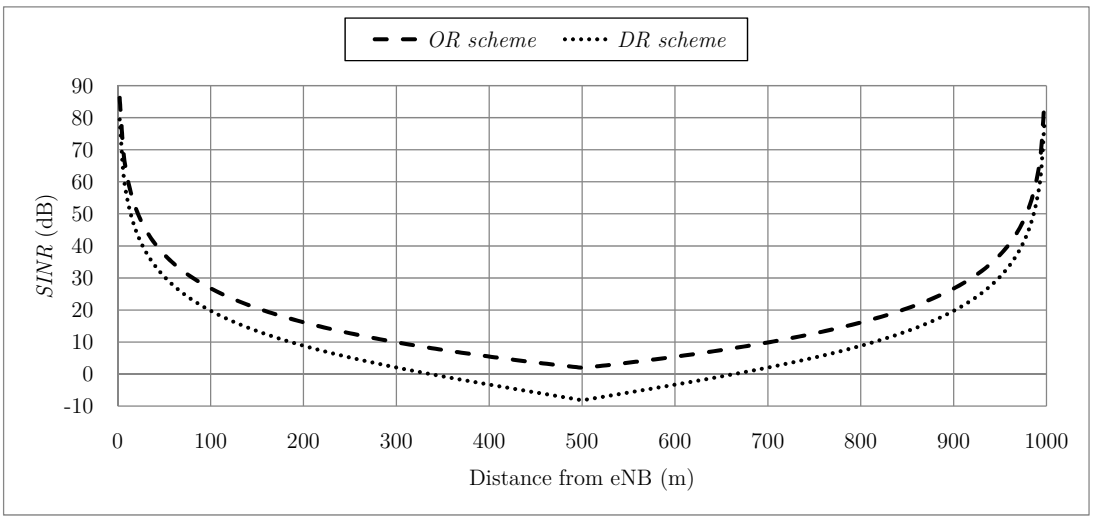

Figure 5.6: Outer *SINR* comparison when the OR and the DR schemes are utilized.

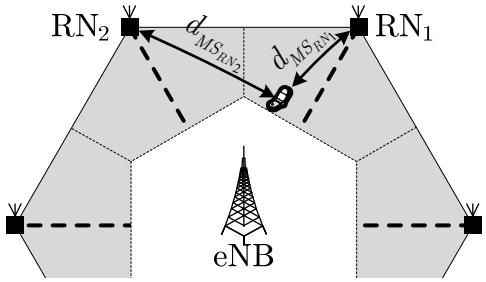

Figure 5.8: MS distances from RN_1 and RN_2.

interference from co-channel relays especially the relays within the cell. In the following section, a proposed transmission scheme is presented such that the effect of high ICI is reduced and consequently the *SINR* is improving for outer users.

5.3 The Enhanced-Directional Relay (E-DR) Transmission Scheme

According to the previous results and discussion, utilizing the DR scheme in the LTE-A network shows degradation in terms of *SINR* profile. This is due to the strong mutual interference from the co-channel relay terminals at the edges of the cell. The severe effect of such interference is noticed in regions between two relays in the same cell. A possible way to solve this issue is to employ a transmission scheme that increases the diversity from the relay terminals and reduce the effect of ICI.

5.3.1 *System Model*

In the DR scheme, the relays in each cell have the same allocated frequency resources. Therefore, the mobile station is able to receive from two relay nodes simultaneously and improve the desired signal power. *Here, we refer to the transmission scheme that utilizes receiving from two relays simultaneously as enhanced-directional relay (E-DR) scheme.*

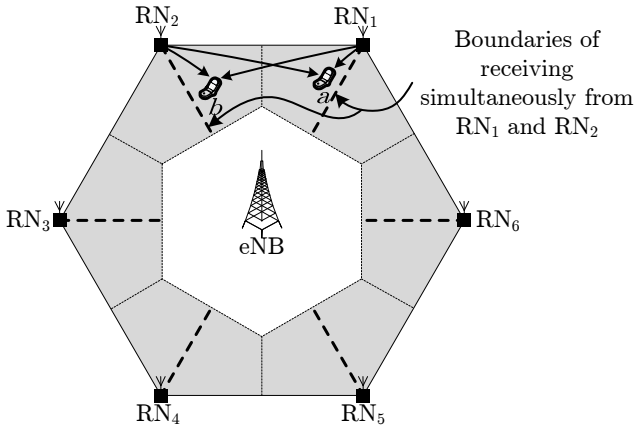

Figure 5.9: The E-DR scheme.

Figure 5.8 shows an example of the E-DR transmission scheme where the mobile stations a and b are hosted by both RN_1 and RN_2. In this scheme, the base station is unable to communicate directly with the outer mobile stations because they operate in different frequency bands, so the base station communicate with RN_1 and RN_2 by, for example, a cable, and RN_1 and RN_2 forward to the mobile station simultaneously. The benefits of employing the E-DR scheme are increased diversity when the mobile station receives from two transmitters, and reduced number of interferers by one since the second relay is now an assisting terminal and not an interferer.

5.3.2 *Performance Analysis*

In order to demonstrate the effect of using the E-DR scheme, the average *SINR* and the average capacity are derived and compared with the DR scheme.

5.3.2.1 Average *SINR* Analysis for the E-DR Scheme

In this section, the average *SINR* is derived for the E-DR scheme. Since the modification on the DR scheme is made for outer users, the average *SINR* analysis

in this section will concern only outer E-DR users. The inner users in both schemes have the same average *SINR* obtained in Section 5.2.2.1.

Referring to Figure 5.9, when the MS is at distance $d_{MS_{RN_1}}$ from RN_1, it experiences an instantaneous *SINR* from RN_1 of

$$SINR_{RN_1}\left(\chi,h,d_{MS_{RN_1}}\right)=\frac{\dfrac{\sqrt{P_{RN}}\left|h_{MS_{RN_1}}\right|^2}{\chi_{MS_{RN_1}}PL\left(d_{MS_{RN_1}}\right)}}{\sum_{j=1}^{10}\left(\dfrac{\sqrt{P_{RN}}\left|h_j\right|^2}{\chi_j PL\left(d_j\right)}\right)+\dfrac{BD}{U_{outer}}}=\frac{d_{MS_{RN_1}}^{-\upsilon}}{\left|h_{MS_{RN_1}}\right|^2 a_{E-DR}/\chi_{MS_{RN_1}}}$$

where $h=\left\{h_{MS_{RN_1}},h_j\right\}$ and $\chi=\left\{\chi_{MS_{RN_1}},\chi_j\right\}$. When the MS is at distance $d_{MS_{RN_2}}$ away from RN_2, the instantaneous *SINR* from RN_2 is

$$SINR_{RN_2}\left(\chi,h,d_{MS_{RN_2}}\right)=\frac{\dfrac{\sqrt{P_{RN}}\left|h_{MS_{RN_2}}\right|^2}{\chi_{MS_{RN_2}}PL\left(d_{MS_{RN_2}}\right)}}{\sum_{j=1}^{10}\left(\dfrac{\sqrt{P_{RN}}\left|h_j\right|^2}{\chi_j PL\left(d_j\right)}\right)+\dfrac{BD}{U_{outer}}}=\frac{d_{MS_{RN_2}}^{-\upsilon}}{\left|h_{MS_{RN_2}}\right|^2 a_{E-DR}/\chi_{MS_{RN_2}}}$$

where a_{E-DR} in both expressions equals

$$a_{E-DR}=\sum_{j=1}^{10}\left(\frac{\left|h_j\right|^2}{\chi_j d_j^{-\upsilon}}\right)+\frac{BD}{\sqrt{P_{RN}}U_{outer}}\left(\frac{4\pi f_c}{c_o}\right)^2$$

Note that in both *SINR* expressions, the summation is taken for 10 co-channel relays and not 11 as in DR scheme. This is because RN_2 is now an assisting relay and not an interferer. Because the MS receives desired signals from RN_1 and RN_2, the instantaneous overall *SINR* received at MS is the sum of *SINR* terms from RN_1 and RN_2, that is,

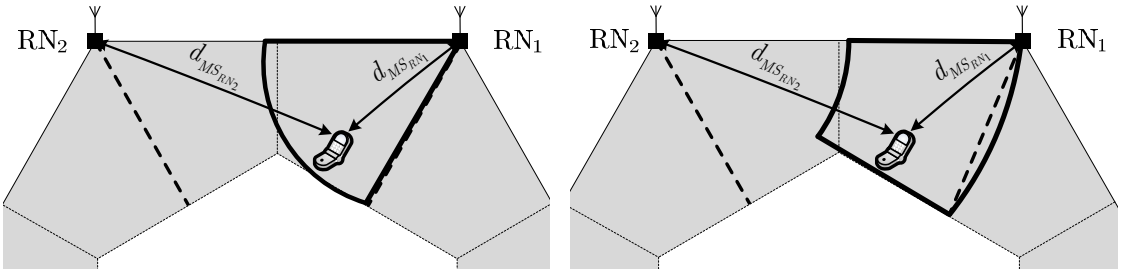

(a) $0 \le d_{RN_1} \le (R - R_o)$ (b) $(R - R_o) \le d_{RN_2} \le R$

Figure 5.10: The ranges of $d_{MS_{RN_1}}$ and $d_{MS_{RN_2}}$ in cell site.

$$\begin{aligned} SINR_{outer}(\chi, h, d) &= SINR_{RN_1}\left(\chi, h, d_{MS_{RN_1}}\right) + SINR_{RN_2}\left(\chi, h, d_{MS_{RN_2}}\right) \\ &= \frac{\chi_{MS_{RN_1}} d_{MS_{RN_1}}^{-\upsilon}}{\left|h_{MS_{RN_1}}\right|^2 a_{E-DR}} + \frac{\chi_{MS_{RN_2}} d_{MS_{RN_2}}^{-\upsilon}}{\left|h_{MS_{RN_2}}\right|^2 a_{E-DR}} \end{aligned} \tag{5.13}$$

where $d = \left\{d_{MS_{RN_1}}, d_{MS_{RN_2}}\right\}$. The average *SINR*, conditioned on knowledge of χ and h, is calculated by integrating the instantaneous overall *SINR* expression in Equation (5.13) over $d_{MS_{RN_1}}$ and $d_{MS_{RN_2}}$ in the ranges shown in Figure 5.10 (a) for $d_{MS_{RN_1}}$ and in Figure 5.10(b) for $d_{MS_{RN_2}}$. That is,

$$\begin{aligned} \overline{SINR}_{outer}(\chi, h) &= \int_0^{R-R_o} \int_{R-R_o}^{R} SINR_{outer}(\chi, h, d)\, \mathrm{d}d_{RN_2}\, \mathrm{d}d_{RN_1} \\ &= \frac{\chi_{RN_1}(R - R_o)\left((R - R_o)^{1-\upsilon} - R^{1-\upsilon}\right)}{|\upsilon - 1|\left|h_{RN_1}\right|^2 a_{outer}(\chi, h)} - \frac{\chi_{RN_2} R_o (R - R_o)^{1-\upsilon}}{|\upsilon - 1|\left|h_{RN_2}\right|^2 a_{outer}(\chi, h)} \end{aligned} \tag{5.14}$$

The average *SINR* will be used to derive the average capacity for E-DR scheme in the next section.

5.3.2.2 Average Capacity Analysis for E-DR Scheme

In E-DR scheme, the overall per-cell capacity is the sum of the capacities provided to the inner and outer MSs. The average capacity for the inner E-DR users is equal to the average capacity for the inner DR users found in Equation (5.11). This is because the DR and the E-DR schemes have the same inner users' *SINR* characteristics. However, the average capacity for outer users is different for the DR and the E-DR schemes. Since $Q_{outer}\left(\chi,h,d\right)=\log_2\left(1+SINR_{outer}\left(\chi,h,d\right)\right)$, the average outer spectrum efficiency, conditioned on χ and h, is given as

$$E\left[Q_{outer}\left(\chi,h\right)\right]=E\left[\log_2\left(1+SINR_{outer}\left(\chi,h\right)\right)\right]$$

Since it is difficult to find a close form for the above expression, the conditional average outer spectral efficiency is upper-bounded as

$$E\left[Q_{outer}\left(\chi,h\right)\right]\le\log_2\left(1+E\left[SINR_{outer}\left(\chi,h\right)\right]\right)$$

Therefore, using the value of $\overline{SINR}_{outer}\left(\chi,h\right)$ found in Equation (5.14), the conditional upper-bound spectrum efficiency equals

$$\begin{aligned}\overline{Q}_{outer}\left(\chi,h\right)&\le\log_2\left(1+\overline{SINR}_{outer}\left(\chi,h\right)\right)\\&=\log_2\left(1+\frac{\chi_{RN_1}\left(R-R_o\right)\left(\left(R-R_o\right)^{1-\upsilon}-R^{1-\upsilon}\right)}{\left|\upsilon-1\right|\left|h_{RN_1}\right|^2 a_{outer}\left(\chi,h\right)}-\frac{\chi_{RN_2}R_o\left(R-R_o\right)^{1-\upsilon}}{\left|\upsilon-1\right|\left|h_{RN_2}\right|^2 a_{outer}\left(\chi,h\right)}\right)\end{aligned}\quad(5.15)$$

After obtaining the conditional average spectrum efficiency for the inner and the outer MSs, the conditional total average capacity is upper-bounded as,

$$\overline{C}\left(\chi,h\right)\le\frac{B\,\overline{Q}_{inner}\left(\chi,h\right)}{\left(1+\Phi\right)}+\frac{\Phi\;B\,\overline{Q}_{outer}\left(\chi,h\right)}{\left(1+\Phi\right)}\quad(5.16)$$

Table 5.2: Semi-analytical and simulated average *SINR*.

		Average *SINR* (dB)	
		Semi-Analytical	**Simulated**
The DR scheme	**inner users**	17.1058	17.011
	outer users	9.9486	9.8977
The E-DR scheme	**inner users**	17.0980	16.9873
	outer users (upper)	22.6610	22.5977

Due to difficulty in averaging the expression in Equation (5.16) over the channel and shadowing parameters, we resort to Monte-Carlo simulation.

5.4 Numerical Results and Discussion

In this section, the performance of the E-DR scheme is compared to the OR and the DR schemes. Semi-analytical results are obtained for the average *SINR* and average capacity that were derived in Section 5.2.2. The parameters for the DR and the E-DR schemes are the obtained from Table 5.1.

Table 5.2 presents the average *SINR* comparisons between analytical and simulated results for DR and E-DR schemes. It is shown that the analytical and simulated results match for both schemes. The average *SINR* for the inner users in both schemes is equal since the modification on the DR scheme is made only for outer users. Meanwhile, the outer users achieve an average *SINR* of 22.661dB when E-DR scheme is utilized, which is higher than 17.1058dB achieved when utilizing the DR scheme. Therefore, transmission with the use of two relays, the E-DR exhibits better average *SINR* than the DR.

Figure 5.11 shows 3D plots for the attainable *SINR* provided by the transmitting terminals to a mobile station roaming within a cell. The figures are obtained to compare the DR scheme in Figure 5.11 (a) and the E-DR scheme in Figure 5.11 (b). Both figures show that the *SINR* is very high for regions close to the

transmitting terminals as seen from the seven peaks for the base station and the six distributed relays. Moreover, when the mobile station is moving away from the transmitters, it encounters low signal level and high interference that yields low *SINR*. It can be seen that the side peaks that represents relays terminals for the E-DR is higher than the side peaks for the DR scheme.

For a clearer demonstration, Figure 5.12 shows the recorded *SINR* contours across the cell for the DR scheme as shown in Figure 5.12 (a), and for the E-DR scheme as shown in Figure 5.12 (b). The figures show that the *SINR* contours for the cell-centre users are similar for the two schemes. However, the *SINR* contours for the outer users are different in both schemes where Figure 5.12 (b) shows higher *SINR*

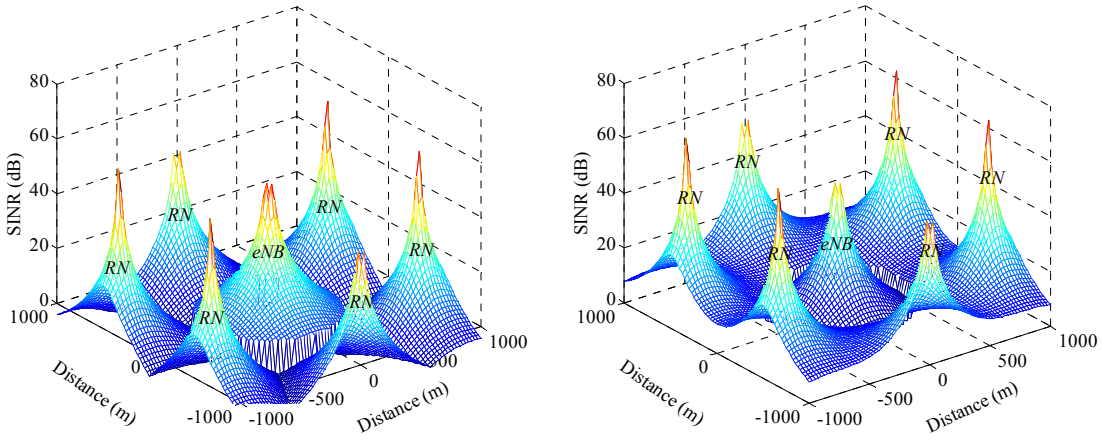

(a) The DR scheme **(b)** The E-DR scheme

Figure 5.11: Analytical *SINR* 3D records.

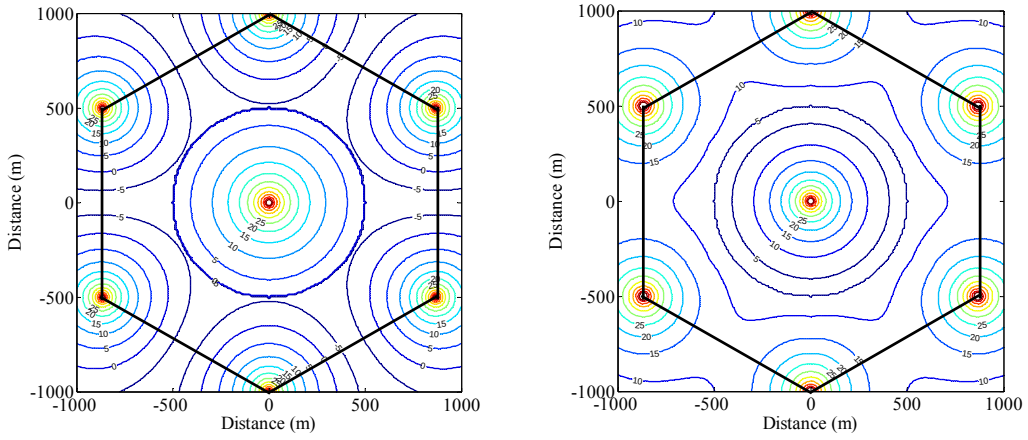

(a) The DR scheme **(b)** The E-DR scheme

Figure 5.12: Analytical *SINR* contours.

than the one in Figure 5.12 (a). Specifically, in Figure 5.12 (a), there are regions within the cell where the mobile station encounters -5dB *SINR*, such as the region between the base station and any relay, as well as the region between two consecutive relays. However, the contours in Figure 5.12 (b) always records *SINR* higher than 5dB. Such significant improvement is due to the diversity improvement in the E-DR scheme.

Figure 5.13 provides an explicit view of the *SINR* profile for the OR, the DR and the E-DR schemes, where the MS is assumed to move from the cell center to the cell edge. All schemes show exponential decrease in *SINR* when inner and outer users are moving away from eNB or RN. As for the outer users, the figure shows that the highest *SINR* is achieved when the E-DR is utilized. For example, at a distance of 520m, the outer DR users achieve an *SINR* of -7dB, the OR users achieve 2dB and the E-DR users achieve 8dB. Despite the improvement for outer region, the inner region requires more improvement for regions where *SINR* drops below 10dB (300m to 500m). This issue will be addressed and solved in Chapter 6.

Figure 5.14 shows the achieved *SINR* for the outer MS users when the OR, the DR and the E-DR schemes are utilized. The results are obtained for a moving mobile station from one RN to another in the same cell. The figure shows significant improvement in *SINR* by the E-DR scheme specifically from distance 300m to 700m, which is due to the diversity improvement made by both relays.

Table 5.3 shows the average analytical and simulated average capacity comparisons for DR and E-DR schemes. The average capacity results are obtained for inner and outer users. The table shows that average capacity for inner users in both schemes is the same due to the similarity of *SINR* characteristics for inner users. However, the outer average capacity for E-DR is higher than the outer average capacity for DR by 3.0713bps/Hz or 44.75%. This is due to the diversity improvement at cell-edge region and ICI reduction that mainly influence the capacity.

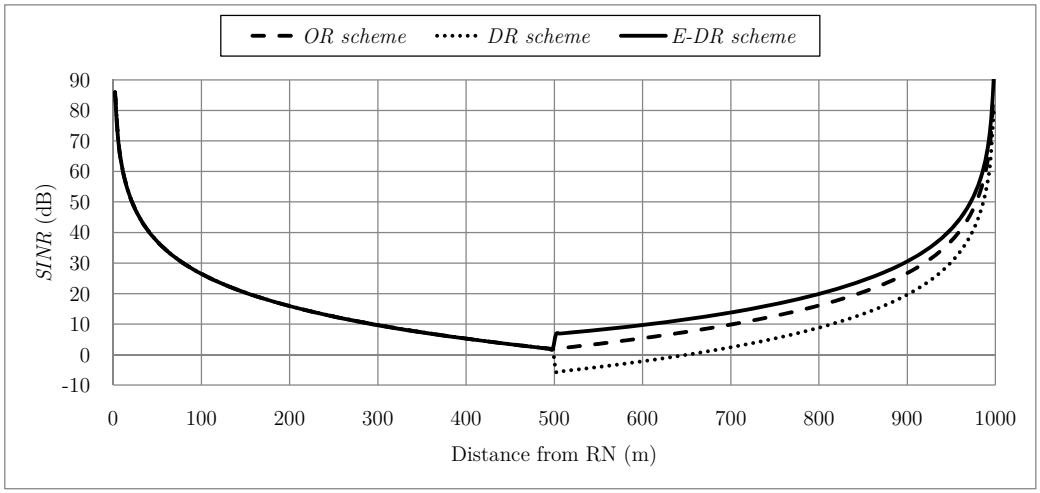

Figure 5.13: *SINR* profile across the cell when the OR, the DR or the E-DR is utilized.

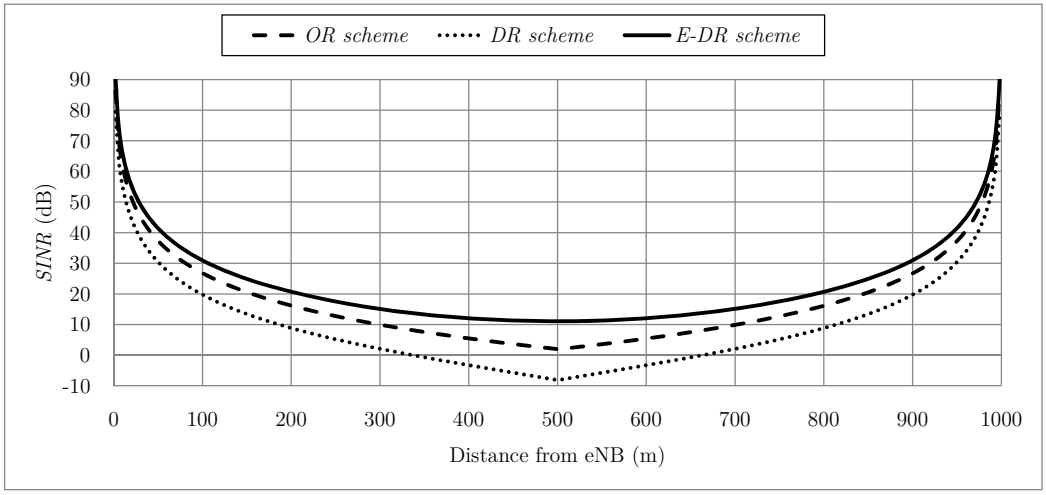

Figure 5.14: Outer *SINR* profile for the OR, the DR and the E-DR schemes.

From all previously provided results, the *SINR* and the capacity of cell-edge users are improved remarkably when utilizing the E-DR scheme. The improvement is due to the diversity gain comes from the cooperation of the edge relay nodes, and due to the interference reduction.

Table 5.3: Semi-analytical and simulated average capacity for the DR and the E-DR schemes.

		Average Capacity (bps/Hz)	
		Semi-analytical	**Simulated**
The DR scheme	**inner users**	5.7102	5.6793
	outer users	3.4439	3.4285
The E-DR scheme	**inner users**	5.7077	5.6716
	outer users (upper)	7.5356	7.5147

5.5 Chapter Summary

In this chapter, a transmission scheme, the directional-relay (DR) scheme, has been proposed to overcome the issues of inter-cell interference and cell-edge users improvement. The scheme also benefits in reducing frequent handover within the cell since the relays serving the outer users carry the same allocated frequency resources. The chapter has included the system model and some performance analyses that measure the validity of the DR scheme. The results from the DR scheme shows deficiency in *SINR* due to strong ICI from co-channel relays within the cell. To overcome the issue of the strong ICI within the cell, the enhanced-DR (E-DR) transmission scheme is proposed by increasing the diversity of the received signal at the mobile terminal. The performance measures of the E-DR were also derived and compared with the DR scheme using theoretical and simulated results. The results show that the E-DR scheme provides better performance in terms of average *SINR* and capacity than the DR due to the diversity gain provided by relay terminals.

Chapter Six: In-band Distributed Relays-Aided LTE-A Cellular System

6.1 Introduction

In Chapters 4 and 5, it was seen that the average *SINR* of cell-edge users was improved by using distributed relay terminals. This improvement is achieved at the expense of spectral efficiency. This is because the total available download bandwidth was divided by a frequency reuse factor of three for the OR scheme and a frequency reuse factor of four for the DR scheme. Since LTE-A requires more per-cell spectral efficiency, it is necessary to have a system with less frequency reuse factor in order to gain higher spectral efficiency. In systems where a universal frequency reuse factor (UFRF) scheme is employed, the channel capacity for each user is improved since each base station exploits the overall available bandwidth. However, this leads to degradation in reception due to high interference from adjacent cells especially for cell-edge users.

In order to achieve a higher degree of spectral efficiency, the conventional UFRF system can be modified by deploying Type II (or in-band) relay terminals at the edges of each cell that utilize the same frequency resources as the base stations. Such modified network setup can provide higher spectral efficiency and improve the *SINR* for cell-edge users. *We shall refer to this as in-band relay* (*IR*) *scheme.*

In Chapter 6, we propose the use of Type II relay terminals at the cell edge area. The objective is to exploit the available bandwidth resources, increase the required link capacity, and improve the cell-edge users. In addition, we propose a cooperative transmission algorithm such that the network terminals (the relay terminals and the base station) can communicate cooperatively. The purpose of this cooperative transmission algorithm is to increase the degree of transmit diversity from network terminals. Moreover, we propose the use of an inter-cell interference cancellation technique jointly with the cooperative transmission to

cancel the interference stemming from the in-band relays. To validate the performance of the in-band relay scheme, its cooperative transmission, and the use of inter-cell interference cancellation technique, we conduct analyses of the *BER* upper-bound, average *SINR*, and the average capacity.

Chapter 6 is organized as follows. Section 6.2 focuses on the system model for the proposed IR scheme. Section 6.3 presents the proposed cooperative transmission algorithm for the IR scheme. It discusses the received signal model as well as inter-cell interference cancellation technique employed in the cooperative transmission. Section 6.4 provides analytical and simulation results for the IR scheme and when employing the proposed cooperative transmission algorithm and interference cancellation technique.

6.2 The In-Band Relay (IR) Scheme

In this section, we present the system model for the proposed IR scheme. We include the received signal model and conventional ML decoder for the IR scheme.

6.2.1 *System Model*

The in-band relay scheme (or simply IR) is a modified UFRF network topology, where Type II relay nodes are deployed at the edges of each cell. When utilizing Type II relay nodes, we allocate frequency resources for each relay node similar to frequency resources for all base stations. The benefit of IR scheme comes from exploiting the available bandwidth resources, as the bandwidth resources here are much higher than any system employing fractional frequency reuse techniques. The system structure for the proposed IR system is illustrated in Figure 6.1, where at the edges of each cell, there exist six-Type II relay nodes, each equipped with a single, omni-directional antenna. The use of relay nodes, particularly at the edges of each cell, provides higher desired signal power for edge users.

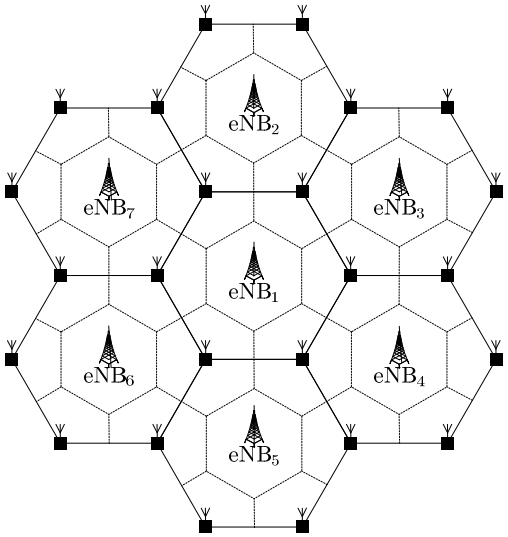

Figure 6.1: The in-band relay (IR) schemes' system model.

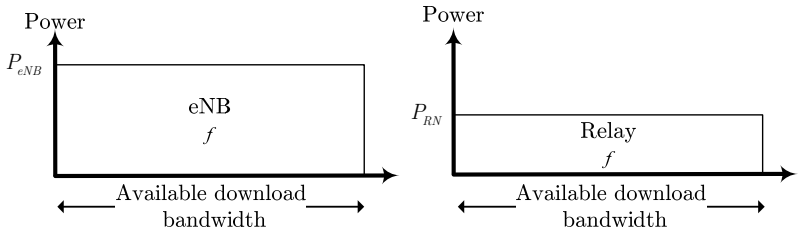

Figure 6.2: Power and frequency resources allocation for the IR transmit terminals.

The power for each relay node (P_{RN}) is set to be equal for all relay nodes and less than the power allocated for the base station (P_{eNB}) with a power ratio of η, which takes a value around 0.1 according to the LTE-A standard [103]. Figure 6.2 shows the power and frequency resources allocation for any base station and relay terminal in the network.

In the IR scheme, since all terminals within the cell are allocated the same frequency resources, the base station and the edge relays can form a virtual cell that performs cooperative transmission of information such as data and CSI from the involved terminals. *We shall refer to this virtual cell as evolved-cell.* The

evolved-cell, or simply E-cell, is illustrated in Figure 6.3, where each E-cell consists of a base station and six distributed relay terminals. The locations and characteristics of the relays make it easier to carry traffic from one E-cell to another, and consequently smoother handover process is achieved. The base station in every E-cell provides centralized coordination between terminals (the base station and the six relays). The coordination between the base station and any two relays is similar to the coordination technique between multiple cell sites called coordinated multipoint transmission (CoMP)[118]-[120]. CoMP is proposed to facilitate the communication between multiple transmitters such that co-channel cells are transmitting desired signals rather than interfering and degraded signals. The coordination between terminals requires centralized radio access network (RAN) point for a group of coordinated base stations. In our proposed E-cell concept, the coordination between terminals is controlled centrally by the host base station. Therefore, there is no need to connect the base station and the distributed relays through an extra RAN device. The transmission between coordinated

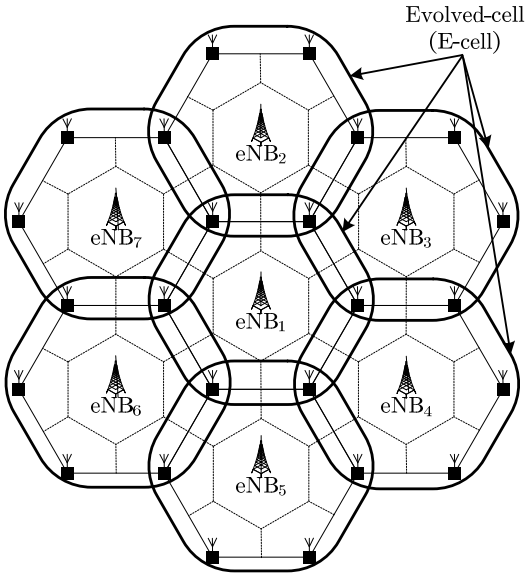

Figure 6.3: Illustration of seven evolved-cells, each consists of one eNB and six relay nodes at the cell edges.

terminals will be discussed in details in section 6.3.

Regardless of the great benefits from edge-relay deployment, strong interference is introduced from the relays within the E-cell and from other adjacent E-cell*s*. This interference reduces the *SINR* and consequently degrades capacity. In the following section, we introduce the effect of this interference by presenting the received signal model as well as the conventional ML decoder.

6.2.2 *Received Signal Model & Conventional ML Decoder for the IR Scheme*

In the IR scheme, the mobile station is communicating through either the base station or a candidate relay within the E-cell and not through both. The candidate relay is selected according to its received signal level. Hence, after allocating the relay, the base station transmits to the relay through, for example, a cable, and the relay retransmits to the mobile station. The data transmission in the IR scheme is similar to direct transmission as the mobile station is receiving from one transmitter, the base station, or the candidate relay node. To further illustrate the IR scheme, consider the E-cell in Figure 6.4.

Assuming RN_1 provides the highest received signal level, the figure shows two cases when the mobile station is receiving desired signals from either eNB_1 in Figure 6.4 (a) or RN_1 in Figure 6.4 (b). When eNB_1 transmits to the mobile station (solid arrow), there exists inter-cell interference delivered by the six distributed relays as well as inter-cell interference delivered by other neighboring E-cells indicated by the dashed arrows. Also, when RN_1 transmits to the mobile station (solid arrow), there exists inter-cell interference delivered by the other five distributed relays and the eNB_1, as well as inter-cell interference delivered by other neighboring E-cells indicated by the dashed arrows. Assuming Rayleigh flat fading channel between terminals, and $s(n)$ is the transmitted symbol sequence, the received signal at the mobile station is given as

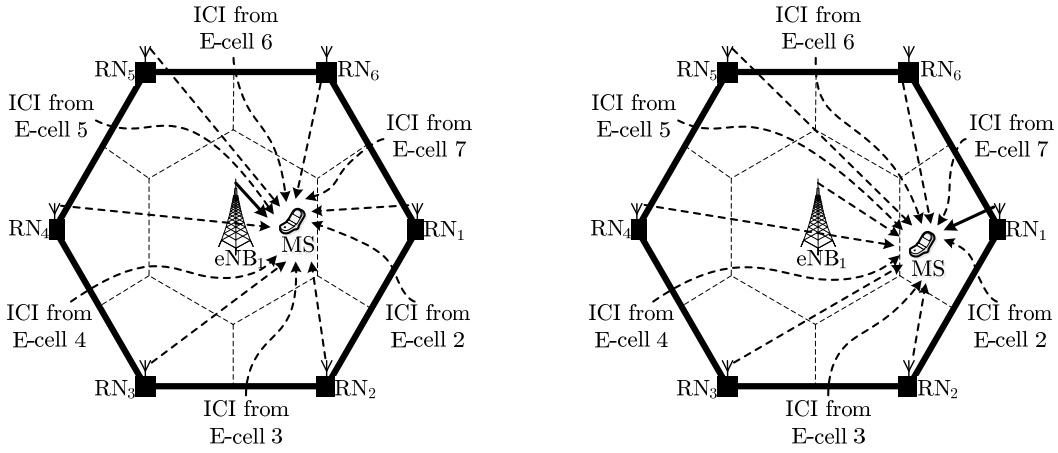

(a) eNB_1 is the desired transmitter (b) RN_1 is the desired transmitter

Figure 6.4: System model for one *Evolved-cell* downlink.

$$y_{eNB}(n) = \sqrt{P_{eNB}}\, h_{eNB_1} s(n) + \sum_{i=1}^{6} \sqrt{P_{RN}}\, h_{RN_i}^{ICI_1} s_i^{ICI_1}(n) + \sum_{j=7}^{\Xi-6} \sqrt{P_{eNB/RN}}\, h_{eNB_j/RN_j}^{ICI_2} s_j^{ICI_2}(n) + w(n) \quad (6.1)$$

when the MS receives directly from the base station, and

$$y_{RN_1}(n) = \sqrt{P_{RN}}\, h_{RN_1} s(n) + \sum_{i=2}^{6} \sqrt{P_{RN}}\, h_{RN_i}^{ICI_1} s_i^{ICI_1}(n) + \sum_{j=7}^{\Xi-6} \sqrt{P_{eNB/RN}}\, h_{eNB_j/RN_j}^{ICI_2} s_j^{ICI_2}(n) + w(n) \quad (6.2)$$

when the MS receives directly from the relay node. In Equations (6.1) and (6.2), h_{eNB_1} and h_{RN_1} are the channel coefficients for the eNB_1-MS and RN_1-MS links, respectively, $h_{RN_i}^{ICI_1}$ is the channel coefficient from the i^{th} co-channel relay within the E-cell to the MS, $h_{eNB_j/RN_j}^{ICI_2}$ is the channel coefficient from the j^{th} co-channel base station / relay from other E-cell*s* to the MS, and $w(n)$ is AWGN. $w(n)$ is modeled as zero-mean, complex Gaussian random variable with variance $\sigma_w^2(n)$. If no ICI cancellation technique is employed, the data at the mobile station can be ML decoded conventionally by computing the decision statistic, which is obtained by multiplying the received signal by the conjugate of the desired channel as

$$\begin{aligned}\hat{y}_{eNB}(n) &\triangleq h_{eNB_1}^{*}\, y_{eNB}(n) \\ &= \sqrt{P_{eNB}} \left|h_{eNB_1}\right|^2 s(n) + \sum_{i=1}^{6} \sqrt{P_{RN}} h_{eNB_1}^{*} h_{RN_i}^{ICI_1} s_i^{ICI_1}(n) + .. + \sum_{j=7}^{\Xi-6} \sqrt{P_{eNB/RN}} h_{eNB_1}^{*} h_{eNB_j/RN_j}^{ICI_2} s_j^{ICI_2}(n) + h_{eNB_1}^{*} w(n)\end{aligned}$$

in Equation (6.1), and

$$\hat{y}_{RN_1}(n) \triangleq h^*_{RN_1}\, y_{RN_1}(n)$$
$$= \sqrt{P_{RN}}\left|h_{RN_1}\right|^2 s(n) + \sum_{i=2}^{6}\sqrt{P_{RN}}\,h^*_{RN_1}h^{ICI_1}_{RN_i}s^{ICI_1}_i(n) + .. + \sum_{j=7}^{\Xi-6}\sqrt{P_{eNB/RN}}\,h^*_{RN_1}h^{ICI_2}_{eNB_j/RN_j}s^{ICI_2}_j(n) + h^*_{RN_1}w(n)$$

in Equation (6.2). Then, the received sequences from the base station and the relay node are selected according to

$$\hat{s}(n) = \arg\min_s \left|\hat{y}_{eNB}(n) - \sum_{n=0}^{N-1}\sqrt{P_{eNB}}\left|h_{eNB}\right|^2 s(n)\right|^2$$

and

$$\hat{s}(n) = \arg\min_s \left|\hat{y}_{RN_1}(n) - \sum_{n=0}^{N-1}\sqrt{P_{RN}}\left|h_{RN_1}\right|^2 s(n)\right|^2,$$

respectively. Assuming each symbol in the sequence has an average energy of $\left|s(n)\right|^2 = 1$, and h_{eNB_1}, $h^{ICI_1}_{RN_i}$ and $h^{ICI_2}_{eNB_j/RN_j}$ are uncorrelated, it can be shown that the instantaneous *SINRs* of the decision statistics are given by

$$SINR\left(h_{eNB_1}, h^{ICI_1}_{RN_i}, h^{ICI_2}_{eNB_j/RN_j}, w(n)\right) = \frac{P_{eNB}\left|h_{eNB_1}\right|^2}{\sum_{i=1}^{6}P_{RN}\left|h^{ICI_1}_{RN_i}\right|^2 + \sum_{j=7}^{\Xi-6}P_{eNB/RN}\left|h^{ICI_2}_{eNB_j/RN_j}\right|^2 + \sigma^2_w(n)} \quad (6.3)$$

and

$$SINR\left(h_{RN_1}, h^{ICI_1}_{RN_i}, h^{ICI_2}_{eNB_j/RN_j}, w(n)\right) = \frac{P_{RN}\left|h_{RN_1}\right|^2}{\sum_{i=2}^{6}P_{RN}\left|h^{ICI_1}_{RN_i}\right|^2 + \sum_{j=7}^{\Xi-6}P_{eNB/RN}\left|h^{ICI_2}_{eNB_j/RN_j}\right|^2 + \sigma^2_w(n)} \quad (6.4)$$

for $\hat{y}_{eNB}(n)$ and $\hat{y}_{RN_1}(n)$, respectively. Note that the ICI from the relay terminals within the E-cell and from other E-cell*s* degrades the performance of decoding the received symbols. In this dissertation, *we shall refer to the IR scheme that decodes the symbols conventionally without any ICI cancellation technique as conventional IR scheme*. In the following section, we propose a cooperative transmission algorithm for the IR scheme to increase the diversity of the received signals.

6.3 Cooperative Transmission Algorithm for the IR Scheme

In an E-cell, communications between the serving base station and the mobile users with the assistance of the relay nodes is achieved using the following algorithm. The base station serves the mobile user whenever the signal level is above a certain threshold. When the received signal level drops below this threshold, the mobile station starts searching for two potential relay nodes that provide the strongest signal levels among the other relays within the E-cell. After locating the two candidate relays, the base station and the two relays start transmitting to the mobile station. In Chapter 3, the transmission protocol Enhanced-Decode-and-Forward (E-DF) has shown remarkable improvements in terms of data rate and diversity gain. Here, the desired eNB and the two candidate relays form a similar structure in the E-DF structure. Hence, E-DF is used as cooperative transmission scheme in IR network.

To further illustrate the cooperative transmission using E-DF cooperative scheme in the IR network, consider the system in Figure 6.5. The base station eNB_1 in the E-cell aims to communicate with MS_1. The figure shows that beside eNB_1, there exist six candidate relay nodes, namely, RN_1, RN_2, RN_3, RN_4, RN_5 and RN_6, that can provide assistance to eNB. It is assumed that RN_1 and RN_2 provide the strongest signal levels among the six relays. Therefore, eNB, RN_1 and RN_2 communicate cooperatively with MS_1. During the transmission, there exists inter-cell interference delivered by the other four relays, as well as inter-cell interference delivered by other neighboring E-cells indicated by the dashed arrows.

6.3.1 *Received Signal Model for IR System with E-DF Cooperative Scheme*

At the eNB, the information bit sequence is first mapped from a complex signal constellation into a desired complex symbol sequence. The complex symbol sequence is then parsed into code vectors $\mathbf{s}_D(n) \triangleq \left[s(2n) \quad s(2n+1) \right]^T$,

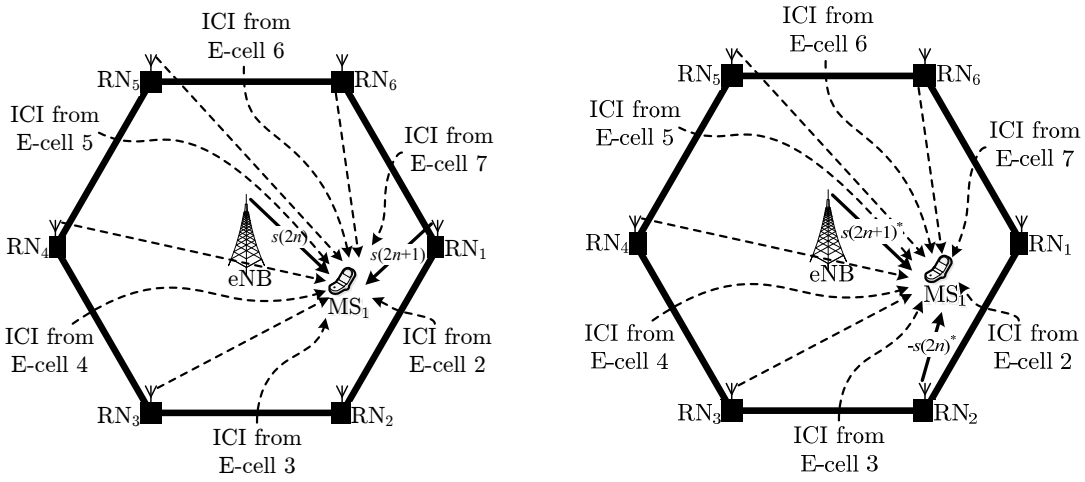

(a) Phase 1 (b) Phase 2

Figure 6.5: System model for one *evolved-cell* downlink using cooperative transmission.

$\left|s(n)\right|^2 = 1, \quad n = 0, 1, 2, ..., N-1$. It is assumed that the channel coherence time is comparable to the symbol duration due to relative motion between transmitter and receiver. The channels between terminals are modeled as uncorrelated frequency-flat but time-selective Rayleigh fading. The channel gains are assumed time-invariant within two signaling intervals but may vary in every two signaling intervals. Each relay power is assumed a fraction of the base station power according to the following relation

$$P_{RN} = \eta P_{eNB} \tag{6.5}$$

where $0<\eta<1$. Let the total number of terminals in the network (base stations plus relay nodes) be denoted by Ξ. The downlink sequence transmission to the MS is accomplished in two phases that are repeated until the end of the entire symbol sequence. The two phases are illustrated in Figure 6.5.

In phase 1, Figure 6.5 (a), eNB transmits the first sequence $s(2n)$ to MS_1, and RN_1 transmits the second sequence $s(2n+1)$ to MS_1, simultaneously. The mobile station MS_1 receives desired signals from eNB and RN_1, and interference from

relays within the E-cell (RN_i, $i = \{3,\ldots,6\}$) and from terminals in other E-cells (eNB_j, RN_j, $j = \{7,\ldots,\Xi\text{-}6\}$) as,

$$y(2n) = \underbrace{\sqrt{P_{eNB}}\, h_{eNB} s(2n) + P_{RN}\, h_{RN_1} s(2n+1)}_{\substack{\text{Desired signals from} \\ \text{eNB and } RN_1}} + \underbrace{\sum_{i=3}^{6} \sqrt{P_{RN}}\, h_{RN_i}^{ICI_1} s_i^{ICI_1}(2n)}_{\substack{\text{Interference from relays} \\ \text{within E-cell}}} + \ldots$$
$$\ldots + \underbrace{\sum_{j=7}^{\Xi-6} \sqrt{P_{eNB/RN}}\, h_{eNB_j/RN_j}^{ICI_2} s_j^{ICI_2}(2n)}_{\substack{\text{Interference from terminals} \\ \text{in other E-cells}}} + w(2n) \tag{6.6}$$

where h_{eNB} and h_{RN_1} are the channel coefficients from base station to MS_1, and from relay node to MS_1, respectively, and $w(2n)$ is additive white Gaussian noise (AWGN). In Equation (6.6), all channel coefficients are combination of path loss, fading and shadowing coefficients. Path loss model is given in Equation (4.2), whereas fading and log-normal shadowing are modeled as zero-mean, complex Gaussian random variables with variances σ_h^2 and σ_χ^2 , respectively. Also, additive white Gaussian noise is modeled as a zero-mean, complex Gaussian random variable with variance $\sigma_w^2(2n)$.

In phase 2, Figure 6.5 (b), eNB and RN_2 modify the constellations of the symbols such that, eNB changes $s(2n+1)$ to $s^*(2n+1)$ and RN_2 changes $s(2n)$ to $s^*(2n)$. Both, eNB and RN_2, transmit the modified symbols to the MS simultaneously. Therefore, the signal received at the MS from eNB, RN_2 and the interferers in phase 2 can be written as

$$y(2n+1) = \underbrace{\sqrt{P_{eNB}}\, h_{eNB} s^*(2n+1) - \sqrt{P_{RN}}\, h_{RN_2} s^*(2n)}_{\substack{\text{Desired signals from} \\ RN_2 \text{ and eNB}}} + \underbrace{\sum_{i=3}^{6} \sqrt{P_{RN}}\, h_{RN_i}^{ICI_1} s_i^{ICI_1}(2n+1)}_{\substack{\text{Interference from} \\ \text{relays within E-cell}}} + \ldots$$
$$\ldots + \underbrace{\sum_{j=7}^{\Xi-6} \sqrt{P_{eNB/RN}}\, h_{eNB_j/RN_j}^{ICI_2} s_j^{ICI_2}(2n+1)}_{\substack{\text{Interference from terminals} \\ \text{in other E-cells}}} + w(2n+1) \tag{6.7}$$

where h_{RN_2} is the channel coefficient from RN_2 to the MS and $w(2n+1)$ is AWGN. In Equation (3.4), $w(2n+1)$ is modeled as a zero-mean, complex Gaussian random variable with variance $\sigma_w^2(2n+1)$. Assuming the channel conditions for all links are quasi-static at least over two consecutive signaling intervals, and taking the conjugate of $y(2n+1)$ in Equation (6.7), Equations (6.6) and (6.7) may be expressed in vector-matrix form as the sum of desired signals, interference from terminals within the E-cell and interference from other E-cell*s* as

$$\mathbf{y}(n) = \underbrace{\mathbf{H}_D \mathbf{s}_D(n)}_{\text{Desired signals}} + \underbrace{\mathbf{H}_{ICI_1} \mathbf{s}_{ICI_1}(n)}_{\substack{\text{ICI within the} \\ \text{Evolved-cell } (\text{ICI}_1)}} + \underbrace{\mathbf{H}_{ICI_2} \mathbf{s}_{ICI_2}(n)}_{\substack{\text{ICI from other} \\ \text{Evolved-cells } (\text{ICI}_2)}} + \mathbf{w}(n) \tag{6.8}$$

where $\mathbf{y}(n) = \left[y(2n) \quad y^*(2n+1) \right]^T$, $\mathbf{y}(n) \in \mathbb{C}^{2\times 1}$ is the received signal vector,

$$\mathbf{H}_D = \begin{bmatrix} \sqrt{P_{eNB}} h_{eNB} & \sqrt{P_{RN}} h_{RN_1} \\ -\sqrt{P_{RN}} h_{RN_2}^* & \sqrt{P_{eNB}} h_{eNB}^* \end{bmatrix}, \qquad \mathbf{H}_D \in \mathbb{C}^{2\times 2}$$

is the channel matrix for the desired signals, $\mathbf{s}_D(n) = \left[s(2n) \quad s(2n+1) \right]^T$, $\mathbf{s}_D(n) \in \mathbb{C}^{2\times 1}$ is the desired signals transmitted from both eNB and RN_1,

$$\mathbf{H}_{ICI_1} \mathbf{s}_{ICI_1}(n) = \sum_{i=3}^{6} \mathbf{H}_{ICI_1}^i \mathbf{s}_{ICI_1}^i(n), \quad \mathbf{H}_{ICI_1}^i \in \mathbb{C}^{2\times 2}, \quad \mathbf{s}_{ICI_1}^i(n) \in \mathbb{C}^{2\times 1}$$

is the interference caused by the interfering relay nodes (i.e. RN_3, …, RN_6) within the E-cell,

$$\mathbf{H}_{ICI_2} \mathbf{s}_{ICI_2}(n) = \sum_{i=7}^{(\Xi-6)} \mathbf{H}_{ICI_2}^i \mathbf{s}_{ICI_2}^i(n), \quad \mathbf{H}_{ICI_2}^i \in \mathbb{C}^{2\times 2}, \quad \mathbf{s}_{ICI_2}^i(n) \in \mathbb{C}^{2\times 1}$$

is the interference caused by the interfering terminals in other E-cell*s* and $\mathbf{w}(n)$, $\mathbf{w}(n) \in \mathbb{C}^{2\times 1}$ is AWGN vector. It can be seen in Equation (6.8) that recovering the desired symbol sequences, $s(2n)$ and $s(2n+1)$, is difficult due to the added inter-cell interfering signals. For this reason, inter-cell interference cancellation technique

must me employed to eliminate the interference and, consequently, decode correctly.

In the literature, several inter-cell interference cancellation and coordination techniques have been proposed to cancel interference or, at least, to regulate it to a minimum acceptable level [121-129]. Examples of such techniques are power control, scheduling, post-coding and pre-coding. Each technique has its characterized performance, implementation complexity, and spectral efficiency improvement. In the following, we propose the use of *Interference Rejection Combining* (IRC) technique as an inter-cell interference cancellation technique that works jointly with the E-DF and the IR schemes.

6.3.2 *IRC-Aided IR Scheme with E-DF Cooperative Systems*

6.3.2.1 Introduction

The idea of lossless interference cancelation in a communication system was first proposed for *Digital-AMPS* (D-AMPS) systems by Bottomley and Jamal in the article "Adaptive Arrays and MLSE Equalization" [130]. The authors considered two processes that corrupt the channel inputs – *interference* and the *noise*, and modeled their sum as a Gaussian process. In their work, Bottomley and Jamal showed that there exists a receiver structure that cancels the interference without incurring any power alteration or rate loss. They named the cancellation technique at the receiver as *Interference Rejection Combining* (IRC). Their idea was later applied to GSM systems [131]. Moreover, several studies have been conducted for the IRC technique in MIMO systems such as [132-135]. The IRC technique and its extensions require knowledge of the interference and noise covariance matrix and uses maximum likelihood sequence estimator (MLSE) equalizer. Estimating this matrix has been conducted such as [133]. To this author's knowledge of the literature, IRC has not been applied for interference cancellation in cooperative

communication systems. In this dissertation, we propose a two-stage processing at the IR scheme with E-DF receiver – decoupling the desired symbols followed by IRC.

In the following, we discuss the received signal model and decoupling the desired symbols by diagonalizing the desired channel matrix. Then, we show, by simulation, that the first and second tier interference at the output of the receiver fit the Gaussian model. Having established this, we eliminate the inter-cell interference using an MLSE equalizer. This requires estimating the covariance matrix of the combined interference and noise. Finally, we derive the average bit-error rate (*BER*) upper bound of the two-step decoding.

6.3.2.2 Signal Model

Due to proximity to the desired transmitting terminals, interfering relay terminals within the E-cell (referred to as tier 1) cause the most effective interference followed by terminals in neighboring E-cell*s* (tier 2 interferers). Therefore, elimination of the effect of ICI_1 and ICI_2 in Equation (6.8) is necessary for reducing the bit-error rate. One way to eliminate the effect of tier 1 and tier 2 interferences is by using interference rejection combining (IRC) technique [130]. IRC has been applied to cancel the interference at the mobile station receiver for D-AMPS [130] and GSM [131] where interference is assumed to be Gaussian. Referring to the received signal in Equation (6.8), ICI_1 and ICI_2 may be combined with the noise elements to yield a new vector $\mathbf{z}(n)$. Hence Equation (6.8) is rewritten as

$$\mathbf{y}(n) = \mathbf{H}_D \mathbf{s}_D(n) + \mathbf{z}(n) \tag{6.9}$$

where $\mathbf{z}(n) = \mathbf{H}_{ICI_1}\mathbf{s}_{ICI_1}(n) + \mathbf{H}_{ICI_2}\mathbf{s}_{ICI_2}(n) + \mathbf{w}(n)$, $\mathbf{z}(n) \in \mathbb{C}^{2\times 1}$ is the combined interference plus the AWGN.

In this dissertation, we propose a two-step decoding approach. In the first step, we decouple the desired symbol sequence by diagonalizing the desired channel matrix.

In the second step, we show that the interference is Gaussian, through simulation, and then apply IRC to cancel the interference. The following subsection derives the diagonalization of the desired channel matrix.

6.3.2.3 The Diagonalization of the Desired Channel Matrix

Consider the channel matrix $\mathbf{H}_D$ and the desired data sequence $\mathbf{s}_D(n)$ in Equation(6.8). Assuming the channel is time-invariant over at least two consecutive signaling periods, multiplying $\mathbf{s}_D(n)$ by $\mathbf{H}_D$ yields

$$\mathbf{H}_D\mathbf{s}_D(n)=\begin{bmatrix} h_{eNB} & \eta h_{RN_1} \\ -\eta h^*_{RN_2} & h^*_{eNB} \end{bmatrix}\begin{bmatrix} s(2n) \\ s(2n+1) \end{bmatrix}=\begin{bmatrix} h_{eNB}s(2n)+\eta h_{RN_1}s(2n+1) \\ -\eta h^*_{RN_2}s(2n)+h^*_{eNB}s(2n+1) \end{bmatrix}$$

Because $s(2n)$ and $s(2n+1)$ appear in every term in the vector $\mathbf{H}_D\mathbf{s}_D(n)$, it is necessary to decouple the two sequences in order to decode correctly. The separation of two sequences can be achieved by diagonalization of the desired channel matrix $\mathbf{H}_D$. One method for matrix diagonalization is using matrix decomposition [143]. This method requires calculating the eigenvalues and eigenvectors, which adds more complexity at the receiver. In this section, we propose the use of Tran & Sesay [105] diagonalization method to decouple the desired data sequences. The method of Tran & Sesay provides less complexity compared to matrix decomposition. In [105], diagonalizing the desired channel matrix is carried out by constructing a matrix $\boldsymbol{\varphi}_D$ such that its product with $\mathbf{H}_D$ is a diagonal matrix. i.e.

$$\boldsymbol{\varphi}_D\mathbf{H}_D=\begin{bmatrix} \lambda_1 & 0 \\ 0 & \lambda_2 \end{bmatrix}\triangleq\boldsymbol{\Lambda}_D \quad \text{and} \quad \boldsymbol{\varphi}_D\mathbf{H}_D\mathbf{s}_D(n)=\begin{bmatrix} \lambda_1 & 0 \\ 0 & \lambda_2 \end{bmatrix}\begin{bmatrix} s(2n) \\ s(2n+1) \end{bmatrix}=\begin{bmatrix} \lambda_1 s(2n) \\ \lambda_2 s(2n+1) \end{bmatrix}$$

where λ_1 and λ_2 are in general complex-valued coefficients that are specified later in this section. Define a 2×2 matrix $\boldsymbol{\varphi}_D$

$$\boldsymbol{\varphi}_D \triangleq \begin{bmatrix} \varphi_{D1} & \varphi_{D2} \\ \varphi_{D3} & \varphi_{D4} \end{bmatrix}$$

Multiplying $\mathbf{H}_D$ by $\boldsymbol{\varphi}_D$ yields,

$$\boldsymbol{\varphi}_D \mathbf{H}_D = \begin{bmatrix} \varphi_{D1} & \varphi_{D2} \\ \varphi_{D3} & \varphi_{D4} \end{bmatrix} \begin{bmatrix} h_{eNB} & \eta h_{RN_1} \\ -\eta h_{RN_2}^* & h_{eNB}^* \end{bmatrix} = \begin{bmatrix} \varphi_{D1} h_{eNB} - \eta \varphi_{D2} h_{RN_2}^* & \eta \varphi_{D1} h_{RN_1} + \varphi_{D2} h_{eNB}^* \\ \varphi_{D3} h_{eNB} - \eta \varphi_{D4} h_{RN_2}^* & \eta \varphi_{D3} h_{RN_1} + \varphi_{D4} h_{eNB}^* \end{bmatrix}$$

In order to diagonalize the product, the elements of $\boldsymbol{\varphi}_D$ are selected to annihilate the off-diagonal terms. That is,

$$\eta \varphi_{D1} h_{RN_1} + \varphi_{D2} h_{eNB}^* = 0 \tag{6.10}$$

and

$$\varphi_{D3} h_{eNB} - \eta \varphi_{D4} h_{RN_2}^* = 0 \tag{6.11}$$

A set of values of φ_{D1} and φ_{D2} that satisfy Equation (6.10) can be obtained intuitively as,

$$\varphi_{D1} = h_{eNB}^* \text{ and } \varphi_{D2} = -\eta h_{RN_1}$$

Also, a set of values of φ_{D3} and φ_{D4} that satisfy Equation (6.11) is given by,

$$\varphi_{D3} = \eta h_{RN_2}^* \text{ and } \varphi_{D4} = h_{eNB}$$

Using the above four values, $\boldsymbol{\varphi}_D$ is written as

$$\boldsymbol{\varphi}_D = \begin{bmatrix} \varphi_{D1} & \varphi_{D2} \\ \varphi_{D3} & \varphi_{D4} \end{bmatrix} = \begin{bmatrix} h_{eNB}^* & -\eta h_{RN_1} \\ \eta h_{RN_2}^* & h_{eNB} \end{bmatrix}$$

Using the above matrix, the gain matrix $\boldsymbol{\Lambda}_D = \boldsymbol{\varphi}_D \mathbf{H}_D$ reduces to a diagonal matrix

$$\boldsymbol{\Lambda}_D = diag(\lambda_1, \lambda_2) = \begin{bmatrix} |h_{eNB}|^2 + \eta^2 h_{RN_2}^* h_{RN_1} & 0 \\ 0 & |h_{eNB}|^2 + \eta^2 h_{RN_2}^* h_{RN_1} \end{bmatrix}$$

where

$$\lambda_1 = \lambda_2 = \left|h_{eNB}\right|^2 + \eta^2 h^*_{RN_2} h_{RN_1} \triangleq \lambda .$$

Now, the received signal is written as

$$\underbrace{\begin{bmatrix} \hat{y}(2n) \\ \hat{y}(2n+1) \end{bmatrix}}_{\hat{\mathbf{y}}(n)} = \sqrt{P_{eNB}} \underbrace{\begin{bmatrix} \lambda & 0 \\ 0 & \lambda \end{bmatrix}}_{\mathbf{\Lambda}_D} \underbrace{\begin{bmatrix} s(2n) \\ s(2n+1) \end{bmatrix}}_{\mathbf{s}_D(n)} + \underbrace{\begin{bmatrix} \hat{z}(2n) \\ \hat{z}(2n+1) \end{bmatrix}}_{\hat{\mathbf{z}}(n)} \tag{6.12}$$

where $\hat{\mathbf{y}}(n) \triangleq \boldsymbol{\varphi}_D \mathbf{y}(n)$ and $\hat{\mathbf{z}}(n) \triangleq \boldsymbol{\varphi}_D \mathbf{z}(n)$. Now $s(2n)$ and $s(2n+1)$ are decoupled and its decoding becomes simpler than before. In the above equation, the vector $\hat{\mathbf{z}}(n)$ is a composition of the first two tiers ICI plus the AWGN multiplied by the diagonalize matrix $\boldsymbol{\varphi}_D$. This vector causes erroneously decoded symbols. In the following, a maximum likelihood sequence estimator (MLSE) equalizer is proposed as a part of the two-step decoding process for the IRC-aided IR with E-DF scheme to eliminate the effect of the vector $\hat{\mathbf{z}}(n)$. We first need to establish that the interference components of $\hat{\mathbf{z}}(n)$ are Gaussian so it agrees with the assumption made in [130] for using IRC.

6.3.2.4 Statistical Characteristics of $\hat{\mathbf{z}}(n)$

Before we proceed to designing the MLSE equalizer for the IRC, it is necessary to understand the statistical characteristics of the vector $\hat{\mathbf{z}}(n) \triangleq \left[\hat{z}(2n) \quad \hat{z}(2n+1)\right]^T$.

Conditioned on the channel parameters for the desired signal, the only random component in $\hat{\mathbf{z}}(n) = \boldsymbol{\varphi}_D \mathbf{z}(n)$ is $\mathbf{z}(n)$. Therefore, we only need to establish that the components of $\mathbf{z}(n)$ are Gaussian. Since

$$\mathbf{z}(n) = \mathbf{H}_{ICI_1} \mathbf{s}_{ICI_1}(n) + \mathbf{H}_{ICI_2} \mathbf{s}_{ICI_2}(n) + \mathbf{w}(n),$$

and $\mathbf{w}(n)$ is Gaussian, we only need to establish that the interference components are Gaussian.

Here, we attempt to show that the interference components are Gaussian through simulation. Figure 6.6 shows the probability density function of the random variable $\hat{\mathbf{z}}(n)$ for two cases – only ICI_1 and $ICI_1 + ICI_2$. The curve for the case where only ICI_1 is considered is obtained for number of eNBs interferers equals 6 and the number of co-channel relays equals 21. Also, the curve for the case where $ICI_1 + ICI_2$ is considered is obtained for number of eNBs interferers equals 12 and the number of co-channel relays equals 33. For each interfere, 10^6 complex channel realizations were generated and used at the desired MS together with other interferers to calculate the probability density function for the first tier interference and for the sum of the first and second tier interferences. The curves show that the two interference components (ICI_1 and ICI_1+ICI_2) both match the Gaussian *PDF* quite well.

In light of the above results, each element of $\mathbf{H}_{ICI_1}\mathbf{s}_{ICI_1}(n)$ vector can be modeled as a zero-mean, complex Gaussian random variable with variance given by

$$\begin{cases} \sigma^2_{eNB_i^{ICI_1}} & i = 1,2,...,6 \\ \sigma^2_{RN_j^{ICI_1}} & j = 1,2,...,21 \end{cases}.$$

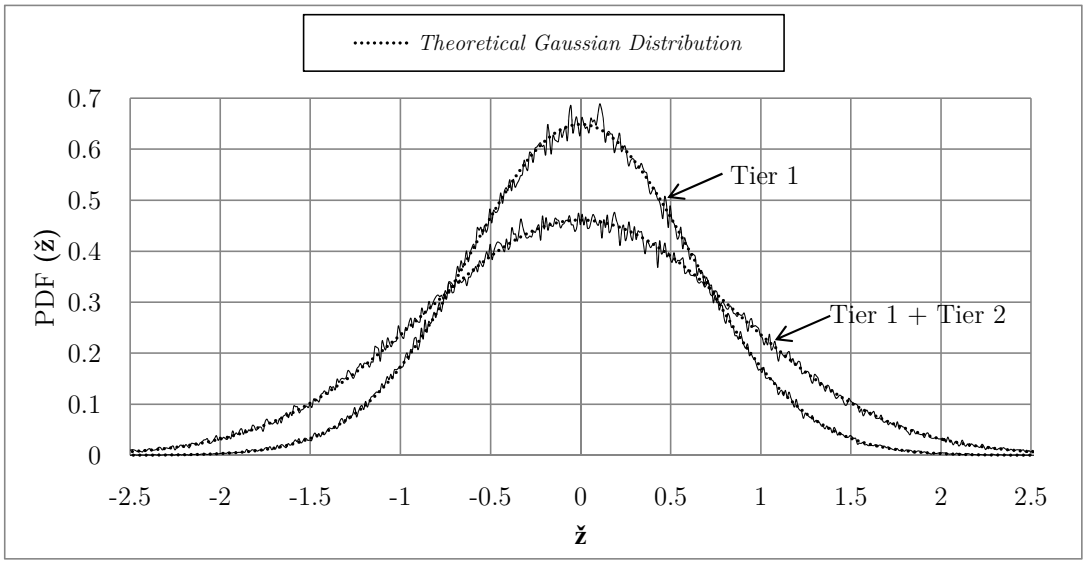

Figure 6.6: Theoretical and simulated *PDF* of $\hat{\mathbf{z}}(n)$

Similarly, each element of $\mathbf{H}_{ICI_2}\mathbf{s}_{ICI_2}(n)$ vector can be modeled as a zero-mean, complex Gaussian random variable with variance given by

$$\begin{cases} \sigma^2_{eNB_k^{ICI_2}} & k=1,2,...,12 \\ \sigma^2_{RN_l^{ICI_2}} & l=1,2,...,33 \end{cases}.$$

Since all the channel components are independent, each component of the vector $\mathbf{z}(n) \triangleq \left[z(2n) \quad z(2n+1) \right]^T$ is modeled as zero-mean, complex Gaussian random variable with variance given, respectively, by

$$\sigma_z^2(2n) = \sigma_w^2(2n) + \sum_{i=1}^{6} \sigma^2_{eNB_i^{ICI_1}} + \sum_{j=1}^{21} \sigma^2_{RN_j^{ICI_1}} + \sum_{k=1}^{12} \sigma^2_{eNB_k^{ICI_2}} + \sum_{l=1}^{33} \sigma^2_{RN_l^{ICI_2}} \tag{6.13}$$

and

$$\sigma_z^2(2n+1) = \sigma_w^2(2n+1) + \sum_{i=1}^{6} \sigma^2_{eNB_i^{ICI_1}} + \sum_{j=1}^{21} \sigma^2_{RN_j^{ICI_1}} + \sum_{k=1}^{12} \sigma^2_{eNB_k^{ICI_2}} + \sum_{l=1}^{33} \sigma^2_{RN_l^{ICI_2}} \quad , \tag{6.14}$$

where $\sigma_w^2(2n)$ and $\sigma_w^2(2n+1)$ are AWGN variances for the noise elements $w(2n)$ and $w(2n+1)$, respectively. Therefore, each element of the interference plus noise vector after the decoder, $\hat{\mathbf{z}}(n) = \boldsymbol{\varphi}_D \, \mathbf{z}(n)$, is modeled as zero-mean, complex Gaussian random variable with variance

$$\sigma_{\hat{z}}^2(2n) = \sigma_z^2(2n)\left(\left| h_{eNB} \right|^2 + \eta^2 \left| h_{RN_2} \right|^2 \right) \tag{6.15}$$

for $\hat{z}(2n)$ and

$$\sigma_{\hat{z}}^2(2n+1) = \sigma_z^2(2n+1)\left(\left| h_{eNB} \right|^2 + \eta^2 \left| h_{RN_1} \right|^2 \right) \tag{6.16}$$

for $\hat{z}(2n+1)$. The overall instantaneous *SINR* of the decision statistics $\hat{y}(2n)$ and $\hat{y}(2n+1)$ is the sum of the *SINR* of the $\hat{y}(2n)$, $\gamma_{IRC}(2n)$, and the *SINR* of $\hat{y}(2n+1), \gamma_{IRC}(2n+1)$. That is

$$SINR_{\hat{\mathbf{y}}(n)}\left(\mathbf{H}_D,\hat{\mathbf{z}}(n)\right)=\gamma_{IRC}(2n)+\gamma_{IRC}(2n+1)$$
$$=\frac{P_{eNB}\left(\left|h_{eNB}\right|^2+\eta^2 h_{RN_2}^{*}h_{RN_1}\right|^2\right)}{\sigma_z^2(2n)\left(\left|h_{eNB}\right|^2+\eta^2\left|h_{RN_2}\right|^2\right)}+\frac{P_{eNB}\left(\left|h_{eNB}\right|^2+\eta^2 h_{RN_2}^{*}h_{RN_1}\right|^2\right)}{\sigma_z^2(2n+1)\left(\left|h_{eNB}\right|^2+\eta^2\left|h_{RN_1}\right|^2\right)} \quad (6.17)$$

where $\sigma_z^2(2n)$ and $\sigma_z^2(2n+1)$ are given in Equations (6.13) and (6.14), respectively. Having established that the co-channel interference is Gaussian, we now proceed to deriving the MLSE equalizer for the IRC.

6.3.2.5 MLSE Equalizer for IRC-Aided IR with E-DF scheme

Denote the covariance matrix for the vector $\hat{\mathbf{z}}(n)$ by

$$\mathbf{\Theta}(n)=E\left[\hat{\mathbf{z}}(n)\hat{\mathbf{z}}^H(n)\right],\ \mathbf{\Theta}(n)\in 2\times 2$$

Let us now derive the maximum likelihood sequence estimator (MLSE). Given the observed sequence

$$\hat{\mathbf{y}}(n)=\left[\hat{y}_1(2n)\quad \hat{y}_2(2n+1)\right]^T=\mathbf{\Lambda}_D\mathbf{s}_D(n)+\hat{\mathbf{z}}(n),$$

and the gain matrix

$$\mathbf{\Lambda}_D=\begin{bmatrix}\left|h_{eNB}\right|^2+\eta^2 h_{RN_2}^{*}h_{RN_1} & 0\\ 0 & \left|h_{eNB}\right|^2+\eta^2 h_{RN_2}^{*}h_{RN_1}\end{bmatrix},$$

we estimate the most probable transmitted sequence $\mathbf{s}_D(n)=\left[s(2n)\quad s(2n+1)\right]^T$. The maximum likelihood estimate of the transmitted sequence $\mathbf{s}_D(n)$ is obtained according to

$$\left\{\hat{s}_D(n)\right\}=\arg\min_{\{s_D(n)\}}\sum_n\left\|\left(\hat{\mathbf{y}}(n)-\mathbf{\Lambda}_D\mathbf{s}_D(n)\right)^H\mathbf{\Theta}(n)^{-1}\left(\hat{\mathbf{y}}(n)-\mathbf{\Lambda}_D\mathbf{s}_D(n)\right)\right\|$$

The MLSE solution can be implemented very efficiently with the Viterbi algorithm [142] (will be discussed in details in the following sub-section). To realize this in practice, it is of course necessary to estimate the noise covariance matrix $\mathbf{\Theta}(n)$. The instantaneous covariance matrix $\mathbf{\Theta}(n)$ can be estimated as

$$\hat{\mathbf{\Theta}}(n) = \frac{1}{\Upsilon}\sum_{n=0}^{\Upsilon-1}\left(\hat{\mathbf{y}}(n) - \mathbf{\Lambda}_D \mathbf{s}_D(n)\right)\left(\hat{\mathbf{y}}(n) - \mathbf{\Lambda}_D \mathbf{s}_D(n)\right)^H$$

where Υ is the number of samples used for the estimation. This way of estimating the $\mathbf{\Theta}(n)$ matrix is well suited for cellular systems, due to the quasi-stationarity assumption of the radio channel during one time slot [73].

6.3.2.6 The Viterbi Algorithm

The maximum likelihood sequence estimation using the Viterbi algorithm [131] can be illustrated by a trellis diagram. Figure 6.7 shows three examples of the states and the state transitions for the convolutional encoder length L = 1, 2 and 3 bit. The dashed line represents 0 transition and the solid line represents 1 transition. At each node of the trellis, there are 2^L states and 2^{L+1} transitions to the next node.

Figure 6.8 shows the trellis of an exemplary MLSE with L = 2-bit convolutional encoder output. At each node, there are $2^L = 4$ states and $2^{L+1} = 8$ transitions to the next node. As an example, the upper all zeros path is assumed the correct path (i.e. $s(n)$={000000000}). Considering the error probability at an arbitrary node k, the incorrect paths diverge at node k from the correct one at Hamming distance $d_H \geq 1$ and merge to the correct one again.

The Viterbi algorithm can be used to implement the ML receiver by searching through all possible trellis states for the most likely transmitted sequence $s(n)$. This search process is called the *maximum likelihood sequence estimation* (MLSE). At an arbitrary node i, the algorithm has stored certain paths through the trellis called surviving paths along with their distances from the received sequence, called

path metrics, and dropped all other paths. After all states have been processed, the whole algorithm repeats when the time is incremented. If the receiver waits until the entire sequence has been received before making a decision, this will cause an i

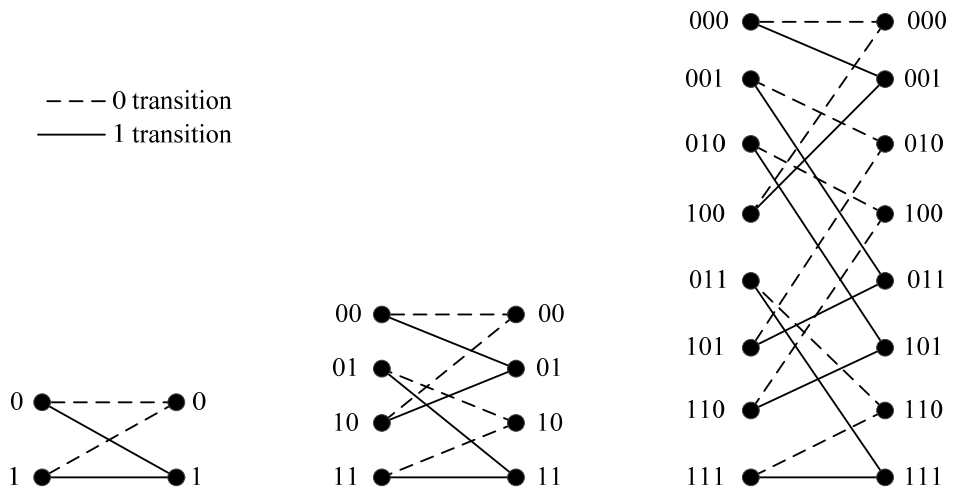

(a) $L = 1$ bit (b) $L = 2$ bits (c) $L = 3$ bits

Figure 6.7: The states and the state transitions for different channel memory sizes.

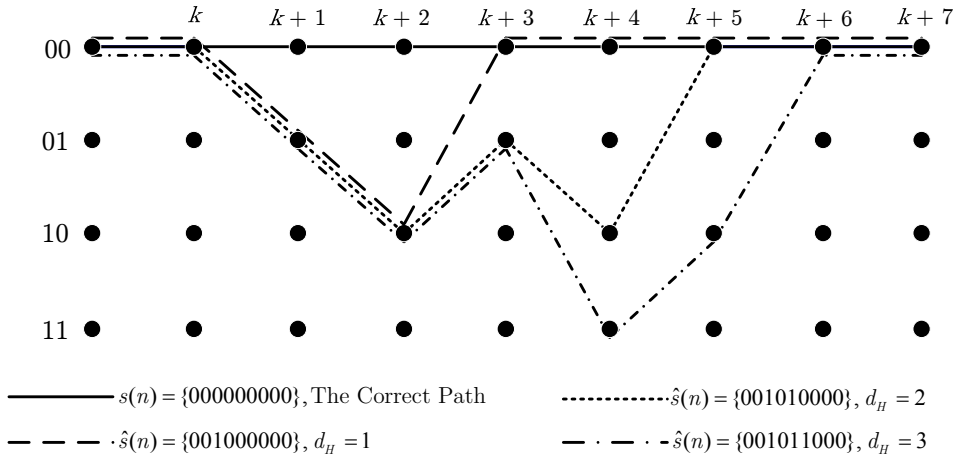

Figure 6.8: The correct path (all-zero) and the exemplary diverging paths at a Hamming distances of $d_H = 1$, 2 and 3 to the correct path.

In Viterbi algorithm, the number of states and transitions grows exponentially as the memory size increases. Hence, the complexity of Viterbi algorithm is directly proportional to the decoder memory size. In the following, the bit-error rate (BER) of the MLSE equalizer is analyzed such that BER upper bound is obtained.

6.3.2.7 Analyzing MLSE Receiver Structure – *BER* Upper Bound Performance

The BER of linear receiver structures is relatively straightforward to compute, since symbols are processed independently and so their errors are independent too. However, this is not the case for non-linear receiver structures (like MLSE equalizer), since consecutive errors are not usually independent.

The exact BER for an MLSE equalizer can be computed as follows. Given a transmitted sequence, the receiver calculates the *path metrics*, which are the sum of Euclidean distances between the received and the transmitted sequences. The receiver also calculates the joint PDF of all hypothesized sequences' path metrics. This can be viewed geometrically as a density function in a multidimensional space. Each hypothesized sequence is assigned its own axis. All the path metrics at the end of transmission can be written as a coordinate vector, specifying a point in this multidimensional space. The value of the density function at this point expresses the likelihood of computing that set of path metrics. The space can be divided into decision regions. Points within the same decision region share the same largest path metric, and so detect the same maximum likelihood sequence. In fact, a hypothesized sequence's decision region encloses the points closer to its axis than any other. When the ML sequence is detected instead of the transmitted sequence, there are a number of bit errors. Each region of the joint PDF is weighted by this number, divided by the total number of bits in the transmitted sequence. Then the bit error rate due to the transmitted sequence is calculated by repeatedly

integrating over all the weighted joint *PDFs* dimensions. The overall average *BER* is then this quantity, averaged across all transmitted sequences.

Clearly this exact method is difficult to compute. The number of path metrics is increasing exponentially with the sequence length, so the jointly *PDF* gets very complicated and the number of integrations gets very large. Therefore, it is necessary to find simpler methods that obtain the bounds of bit error events rather than the more complex exact method.

Several techniques were presented in the literature for calculating *BER* performance of Viterbi decoder in fading channels. These techniques can be broadly classified into three categories – simulation, upper bounds on individual *BER* [137-139], and analytical approximation based on the computation of the exact *BER* of a small set of error events [140]. The disadvantage of simulation-based technique is that it can be very time-consuming. As for the upper bound techniques, they are easy to compute but may be loose. Finally the disadvantage of analytical approximation is that the result is not a true upper bound. In this dissertation, we consider the upper bound techniques for calculating *BER* performance of our decoder.

In the upper bound techniques, the probability that the sequence with the largest path metric is not the transmitted sequence can be upper bounded by the probability that any error sequence has a larger path metric than the transmitted sequence's path metric. Thus a joint *PDF* is not needed, only the *PDF* of the path metric difference, for all possible transmitted and error sequences. Furthermore, there is no need to compute the *PDF* over the whole transmission interval. An error sequence follows the same states as the transmitted sequence until the first error. Errors follow until the two sequences merge at a common state again. This sequence of errors is called an *error event*. In communication systems with low *BER*, the error events are normally short compared to the mean time between them. Accordingly, they can be considered independent, so their probability can be calculated by only considering the *PDF* of the path metric difference in the vicinity

of the error event. Examples of upper bounds techniques are Chernoff bound [137,138] and union bound[139].

Given the erroneous sequence $\mathbf{e}(n)=\{e(n)\}$ and the transmitted sequence $\mathbf{s}_D(n)=\{s_D(n)\}$. In general, the MLSE-based receiver will choose the incorrect sequence $\mathbf{s}_D(n)\rightarrow\mathbf{e}(n)$ if the squared Euclidean distance for the error sequence $d_{\mathbf{e}(n)}$ is greater than the squared Euclidean distance for the transmitted sequence $d_{\mathbf{s}(n)}$. i.e.

$$d_{\mathbf{e}(n)} \geq d_{\mathbf{s}(n)}$$

where $d_{\mathbf{e}(n)}=\left\|\mathbf{s}_D(n)-\mathbf{e}(n)\right\|^2$, $d_{\mathbf{s}(n)}=\left\|\mathbf{s}_D(n)\right\|^2$ and $\|.\|^2$ is squared Euclidean distance. Therefore, the probability of bit error of the Viterbi decoder is the sum of erroneous bits when the decoder chooses sequence the erroneous sequence instead of the transmitted sequence. is given by

$$BER(n) \leq \sum_n \Pr\left[\left\|\mathbf{s}_D(n)-\mathbf{e}(n)\right\|^2 \geq \left\|\mathbf{s}_D(n)\right\|^2\right]$$

Considering Chernoff upper bound method, this quantity equals to

$$BER(n) \leq \sum_n E\left[\exp\left[\left\|\mathbf{s}_D(n)-\mathbf{e}(n)\right\|^2 \geq \left\|\mathbf{s}_D(n)\right\|^2\right]\right] \tag{6.18}$$

The performance of Chernoff bounds is shown to be loose for low *SINR* scenarios [141]. On the other hand, union bound technique shows tighter upper bound than Chernoff bound and is more straightforward to compute [139].

On the other hand, *BER* performance is upper-bounded using union bound method by

$$BER(n) \leq \sum_{\mathbf{s}_D(n)\neq\mathbf{e}(n)} b_e\left(\mathbf{s}_D(n),\mathbf{e}(n)\right)\ \Pr\left[\mathbf{e}(n)\middle|\mathbf{s}_D(n)\right]\ \Pr\left[\mathbf{s}_D(n)\right] \tag{6.19}$$

where $b_e\left(\mathbf{s}_D(n),\mathbf{e}(n)\right)$ is the number of bit errors in the error event, $\Pr\left[\mathbf{e}(n)\middle|\mathbf{s}_D(n)\right]$ is the probability of error event $\mathbf{s}_D(n)\to\mathbf{e}(n)$ and $\Pr\left[\mathbf{s}_D(n)\right]$ is the probability that the transmitter sent sequence $\mathbf{s}_D(n)$. Since the MLSE-based receiver will choose the incorrect sequence $\mathbf{s}_D(n)\to\mathbf{e}(n)$ if the squared Euclidean distance for the error sequence is greater than the squared Euclidean distance for the transmitted sequence, the *BER* can be written as

$$\begin{aligned} BER(n) &\le \sum_n b_e\left(\mathbf{s}_D(n),\mathbf{e}(n)\right)\Pr\left[d_{\mathbf{e}(n)}\ge d_{\mathbf{s}(n)}\right]\ \Pr\left[d_{\mathbf{s}(n)}\right] \\ &= \sum_n b_e\left(\mathbf{s}_D(n),\mathbf{e}(n)\right)\Pr\left[\left\|\mathbf{s}_D(n)-\mathbf{e}(n)\right\|^2\ge\left\|\mathbf{s}_D(n)\right\|^2\right]\ \Pr\left[\left\|\mathbf{s}_D(n)\right\|^2\right] \end{aligned} \quad (6.20)$$

Assuming MPSK modulation is used, and the incorrect path through the trellis diverges from the correct path at time k and remerges with the correct path at time $k + l$, therefore, the *BER* in Equation (6.20) becomes [142]

$$BER(n) \le \sum_n \frac{2b_e\left(\mathbf{s}_D(n),\mathbf{e}(n)\right)}{\log_2 M} Q\left[\sqrt{2\log_2 M\sum_{n=k}^{k+l-1} SINR(n)}\sin\left(\frac{\pi}{M}\right)\right] \quad (6.21)$$

where M ($M = 2^i$, $i = 1, 2, \ldots$) is the modulation constellation size, $SINR(n)$ is the signal-to-interference plus noise ratio for the received error sequence and $Q[.]$ is the Q-function. The *BER* expression in Equation (6.21) is called *Forney's union bound* [139].

In Equation (6.21), Chernoff bound can be used for high $SINR(n)$, ($SINR(n) \gg 0$). This new bound is referred to as *Chernoff-union bound method* [142]. According to [137], the Q-function can be approximated for high $SINR(n)$ to

$$Q[\varsigma] \le \frac{\exp\left(-\varsigma^2/2\right)}{\varsigma\sqrt{2\pi}}$$

Therefore, the *BER* in Equation (6.21) can be expressed using Chernoff-union bound method as

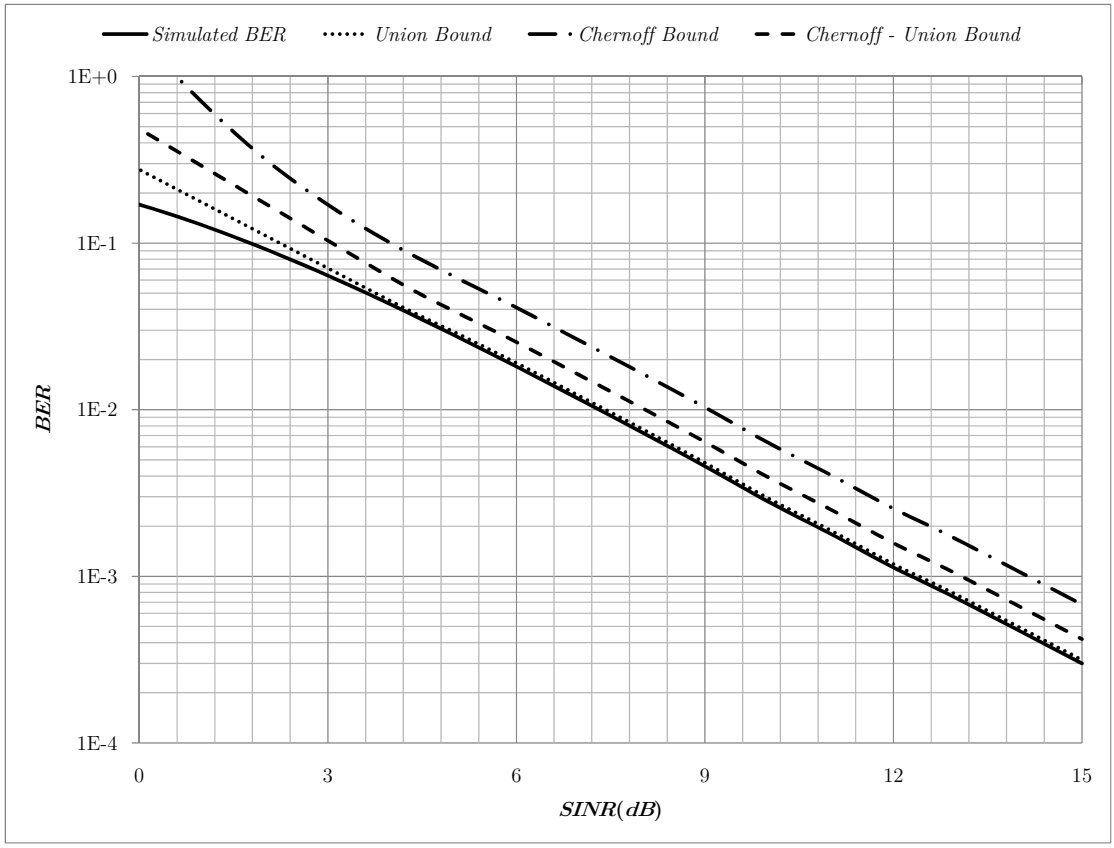

Figure 6.9: A comparison between the simulated, Chernoff upper bound, union bound and Chernoff-union *BER* bounds.

$$BER(n) \le \sum_{n} \frac{2b_e\left(\mathbf{s}_D(n), \mathbf{e}(n)\right)}{\log_2 M} \frac{\exp\left(-2\log_2 M \sum_{n=k}^{k+l-1} SINR(n)\sin^2\left(\frac{\pi}{M}\right)\right)}{\sqrt{2\pi}\sin\left(\frac{\pi}{M}\right)\sqrt{2\log_2 M \sum_{n=k}^{k+l-1} SINR(n)}} \tag{6.22}$$

This Chernoff-union bound method is used to avoid calculating the Q-function in Equation (6.21).

Figure 6.9 shows the curves of *BER* versus *SINR*(dB) for simulated, Chernoff upper bound, union upper bound and Chernoff-union upper bound *BERs*. The simulated curve is obtained using Viterbi algorithm for decoded sequences

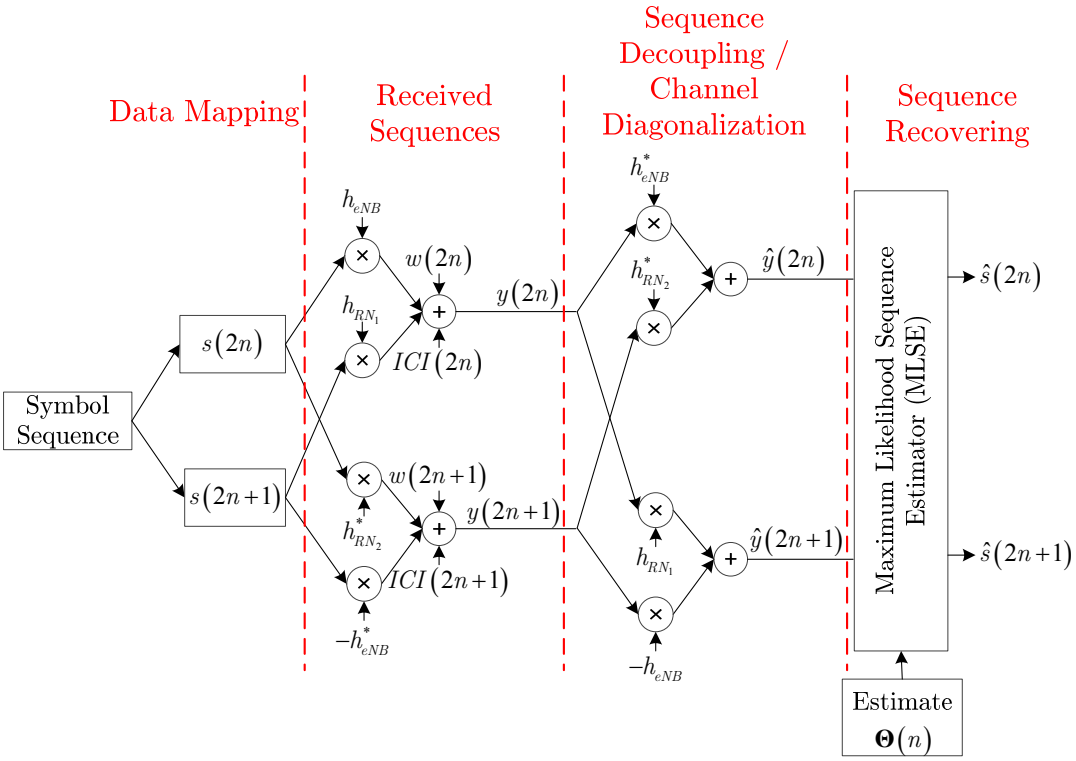

Figure 6.10: The proposed IRC decoder model for sequence recovery using MLSE.

compared to the correct or transmitted sequences. The rest of the curves are obtained by using Equation (6.18) for Chernoff bound, Equation (6.21) for union bound and Equation (6.22) for Chernoff-union bound. It can be noticed from Figure 6.9 that the Chernoff bound is loose for *SINR*<3dB. At high *SINR*, the Chernoff bound curve follows the trend of simulated *BER* with gap between the two curves widens to within 2dB. However, the Chernoff-union bound achieves better than Chernoff bound. The *BER* curve is tighter than Chernoff bound at low *SINR* and the gap between the exact and Chernoff-union curves widens to within 1dB. Finally, the union bound shows the tightest performance among the two bounds. The union bound at low *SINR* (from -10 to 3dB) achieves from 0dB to 5dB curve difference to the simulated *BER*, and matches it very well when *SINR* > 3dB.

In light of the above results, the derived union upper bound *BER* is the tightest bound compared to the Chernoff and Chernoff-union bounds, although its expression includes integration (Q-function). For simpler calculations, Chernoff-union bound shows simpler *BER* expression and acceptable performance compared to the exact *BER*.

Figure 6.10 summarizes the IRC decoder model to recover the transmitted symbol sequences $s(2n)$ and $s(2n+1)$ using MLSE. At the transmitter, the symbol sequences are mapped and transmitted according to the E-DF cooperative relaying

Table 6.1: System parameters.

Parameter	**Value**
Carrier frequency (f_c)	2 GHz
Frequency bandwidth (B)	10 MHz
eNBs' transmission power (P_{eNB})	46 dBm
eNBs' transmission power (P_{RN})	40dBm
eNB antenna pattern	Omni-directional
Path loss exponent (υ)	3.5
noise power density (D)	-174 dBm.user/Hz
Cell radius (R)	1000 m
Relay radius	500 m
RN antenna pattern	Omni-directional
Modulation type	QPSK
Number of relays per cell	6
Path loss model	$PL(dB) = 35.46 + 35 \log(d)$, d in km
Channel model	Rayleigh flat fading channel
Rayleigh fading variance (σ_h^2)	1
Log-normal shadowing variance (σ_χ^2)	6.31
Number of *E-cells*	21

protocol. At the receiver side, the received sequences are decoupled and the noise covariance matrix $\mathbf{\Theta}(n)$ is estimated. $\mathbf{\Theta}(n)$ is then used at the MLSE to estimate the sequences $s(2n)$ and $s(2n+1)$ using the Viterbi algorithm.

6.4 Numerical Results and Discussion

In this section, the performances of the IR scheme and the IRC-aided IR with E-DF scheme are compared. Semi-analytical results for the *BER*, the average *SINR*, and the average capacity are obtained from the expressions derived in Section 6.3. The parameters for the IR system are shown in Table 6.1. The results are obtained for different schemes to show the improvement when the cooperative transmission scheme, E-DF, and the interference cancellation technique, IRC, are employed in every E-cell.

6.4.1 *The Effect of ICI from tier 1 and tier 2 interferers on Average BER*

Figure 6.11 shows simulated *BER* versus *SINR* curves for the conventional IR scheme and the IRC-aided IR with E-DF scheme when QPSK modulation is employed. The curves are obtained for systems when received signal impairment is (a) AWGN only, (b) a combination of ICI from tier1 and AWGN, and (c) a combination ICI from tier1 and tier2 and AWGN. All channel coefficients are modeled as zero-mean, complex Gaussian random variables with equal variances of $\sigma_h^2 = 1$. Also, the ratio between the relay power and the base station power is set to $\eta = 0.1$. The figure is obtained to show the effect of tier1 and tier2 inter-cell interferers as well as the effect of using IRC in IR system.

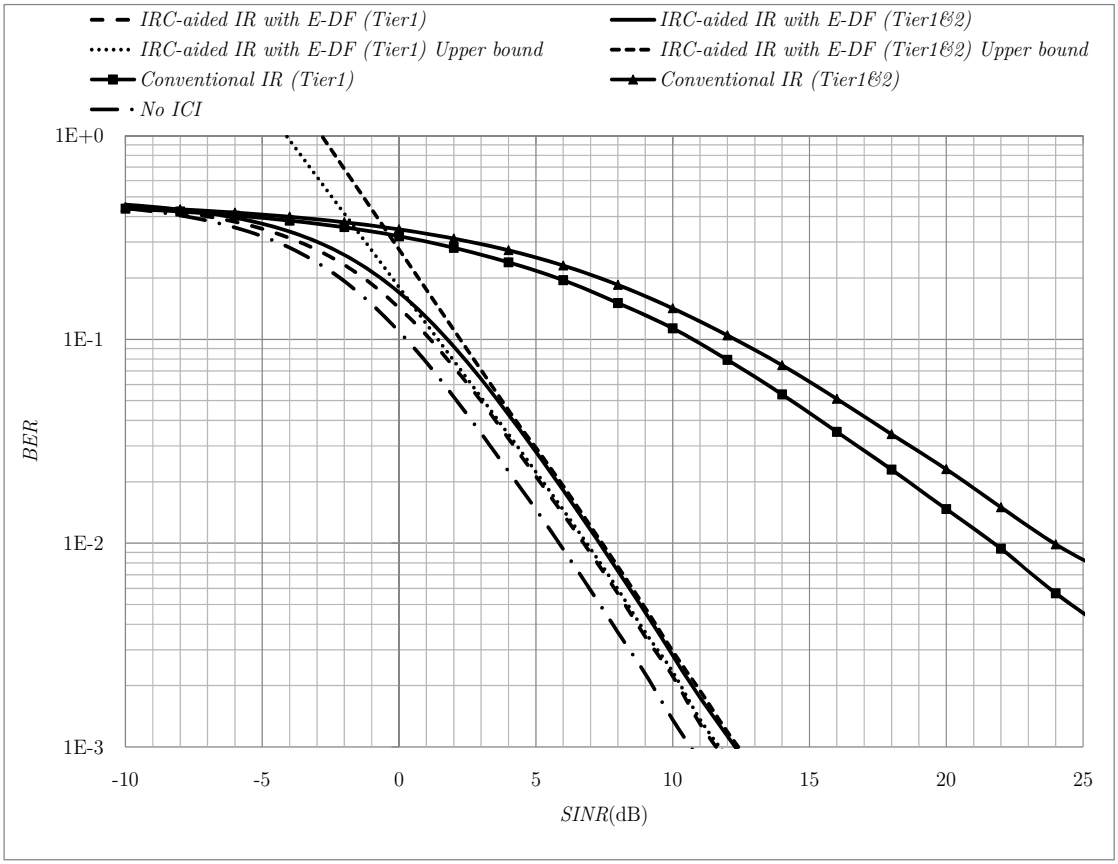

Figure 6.11: *BER* comparison for the conventional IR and the IRC-aided IR with E-DF schemes.

In Figure 6.11, when IRC is employed, the *BER* is significantly reduced compared to the IR scheme with no IRC. Also, we observe that the *BER* when IRC is applied is within 1dB of the case when there is no ICI. Furthermore, the gap between the *BERs* when only tier1 ICI is present and when both tier1 and tier2 ICI are present is significantly small (within 1dB). Therefore, ICI from tier2 may be ignored for simply implementation of the IRC. However, when no IRC is used, the gap between the *BERs* in the presence of tier1 only and tier1 plus tier2 widens to within 0.75dB at high *SINR*.

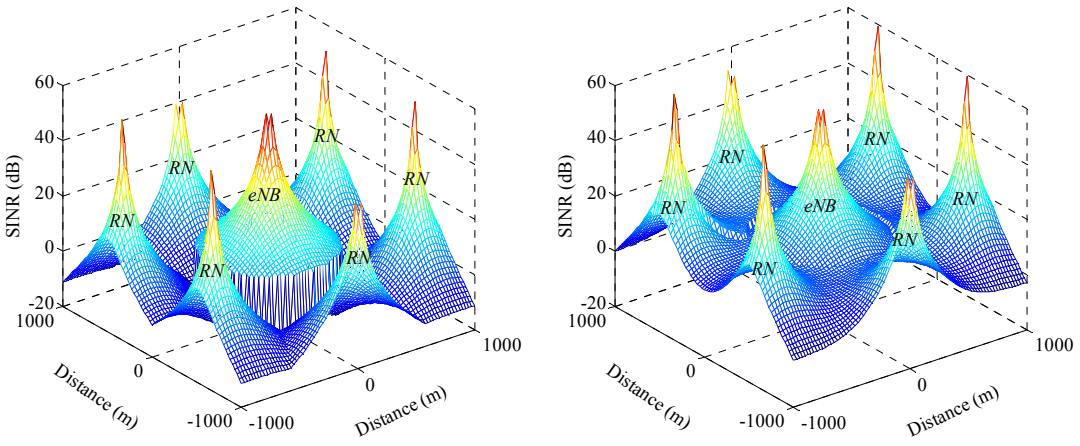

(a) The IR scheme **(b)** The IRC with E-DF aided IR schemes

Figure 6.12: Average *SINR* 3D plot for one E-cell.

6.4.2 *The Effect of the Cooperative Transmission Algorithm on Average SINR*

Figure 6.12 shows a 3D plot for the *SINR* level for the conventional IR and the IRC with E-DF aided IR schemes. In Figure 6.12 (a), average *SINR* is obtained for signals from either the eNB or one of the candidate relay nodes to a mobile station roaming within the E-cell. *SINR* is averaged over channel realizations for each mobile station location. The figure shows that the *SINR* is very high for regions close to the transmitting terminals indicated by the seven peaks for the base station and the six distributed relays. Moreover, when the mobile station is moving away from the transmitter, it encounters low signal level and high interference that yields low *SINR*. Figure 6.12 (b) shows average *SINR* when the IRC is combined with E-DF cooperative scheme in IR network. It is seen that the side peaks, representing the relay terminals, have improved when IRC is used with the E-DF compared to the conventional IR scheme.

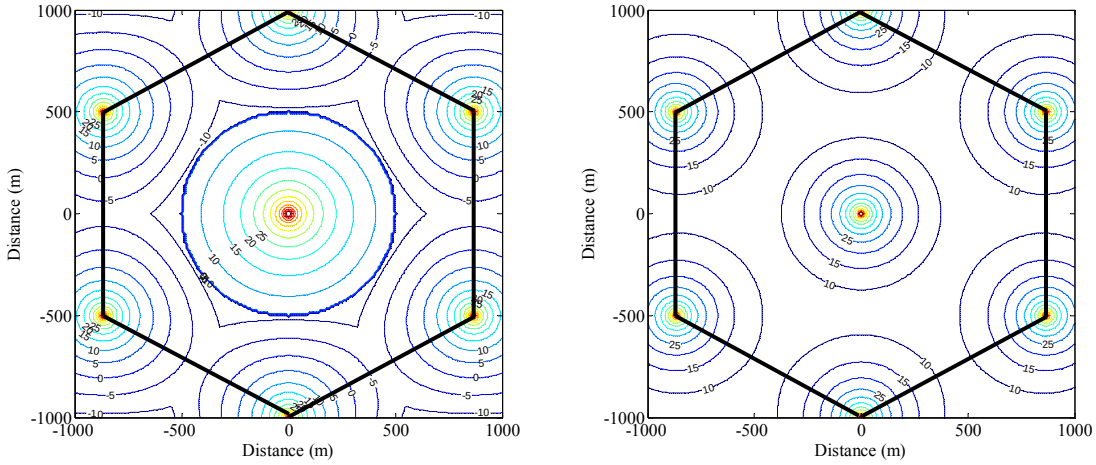

(a) The IR scheme **(b)** The IRC-aided IR with E-DF scheme

Figure 6.13: Average *SINR* counters.

For clearer demonstration, Figure 6.13 shows the attainable *SINR* contours across the cell for conventional IR and the IRC with E-DF aided IR schemes. Figure 6.13 (a) shows that for the conventional IR scheme, the areas around the base station (up to 500m - distance from the base station) and the relay terminals (up to 300m - distance from each relay) carry positive *SINR*; however, the regions between the base station and the relay terminals (from 500m to 700m - distance from the base station), as well as the regions between two consecutive relays (from 300m to 700m - distance from the relay) carry negative *SINR*. This is due to the strong ICI component from other adjacent E-cell*s* and adjacent relays within the E-cell. Figure 6.13 (b) shows that for the IRC with E-DF aided IR scheme, the least recorded average *SINR* value reaches 10dB in areas where *SINR* recorded less than 10dB in the conventional IR scheme. Such significant improvement has effects on the link capacity as well as the overall per-cell throughput.

Table 6.2 compares the semi-analytical average *SINR* (in dB) as well as the average capacity (in bps/Hz) for the two schemes. The table shows that both average *SINR* and capacity are improved significantly when jointly using the E-DF and the IRC for inner and outer mobile station users. For example, about 2dB average *SINR*

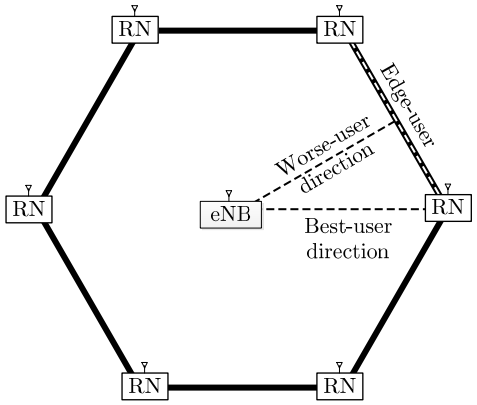

Figure 6.14: Illustration of best-user direction, worse-user direction and edge-user cases.

improvement for inner MSs is achieved when switching from conventional IR to the IRC with E-DF aided IR scheme, and the average *SINR* is tripled for outer MSs.

6.4.3 *Special Cases*

For better comparison, consider the three cases illustrated for the two schemes. The first case is the *best-user direction*, where the mobile station is traveling from the cell centre toward any assisting relay at the cell edge. The second case is the *worse-user direction*, where the mobile station travels from the cell centre to the midpoint between two adjacent relays. Finally, the third case is the *edge-user*, where the mobile station moves from one relay to another neighboring relay. Figure 6.14 illustrates the three cases under study.

6.4.3.1 Case 1: The Best-User Direction

Figure 6.15 compares the average *SINR* for the conventional IR scheme and the IRC with E-DF aided IR scheme. When inner region is considered (0 – 500m), the average *SINR* for the IRC-aided IR with E-DF scheme is better than the

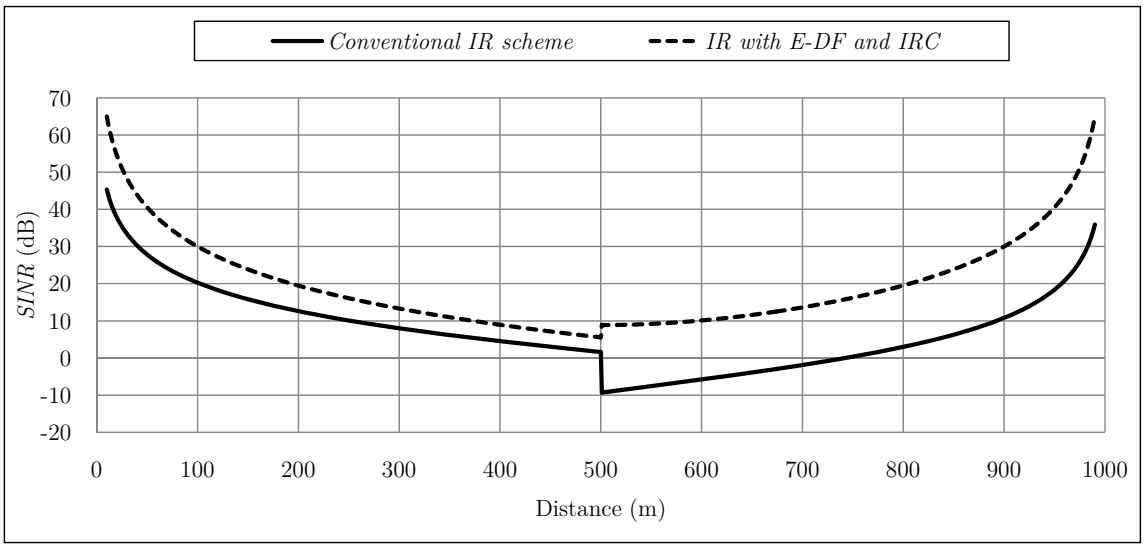

Figure 6.15: Average analytical *SINR* for the best-case direction.

conventional IR scheme. This is due to suppression of interference from the adjacent relays. In the cell-edge or outer region (500m – 1000m), the mobile station experiences low *SINR* when using the conventional IR scheme. However, utilizing the IRC with E-DF shows significant improvement for the cell-edge users in excess of 10dB in the worst case.

6.4.3.2 Case 2: The Worse-User Direction

Figure 6.16 compares the semi-average analytical *SINR* profiles for the two different schemes. The inner region average *SINR* when the IRC-aided IR with E-DF scheme is utilized is only slightly better (within about 2dB) than the conventional IR scheme. However, for the outer region the average *SINR* with IRC and E-DF scheme is significantly higher (within 25dB in the worst case) despite the low signal level and the strong interference from other E-cell*s*.

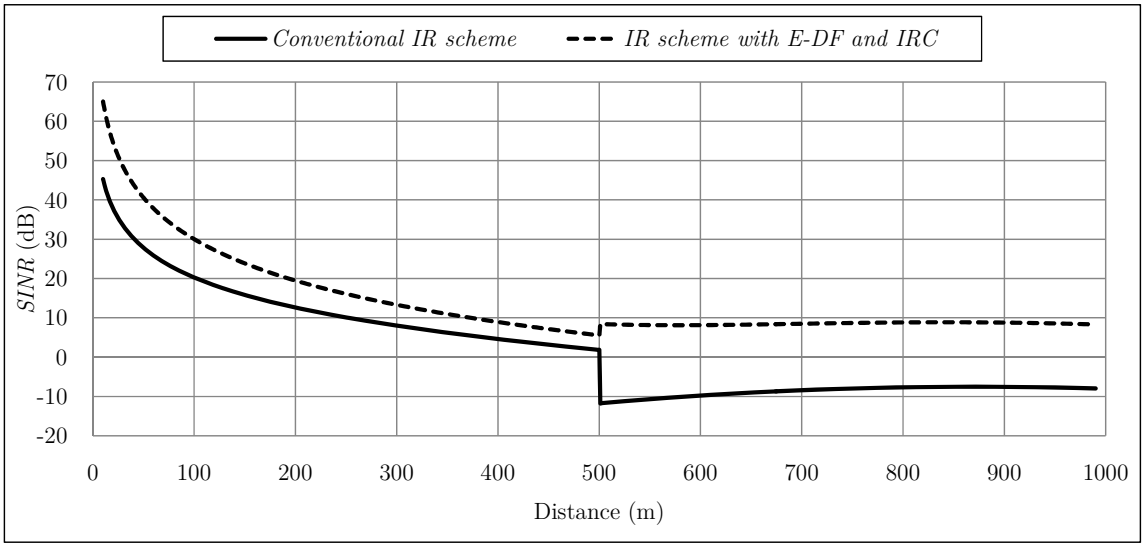

Figure 6.16: Average semi-analytical *SINR* profile for the worse-case direction

6.4.3.3 Case 3: The Edge-User Direction

The final case is the edge-user case where the mobile station is moving from one relay to another adjacent relay. Figure 6.17 shows the *SINR* records for the two different schemes. The figure shows great improvement when E-DF with the interference rejection technique is employed. For example, the lowest recorded *SINR* of -7dB occurs when the conventional IR scheme is utilized at 500m distance from either the two relays. However, at the same distance, a 14dB *SINR* improvement is achieved when the IRC with E-DF is utilized.

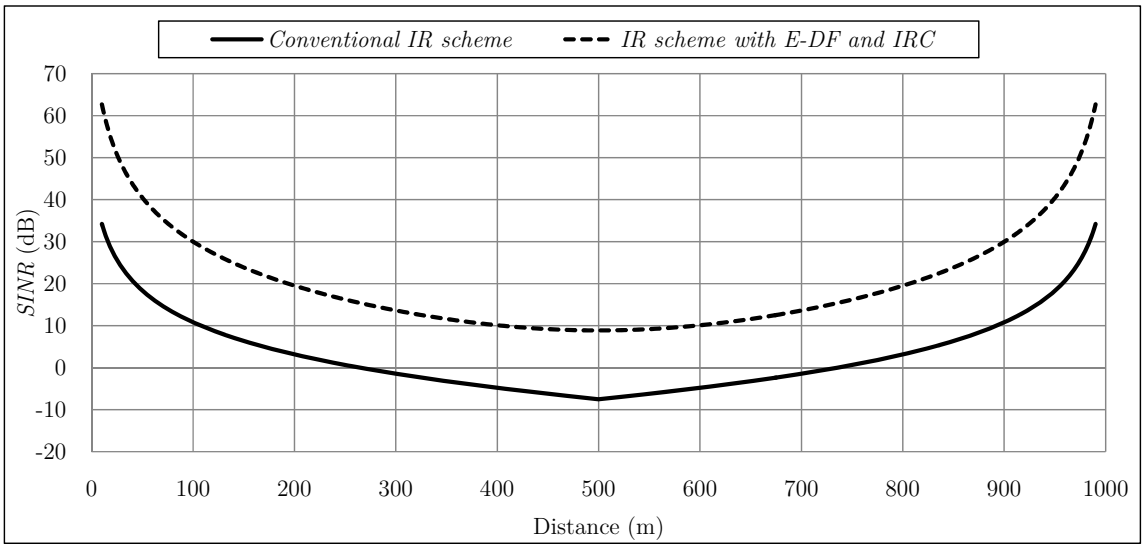

Figure 6.17: Average semi-analytical *SINR* profile for the edge-user direction.

6.5 Chapter Summary

In this chapter, a transmission scheme, the in-band relay (IR), has been proposed to improve the performance of LTE-A systems and meet its standardized requirements. The IR scheme is based on distributing transparent relay nodes at the edges of each cell. These relays are allocated the same spectral resources as the base station to increase the per-cell spectral efficiency. Due to the need to increase the degree of diversity from the transmitting terminals, the cooperative relaying scheme, Enhanced-Decode-and-Forward (E-DF), is employed such that the base station and two candidate relays are transmitting to the mobile station. Despite the improvement in diversity, the E-DF aided IR scheme suffers from high interference from co-channel relays and base station. To overcome this issue, the E-DF is utilized jointly with the Interference Rejection Combining (IRC) technique to eliminate the interference from the adjacent relays in each cell.

To validate the cooperative transmission scheme using E-DF and IRC, analytical *BER* upper bound, *SINR*, and capacity results are obtained for the IR scheme and the IRC aided IR with E-DF scheme. The results show significant improvement in terms of *BER* reduction, *SINR* and capacity improvement when jointly utilizing

the E-DF and the IRC in the IR network. Such impressive results are due to the improvement in desired signal power from the distributed relays, the improvement in diversity gain when cooperatively receiving from two terminals, and the reduction of interference from adjacent relays in the cell when utilizing the IRC technique.

Chapter Seven: Summary, Conclusions and Future Work

This chapter presents a brief summary and conclusions of the work accomplished in this dissertation. Some topics for future work to continue research in this area are also discussed. Section 7.1 provides the conclusions important points of the dissertation. Some possible topics for future investigations are suggested in Section 7.2.

7.1 Conclusions

The overall objective of this research is to propose and investigate improved and efficient transmission techniques for LTE-A systems that can achieve high average *SINR* and high average capacity under various impairments such as fading, interference and noise in the wireless channels. The work is mainly divided into two parts – the first part (Chapter 3) involved modifying a DF cooperative relaying protocol to achieve a higher data rate with diversity. The second part (Chapters 4, 5 and 6) involved the integration of relay terminals in cellular LTE-A systems. We encountered three major issues that were solved at the end of this work. Firstly, the issues of improving the desired signal level and coordinating the inter-cell interference. Secondly, the issue of frequent handover caused by the deployed relay terminals. Finally, the issue of high interference caused from co-channel relay terminals.

In Chapter 2, we provided the reader with a review of a number of concepts that were useful throughout this dissertation such as – the characteristics of wireless channels, the diversity and MIMO concepts, relay communications and the LTE and the LTE-A systems.

In Chapter 3, we proposed and investigated the performance of a new cooperative relaying protocol called *the Enhanced-Decode-and-Forward* (*E-DF*) *scheme*. Based

on the system and the received signal model of the E-DF scheme, we proposed a modified maximum likelihood (ML) decoder to recover the received symbols over a quasi-static fading channel. In addition, the analysis of the average signal-to-noise ratio (*SNR*) was conducted, in which the exact *SNR*, the *SNR* upper bound, and an approximate *SNR* upper bound were derived for the E-DF scheme. Based on the approximate *SNR* upper bound, we performed the analysis of the exact symbol error rate (*SER*) via the moment generating function (*MGF*). Expressions for a worse-case *SER* upper bound and an approximate worse-case *SER* were derived to simplify the calculations when obtaining the exact *SER* expression. Also, we conducted analysis of other information-theoretic measures include – mutual information, the achieved rate and the outage probability for the E-DF, the conventional DF and the non-relay schemes. Finally, semi-analytical and simulation results including – *SER,* outage probability and achieved rate were obtained for the E-DF scheme and compared with the conventional DF and the non-relay schemes. The results showed significant improvement for the E-DF scheme over the non-relay and the DF schemes in terms of symbol error rate. Also, the results showed higher transmission rate and lower outage probability are achieved when employing the E-DF scheme than the conventional DF and the non-relay schemes.

In Chapter 4, we proposed a relay-assisted scheme with omni-directional antennas called *the omni-relay* (*OR*) *scheme*. Also, we proposed a relay frame structure for the OR scheme that is compatible with the long-term evolution (LTE) standard. In addition, analyses of the average signal-interference plus noise ratio (*SINR*) and the average capacity were carried out for the conventional UFRF and the OR schemes. Finally, semi-analytical and simulation results for the achieved average *SINR* and the achieved average capacity were obtained for the OR scheme and compared with the conventional UFRF. In terms of average *SINR*, the results showed that more than double the average *SINR* of UFRF is achieved when utilizing the OR scheme, and about 40 percent of the UFRF users experience a *SINR* less than 10dB and about 15 percent for the OR users. In terms of average capacity, the results showed that 50 percent of the OR users result in an average capacity higher than 7bps/Hz.

On the other hand, 50 percent of UFRF users result in an average capacity higher than 5bps/Hz. These impressive results are due to the use of the distributed relay terminals at the edge of cells. Despite the remarkable improvement in *SINR* and capacity compared to the conventional UFRF, utilizing the OR scheme have generated high interference from the distributed relay terminals in particular regions inside cells.

In Chapter 5, we proposed the use of relay terminals at the cell-edges, where each relay is equipped with directional antennas. This scheme is called *the directional-relay* (*DR*) *scheme*. We also proposed a new download transmission scheme for the DR, called *Enhanced-DR* (E-DR) scheme, to overcome the issues of high interference and low desired signal level in particular regions inside cells. In addition, analyses of the average signal-interference plus noise ratio (*SINR*) and the average capacity were carried out for the DR and the E-DR schemes. Finally, semi-analytical and simulation results for the achieved average *SINR* and the achieved average capacity were obtained for the DR and the E-DR schemes and compared with the OR scheme. The results showed that, when utilizing the DR, the average *SINR* for the DR users is less than the average *SINR* for the OR users. However, when the enhanced transmission scheme, the E-DR, is utilized, the average *SINR* is improved remarkably. Specifically, the E-DR cell-edge users have achieved double the average *SINR* compared to the DR. Also, E-DR has improved average capacity such that more than double the capacity is achieved when utilizing E-DR compared to the DR.

Despite the remarkable improvement in *SINR* and capacity when utilizing the OR and the E-DR schemes, the spectral efficiency degrades because the total available download bandwidth was divided by a frequency reuse factor of three for the OR scheme and a frequency reuse factor of four for the DR scheme.

In Chapter 6, we proposed the use of relay terminal at the cell edges, each with omni-directional antennas and the same frequency resources allocated to the base station. This scheme is called *the in-band relay* (*IR*) *scheme*. The IR scheme

increases the spectral efficiency since each relay utilizes the same frequency resources allocated to the base station. We also proposed the concept of *the evolved-cell* (*E-cell*) for the IR scheme that can perform cooperative transmission of information between the terminals of interest within the E-cell. The cooperative transmission is accomplished by using the E-DF relaying protocol (introduced in Chapter 3) to increase diversity and data rate. Due to high interference, we proposed the use of an interference cancelling technique, known as *Interference Rejection Combining* (*IRC*), in each E-cell. In addition, decoding the received symbols was carried out by decoupling the desired symbols first and then applying the conventional ML symbol decoder. The derivations of the average *SINR* and the average capacity were also carried out for the IR and the IRC-aided IR schemes. Finally, we obtained semi-analytical and simulation results for the achieved average *SINR* and the achieved average capacity when utilizing the IR and the IRC-aided IR schemes. The results showed that, for the IRC-aided IR scheme, the average *SINR* and the average capacity are improved remarkably for the cell-edge users compared to the IR that has no cooperative transmission scheme.

To conclude, three different relay-assisted schemes were investigated – the OR scheme, the DR scheme (including its enhanced version E-DR) and the IR scheme (including the cooperative transmission scheme). The OR scheme have showed remarkable improvement in average *SINR* and capacity compared to the conventional UFRF scheme, however, it generates interference from the distributed relay terminals and increases the frequency of handovers. On the other hand, the DR reduces the frequency of handovers and the interference from the distributed relay terminals. Both, the OR and the DR schemes have shown low spectral efficiency because each base station or relay in the network is utilizing only a fraction of the available spectral resources. The scheme also cancels the effect of interference from the deployed relays. The IR scheme has shown improvements in terms of *SINR* and capacity and high spectral efficiency compared to the conventional UFRF scheme, the OR scheme and the DR schemes. One

disadvantage of the IR scheme is that the receiver is required to estimate the interference and noise covariance matrix in order to be able to decode correctly.

7.2 Future Work

During the time frame of this research, many important issues have not been dealt with, or have been sometimes considered with simplified assumptions. Hence, there are many areas to extend the work of this dissertation. In this section, we suggest some topics for future research in the direction of this dissertation. We recommend the following issues for further study …

- Among the work considered in Chapter 3, we have assumed complete knowledge of the channel state information at the receiver. The work can be extended to include a channel estimator with a study of the effect on the overall performance.

- The work in Chapter 3 is conducted for a quasi-static Rayleigh flat fading channel. A future work in investigating the model for different transmission environment such as, time variant flat fading channel or frequency selective channel. Designing and investigating decoders for such environment is another open issue.

- The work in Chapter 3 can be studied further in terms of the effect of non-ideal conditions such as timing and carrier offset errors.

- The works in Chapters 4 to 6 can be extended further to study the issue of peak-to-average ($PAPR$) for each relay-assisted scheme. Furthermore, the work can be extended to include channel estimation for each relay-assisted scheme and its effect on the overall performance.

- Recently, the research trend is toward employing relay terminals in powerline communication (PLC) networks. Designing relaying protocols that

suits PLC network receives lots of consideration. The work in Chapter 3 can be extended by employing the E-DF relaying protocol to PLC network.

References

1. Special issue, "Wireless Personal Communications," *IEEE Communications Magazine*, Vol. 33, Jan 1995.

2. K. S. Gilhousen, I. M. JacoBS, R. Padovani, A. J. Viterbi, L. A. Weaver, and C. E. Wheatley III, "On the Capacity of a Cellular CDMA System," *IEEE Transaction on Vehicular Technology*, Vol. 40, pp.305-312, May 1991

3. Special Issue, "Wideband CDMA," *IEEE Communications Magazine*, Vol. 36, Sept. 1998.

4. D.N. Knisely, S. Kumar, S. Laha, and S. Nanda, "Evolution of Wireless Data Services: IS-95 to CDMA2000," *IEEE Communication Magazine*, pp. 140-149, Oct., 1998.

5. 3GPP2 TSG C.S0024-0 v2.0, CDMA2000 High Rate Packet Data Air Interface Specification.

6. 3GPP TSG RAN TR 25.848 v4.0.0, Physical Layer Aspects of UTRA High Speed Downlink Packet Access.

7. 3GPP2TSG C.S0002-C v1.0, Physical Layer Standard for CDMA2000 Spread Spectrum Systems, Release C.

8. 3GPP TSG RAN TR 25.912 v7.2.0, Feasibility Study for Evolved Universal Terrestrial Radio Access (UTRA) and Universal Terrestrial Radio Access Network (UTRAN).

9. 3GPP2 TSG C.S0084-001-0 v2.0, Physical Layer for Ultra Mobile BroadBand (UMB) Air Interface Specification.

10. 3GPP TSG RAN TR 25.913 v7.3.0, Requirements for Evolved Universal Terrestrial Radio Access (UTRA) and Universal Terrestrial Radio Access Network (UTRAN).

11. 3GPPTSG RANTR 23.882 v1.15.1, 3GPP System Architecture Evolution: Report on Technical Options and Conclusions.

12. 3GPP TSG RAN TR 36.913 v8.0.0, Requirements for Further Advancements for E-UTRA (LTE-A).

13. IEEE802.16m-07/002r4, TGm System Requirements Document (SRD).

14. H. Yanikomeroglu, "Cellular Multihop Communications: Infrastructure-Based Relay Network Architecture for 4G Wireless Systems," *The 22nd Biennial Symposium on Communications*, Queen's University, Kingston, Canada, June 2004.

15. R. Pabst, B. H. Walke, D. C. Schultz, et al., "Relay-Based Deployment Concepts for Wireless and Mobile Broadband Radio," *IEEE Communications Magazine*, Vol. 42, no. 9, pp. 80–89, 2004.

16. L. Le and E. Hossain, "Multihop Cellular Networks: Potential Gains, Research Challenges, and A Resource Allocation Framework," *IEEE Communications Magazine*, Vol. 45, no. 9, pp. 66–73, 2007.

17. O. Oyman, N. J. Laneman, and S. Sandhu, "Multihop Relaying for Broadband Wireless Mesh Networks: From Theory to Practice," *IEEE Communications Magazine*, Vol. 45, no. 11, pp. 116–122, 2007.

18. Y.-D. Lin and Y.-C. Hsu, "Multihop Cellular: A New Architecture for Wireless Communications," *The 19th Annual Joint Conference of IEEE Computer and Communications Societies* (*INFOCOM* '00), Vol. 3, pp. 1273–1282, Tel Aviv, Israel, March 2000.

19. H. Wu, C. Qiao, S. De, and O. Tonguz, "Integrated Cellular and ad hoc Relaying Systems: iCAR" , *IEEE Journal on Selected Areas in Communications*, Vol. 19, no. 10, pp. 2105–2115, 2001.

20. V. Sreng, H. Yanikomeroglu, and D. Falconer, "Coverage Enhancement Through Two-hop Relaying in Cellular Radio Systems," *IEEE Wireless Communications and Networking Conference* (*WCNC* '02), Vol. 2, pp. 881–885, March 2002.

21. A. Bletsas, A. Khisti, D. P. Reed, and A. Lippman, "A Simple Cooperative Diversity Method Based on Network Path Selection," *IEEE Journal on Selected Areas in Communications*, Vol. 24, no. 3, pp. 659–672, 2006.

22. M. Qin and R. S. Blum, "Capacity of Wireless ad hoc Networks with Cooperative Diversity: A Warning on the Interaction of Relaying and Multi-hop Routing," *IEEE International Conference on Communications*, Vol. 2, pp. 1128–1131, May 2005.

23. G. Scutari, S. Barbarossa, and D. Ludovici, "Cooperation diversity in multihop wireless networks using opportunistic driven multiple-access," *IEEE Workshop on Signal Processing Advances in Wireless Communications* (*SPAWC* '03), pp. 170–174, June 2003.

24. E. C. van der Meulen. "Three-terminal communication channels." *Advances in Applied Probability*, 3:120–154, 1971.

25. E. C. van der Meulen. "A survey of multi-way channels in information theory: 1961–1976." *IEEE Transactions on Information Theory*, 23(1):1–37, January 1977.

26. G. Kramer, M. Gastpar, and P. Gupta. "Cooperative strategies and capacity theorems for relay networks". *IEEE Transactions on Information Theory*, 51(9):3037–306, September 2005.

27. A. Reznik, S. R. Kulkarni, and S. Verdu. "Degraded Gaussian multi-relay channel: capacity and optimal power allocation". *IEEE Transactions on Information Theory*, 50(12):3037–3046, December 2004.

28. A. A. El Gamal and S. Zahedi. "Capacity of a class of relay channels with orthogonal components". *IEEE Transactions on Information Theory*, 51(5):1815–1817, May 2005.

29. J. N. Laneman and G.W. Wornell. "Distributed space-time coded protocols for exploiting cooperative diversity in wireless networks" *IEEE Transactions Information Theory*, 49(10):2415–2425, October 2003.

30. J. N. Laneman, D. N. C. Tse, and G. W. Wornell. "Cooperative diversity in wireless networks: efficient protocols and outage behavior." *IEEE Transactions on Information Theory*, 50(12):3062–3080, December 2004.

31. G. Kramer, M. Gastpar, and P. Gupta. "Cooperative strategies and capacity theorems for relay networks". *IEEE Transactions on Information Theory*, 51(9):3037–306, September 2005.

32. Z. Xiong, A. D. Liveris, and S. Cheng. "Distributed source coding for sensor networks". *IEEE Signal Processing Magazine*, 21:80–94, September 2004.

33. T. Cover and A. E. Gamal. "Capacity theorems for the relay channel". *IEEE Transactions on Information Theory*, 25(5):572–584, September 1979.

34. B. Zhao and M.C. Valenti. "Practical relay networks: a generalization of hybrid-ARQ". *IEEE Journal on Selected Areas in Communications*, 23(1):7–18, January 2005.

35. M. Zorzi and R. R. Rao. "Geographic random forwarding (geraf) for ad hoc and sensor networks: multihop performance". *IEEE Transactions on Mobile Computing*, 2(4):337–348, Oct.-Dec. 2003.

36. J. Luo, R. S. Blum, L. J. Greenstein, L. J. Cimini, and A. M. Haimovich. "New approaches for cooperative use of multiple antennas in ad hoc wireless networks". *IEEE Vehicular Technology Conference* (*VTC*'04) Vol. 4, pp. 2769–2773, Sept. 2004.

37. A. Ibrahim, A. Sadek, W. Su, and K. J. R. Liu. "Cooperative communications with partial channel state information: when to cooperate?", *The IEEE Global Telecommunications Conference* (*GLOBECOM*), 5:3068–3072, Nov. 2005.

38. A. Ibrahim, A. Sadek,W. Su, and K. J. R. Liu. "Relay selection in multi-node cooperative communications: when to cooperate and whom to cooperate with?", *The IEEE Global Telecommunications Conference* (*GLOBECOM*), Nov. 2006.

39. A. K. Sadek, W. Su, and K. J. R. Liu. "A class of cooperative communication protocols for multi-node wireless networks." *The IEEE International Workshop on Signal Processing Advances in Wireless Communications* (*SPAWC*), pp. 560–564, June 2005.

40. A. K. Sadek, W. Su, and K. J. R. Liu. "Multinode cooperative communications in wireless networks." *IEEE Transactions on Signal Processing*, 55(1):341–355, January 2007.

41. K. G. Seddik, A. K. Sadek, W. Su, and K. J. R. Liu. "Outage analysis and optimal power allocation for multi-node relay networks". *IEEE Signal Processing Letters*, 14:377-380, June 2007.

42. H. Mheidat, M. Uysal, and N. Al-Dhahir, "Comparative analysis of equalization techniques for STBC with application to EDGE," *IEEE Vehicular Technology Conference* (*VTC*'04) Spring, Milan, Italy, May 2004.

43. T. L. Marzetta and B. M. Hochwald, "Capacity of a mobile multiple-antenna communication link in Rayleigh flat-fading," *IEEE Transactions on Information Theory*, Vol. 45, pp. 139–157, Jan. 1999.

44. B. L. Hughes, "Differential space-time modulation," *IEEE Transactions on Information Theory*, Vol. 46, pp. 2567–2578, Nov. 2000.

45. B. M. Hochwald and T. L. Marzetta, "Unitary spacetime modulation for multiple-antenna communications in Rayleigh flat fading," *IEEE Transactions on Information Theory*, Vol. 46, pp. 543-564, March 2000.

46. B. M. Hochwald and W. Sweldens, "Differential unitary space-time modulation," *IEEE Transactions on Communications*, Vol. 48, pp. 2041–2052, Dec. 2000.

47. V. Tarokh and H. Jafarkhani, "A differential detection scheme for transmit diversity," *IEEE Journal on Selected Areas in Communications*, Vol. 18, pp. 1169–1174, July 2000.

48. Z. Chen, G. Zhu, J. Shen, and Y. Liu, "Differential space time block codes from amicable orthogonal designs," *Wireless Communications and Networking Conference*, Mar. 2003, pp. 768-772.

49. B. Maham and A. Hjørungnes, "Power allocation in cooperative networks using differential space-time codes," *IEEE International Symposium in Information Theory* (*ISIT*), Nice, France, June 24-29, 2007.

50. W. Cho and L. Yang, "Distributed differential schemes for cooperative wireless networks," *IEEE International Conference on · Acoustics Speech and Signal Processing* (ICASSP), Toulouse, France, May 2006.

51. Q. Zhao, H. Li, "Decode-based differential modulation for wireless relay networks," *IEEE International Conference on Acoustics Speech and Signal Processing* (ICASSP), Philadelphia, USA, March 2005.

52. R. Zhang and L. Hanzo, "Interleaved Random Space-Time Coding for Multisource Cooperation," *IEEE Transactions on Vehicular Technology*, Vol. 58, no. 4, pp. 2120–2125, May 2009.

53. E. H. Drucker, "Development and application of a cellular repeater," *IEEE Vehicular Technology Conference* (*VTC* '88), pp. 321–325, June 1988.

54. O. Muñoz-Medina, J. Vidal, and A. Agustín, "Linear transceiver design in non-regenerative relays with channel state information," *IEEE Transactions on Signal Processing*, Vol. 55, no. 6, pp. 2593–2604, 2007.

55. X. Tang and Y. Hua, "Optimal design of non-regenerative MIMO wireless relays," *IEEE Transactions on Wireless Communications*, Vol. 6, no. 4, pp. 1398–1406, 2007.

56. S. W. Peters and R. W. Heath Jr., "Nonregenerative MIMO relaying with optimal transmit antenna selection," *IEEE Signal Processing Letters*, Vol. 15, pp. 421–424, 2008.

57. D. Chen and J. N. Laneman, "Modulation and demodulation for cooperative diversity in wireless systems," *IEEE Transactions on Wireless Communications*, Vol. 5, no. 7, pp. 1785–1794, 2006.

58. K. Azarian, H. El Gamal, and P. Schniter, "On the achievable diversity-multiplexing tradeoff in half-duplex cooperative channels," *IEEE Transactions on Information Theory*, Vol. 51, no. 12, pp. 4152–4172, 2005.

59. B. Rankov and A. Wittneben, "Spectral efficient signaling for half-duplex relay channels," *Asilomar Conference on Signals, Systems and Computers*, pp. 1066–1071, November 2005.

60. B. Wang, J. Zhang, and A. Høst-Madsen, "On the capacity of MIMO relay channels," *IEEE Transactions on Information Theory*, Vol. 51, no. 1, pp. 29–43, 2005.

61. C. K. Lo, S. Vishwanath, and R. W. Heath Jr., "Rate bounds for MIMO relay channels," *Journal of Communications and Networks*, Vol. 10, no. 2, pp. 194–203, 2008.

62. C.-B. Chae, T. Tang, R. W. Heath Jr., and S. Cho, "MIMO relaying with linear processing for multiuser transmission in fixed relay networks," *IEEE Transactions on Signal Processing*, Vol. 56, no. 2, pp. 727–738, 2008.

63. Mohamed-salim Alouni and Andrea Goldsmith," Area spectral efficiency of cellular mobile radio systems", IEEE transactions on Vehicular Technology, Vol. 48, No. 4, July 1999. PP. 1047-1066.

64. R. Steele, "*Mobile Radio Communications*," Pentech Press, 1992.

65. T. S. Rappaport, "Wireless Communications: Principle and Practice," 2nd ed., Prentice Hall, 2002.

66. G. L. Stüber, "*Principles of Mobile Communication*" Kluwer Academic Publishers, 1996.

67. H. B¨olcskei, D. Gesbert, and A. J. Paulraj, "On the capacity of OFDM-based spatial multiplexing systems," *IEEE Transactions on Communications*, Vol. 50, no. 2, pp. 225–234, Feb. 2002.

68. G. J. Foschini, "Layered space–time architecture for wireless communication in a fading environment when using multi-element antennas," *Bell Labs Technical Journal*, pp. 41–59, 1996.

69. A. J. Paulraj and T. Kailath, "Increasing capacity in wireless broadcast systems using distributed transmission/directional reception," *U.S. Patent*, 1994, no. 5,345,599.

70. I. E. Telatar, "Capacity of multi-antenna Gaussian channels," *European Transactions on Telecommunications*, Vol. 10, no. 6, pp. 585–595, Nov./Dec. 1999.

71. L. Zheng, and D.N.C. Tse, "Diversity and multiplexing: a fundamental tradeoff in multiple-antenna channels," *IEEE Transactions on Information Theory* Vol. 49(no. 5): 1073–1096.

72. V. Tarokh, N. Seshadri, and A.R. Calderbank, "Space-time codes for high data rate wireless communication: Performance criterion and code construction," *IEEE Transactions on Information Theory* Vol. 44(no. 2): 744–765.

73. S.M. Alamouti, "A simple transmit diversity technique for wireless communications," *IEEE Journal on Selected Areas in Communications* Vol. 16(no. 8): 1451–1458.

74. A. Ghrayeb, "A survey on antenna selection for MIMO communication systems," *Information and Communication Technologies* (*ICTTA*) pp. 2104–2109.

75. S. Mallick, P. Kaligineedi, M. M. Rashid, and V. K. Bhargava, "Radio resource optimization in cooperative wireless communication networks," *Chapter 8, in Cooperative Cellular Wireless Networks*, Cambridge University Press, 2011.

76. L. B. Le, S. A. Vorobyov, K. Phan, and T. L. Ngoc, "Resource allocation and QoS provisioning for wireless relay networks," in Quality-of-Service Architectures for Wireless Networks: Performance Metrics and Management. *IGI Global*, 2009.

77. A. Goldsmith, "Capacity limits of MIMO Channels," *IEEE Journal in Selected Areas in Communications*, vol. 21, no. 5, June 2003.

78. M. Salem, A. Adinoyi, H. Yanikomeroglu, and D. Falconer, "Opportunities and challenges in OFDMA-based cellular relay networks: A radio resource management perspective," *IEEE Transactions on Vehicular Technology*, Vol. 59, no. 5, pp. 2496-2510, June 2010.

79. A. Sendonaris, E. Erkip, and B. Aazhang, "User cooperation diversity-part I: System description," *IEEE Transactions on Communications*, vol. 51, no. 11, pp. 1927–1938, Nov. 2003.

80. A. Sendonaris, E. Erkip, and B. Aazhang, "User cooperation diversity-part II: Implementation aspects and performance analysis system," *IEEE Transactions on Communications*, vol. 51, no. 11, pp. 1939–1948, Nov. 2003.

81. A.Nosratinia, T.E.Hunter, and A. Hedayat, "Cooperative communication in wireless networks," *IEEE Communications Magazine*, vol.42, no.10, pp.74–80, Oct. 2004.

82. Y. W. Hong, W. J. Huang, F. H. Chiu, and C. C. J. Kuo, "Cooperative communications in resource-constrained wireless networks," *IEEE Signal Processing Magazine*, vol. 24, no. 3, pp. 47–57, May 2007.

83. Y. Liang and V. V. Veeravalli, "Gaussian orthogonal relay channel: Optimal resource allocation and capacity," *IEEE Transactions in Information Theory*, vol. 51, no.9, pp. 3284–3289, Sept. 2005.

84. M. Dohler, "Virtual antenna arrays", Ph.D. dissertation, King's College London, London, UK, 2003.

85. *IEEE* P802.16j/D9, "Draft Amendment to *IEEE* Standard for Local and Metropolitan Area Networks Part 16: Air Interface for Fixed and Mobile Broadband Wireless Access Systems: Multihop Relay Specification," Feb. 2009.

86. M. Iwamura, H. Takahashi and S. Nagata, "Special Articles on LTE-A Technology – ongoing evolution of LTE toward IMT-Advanced," *NTT DOCOMO Technical Journal*, Vol. 12, no. 2, 2010

87. S. W. Peters and R. W. Heath Jr., "The Future of WiMAX: Multihop Relaying with *IEEE* 802.16j," *IEEE Communications Magazine*, Vol. 47, no. 1, Jan. 2009, pp. 104–11.

88. V. Genc et al., "*IEEE* 802.16j Relay-Based Wireless Access Networks: An Overview," *IEEE Transactions on Wireless Communications*, Vol. 15, no. 5, Oct. 2008, pp. 56–63.

89. R. U. Nabar, H. Bolcskei and F. W. Kneubuhler, “Fading relay channels: performance limits and space-time signal design,” *IEEE Journal on Selected Areas in Communications*, Vol.22, no.6, pp. 1099- 1109, Aug. 2004.

90. F. Khan, “*LTE for 4G Mobile Broadband – Air Interface Technologies and Performance*,” Cambridge University Press, 2009.

91. 3GPP TR 36.814 V1.2.1, “Further Advancements for EUTRA: Physical Layer Aspects,” Technical Specifications Group Radio Access Network Rel. 9, June 2009.

92. M. G. Hyung, J. Lim, and D. J. Goodman, “Single carrier FDMA for uplink wireless transmission,” *IEEE Vehicular Technology Conference*, pp. 30–38, Sept. 2006.

93. CISCO, USA, White paper, “Cisco Visual Networking Index: Global Mobile Data Traffic Forecast Update,” Jan. 2009.

94. Y. Lin and Y. Hsu, “Multihop Cellular: A New Architecture for Wireless Communications," in IEEE Infocomm, (Tel Aviv, Israel), March 2000.

95. N. Esseling, B. H. Walke, and R. Pabst, Fixed Relays For Next Generation Wireless Systems, ch. 5, pp. 71-91. New York, USA: Springer Science+Buisness Media, Inc., 2005.

96. "802.16j-2009, IEEE Standard for Local and metropolitan area networks Part 16: Air Interface for Broadband Wireless Access Systems Amendment 1: Multihop Relay Specification," June 2009.

97. Khakurel, S.; Mehta, M.; Karandikar, A. "Optimal Relay Placement for Coverage Extension in LTE-A Cellular Systems" 2012 National Conference on Communications (NCC) 2012 , Page(s): 1-5.

98. Hamdi, A.; El-Khamy, M.; El-Sharkawy, M. "Optimized Dual Relay Deployment for LTE-Advanced Cellular Systems" 2012 IEEE Wireless

Communications and Networking Conference (WCNC), 2012 , Page(s): 2869-2873.

99. Yilmaz, E.; Gesbert, D.; Knopp, R. "Interference Relay Channel in 4G Wireless Networks" 2012 IEEE Wireless Communications and Networking Conference (WCNC), 2012 , Page(s): 364-368.

100. Wei Hong; Jing Han; Haiming Wang, "Full Uplink Performance Evaluation of FDD/TDD LTE-Advanced Networks with Type-1 Relays" 2011 IEEE Vehicular Technology Conference (VTC Fall) 2011 , Page(s): 1-5

101. Wei Hong, Jing Han, Haiming Wang, "UL Performance of Type-1 Relay Enhanced FDD LTE-A Networks with Unaligned Backhaul Subframes" IEEE 73rd Vehicular Technology Conference (VTC Spring), 2011, Page(s): 1- 5.

102. Chandwani, G.; Datta, S.N.; Chakrabarti, S., "Relay Assisted Cellular System for Energy Minimization" 2010 Annual IEEE India Conference (INDICON), 2010, Page(s): 1-4.

103. 3GPP TS 36.211 “Physical Channels and Modulation (Release 8)”.

104. 3GPP TR 36.912 V 9.1.0: Technical Specification Group Radio Access Network; Feasibility study for further advancements for E-UTRA (LTE-A), Release 9 December 2009.

105. A. Tuan Tran and Abu B. Sesay, “A generalized linear quasi-ML decoder of OSTBCs for wireless communications over time-selective fading channels” *IEEE Transactions on Wireless Communications* 3(3): 855-864 (2004).

106. Mohamed A. Khamsi and William A. Kirk, "An introduction to metric spaces and fixed point theory", John Wiley & Sons, 2001.

107. J. G. Proakis , “*Digital communications*”, 4th ed. 2001 New York: McGraw-Hill.

108. A. Papoulis, "*Probability, Random Variables and Stochastic Processes*", Mcgraw-Hill College 3rd ed., 1991

109. C. Tellambura, A. J. Mueller and V. K. Bhargava, "Analysis of M-ary phase-shift keying with diversity reception for land-mobile satellite channels," IEEE Trans. Veh. Technol., vol. 46, pp. 910–922, Nov. 1997.

110. M. K. Simon and M.-S. Alouini, "A unified approach to the performance analysis of digital communication over generalized fading channels," Proc. IEEE, vol. 86, no. 9, pp. 1860–1877, Sept. 1998.

111. A. Jeffrey, "*Table of Integrals*, *Series*, *and Products*" Academic Press; 5th ed., 1996.

112. S. Parkvall and D. Astely, "The Evolution of LTE towards IMT-Advanced", *Journal of Communications*, Vol. 4, no. 3, April 2009

113. C. E. Shannon. "A mathematical theory of communication". *The Bell System Technical Journal*, Vol. 27, pp. 379-423, 623-656, July, October, 1948.

114. R. V. L. Hartley, "Transmission of Information," *Bell System Technical Journal*, July 1928, p. 535.

115. 3GPP TS 36.300, "Evolved Universal Terrestrial Radio Access (E-UTRA) and Evolved Universal Terrestrial Radio Access Network (E-UTRAN); Overall Description Stage 2", version 8.7.0, December 2008

116. 3GPP TS 36.214, "Evolved Universal Terrestrial Radio Access (E-UTRA) Physical Layer – Measurements", version 8.5.0, December 2008.

117. 3GPP Project Document R1-060 291. "OFDMA Downlink Inter-Cell Interference Mitigation." Feb. 2006.

118. Sawahashi, M.; Kishiyama, Y.; Morimoto, A.; Nishikawa, D.; Tanno, M. "Coordinated multipoint transmission/reception techniques for LTE-advanced"

Wireless Communications, IEEE Volume: 17 , Issue: 3 Publication, 2010 , Page(s): 26- 34

119. Lee, J.; Kim, Y.; Lee, H.; Ng, B.L.; Mazzarese, D.; Liu, J.; Xiao, W.; Zhou, Y. "Coordinated multipoint transmission and reception in LTE-advanced systems" IEEE Communications Magazine, Volume: 50 , Issue: 11 2012 , Page(s): 44-50

120. Daewon Lee; Hanbyul Seo; Clerckx, B.; Hardouin, E.; Mazzarese, D.; Nagata, S.; Sayana, K. "Coordinated multipoint transmission and reception in LTE-advanced: deployment scenarios and operational challenges" IEEE Communications Magazine, Volume: 50 , Issue: 2 2012 , Page(s): 148 - 155.

121. Qualcomm R1-050896. "Description and Simulations of Interference Management Technique for OFDMA Based E-UTRA Downlink Evaluation," 3GPP RAN WG1 #42, London, UK.

122. Nokia R1-060298. "Uplink Inter Cell Interference Mitigation and Text Proposal," 3GPP RAN WG1 #44, Denver, USA.

123. Samsung R1-051341. "Flexible Fractional Frequency Reuse Approach," 3GPP RAN WG1 #43, Seoul, Korea.

124. L.J. Cimini, J. C. Chuang, and N. R. Sollenberger, "Advanced cellular internet service (ACIS)." *IEEE Communication Magazine*, 36(10), 150–159.

125. S. B. Yun, S. Y. Park, Y. W. Lee, "Hybrid division duplex system for next-generation cellular services." *IEEE Transactions on Vehicular Technology*, 56(5), 3040–3059.

126. D. G. Jeong, and W. S. Jeon "Comparison of time slot allocation strategies for CDMA/TDD systems." *IEEE Journal on Selected Areas in Communications*, 18(7), 1271–1278.

127. G. Auer, "On modeling cellular interference for multi-carrier based communication systems including a synchronization offset." *International Symposium on Wireless Personal Multimedia Communications* (WPMC'03), pp. 290–294.

128. Ericsson R1-050764. "Inter-cell Interference Handling for E-UTRA," 3GPP RAN WG1 #42, London, UK.

129. RITT R1-050608. "Inter-cell Interference Mitigation based on IDMA," *3*GPP *TSG RAN WG1 Ad Hoc on* LTE, Sophia Antipolis, France.

130. Gregory E. Bottomley and Karim Jamal, "Adaptive Arrays and MLSE Equalization," *IEEE Vehicular Technology Conference*, pp. 50-54, Chicago, 1995

131. J. Karlsson and J. Heinegard, "Interference Rejection Combining for GSM," *IEEE International Conference on Universal Personal Communications* 1996, pp. 433–437.

132. O. Oteri and A. Paulraj "Multicell Optimization for Diversity and Interference Mitigation" *IEEE Transactions on Signal Processing*, Vol. 56, no. 5, MAY 2008.

133. L. Thiele, M. Schellmann, S. Schiffermuller, V. Jungnickel and W. Zirwas, "Multi-Cell Channel Estimation using Virtual Pilots", *IEEE Vehicular Technology Conference* Spring 2008, pp. 1211-1215.

134. L. Thiele, T. Wirth, M. Schellmann, Y. Hadisusanto and V. Jungnickel, "MU-MIMO with Localized Downlink Base Station Cooperation and Down-tilted Antennas", *IEEE International Conference on Communications Workshops*, 2009. *ICC Workshops* 2009. pp. 1-5.

135. L. Thiele, M. Schellmann, T. Wirth and V. Jungnickel, "Cooperative Multi-User MIMO Based on Limited Feedback in Downlink OFDM Systems" 42^{nd} *Asilomar Conference on Signals, Systems and Computers*, 2008, pp: 2063 - 2067.

136. A. M. D. Turkmani, "Performance Evaluation of a Composite Microscopic Plus Macroscopic Diversity System," *IEE Proceedings I.*, Vol. 138, pp. 15–20, 1991.

137. H. Chernoff, "A Measure of Asymptotic Efficiency for Tests of a Hypothesis Based on the Sum of Observations", *Annals of Mathematical Statistics*, 23 (4): 493–507.

138. H. Chernoff, "A Note on an Inequality Involving the Normal Distribution", *Annals of Probability* 9 (3): 533.

139. G. D. Forney, "Maximum-Likelihood sequence Estimation of Digital Sequences in the Presence of Inter- symbol Interference," *IEEE Transactions in Information Theory*, vol. 18, no. 3, pp363-378, May 1972.

140. J.K. Cavers and P. Ho, "Analysis of the error performance of trellis coded modulations in Rayleigh fading channels", *IEEE Transactions on Communications,* vol. 40, pp. 74-80, Jan 1992.

141. A. J. Viterbi, J. K. Omura, "*Principles of Digital Communication and Coding*" McGraw-Hill, Inc. 1979

142. G.L. Stüber, "*Principles of mobile communication*", Kluwer Academic Publishers, 1996.

143. G. Strang, "*Introduction to linear algebra*" Cambridge (MA): Wellesley-Cambridge Press, 1998.